Impact of Channel Estimation Error and PAPR Reduction for Precoding Techniques in TDD-CDMA System

by

NORHARYATI BINTI HARUM

A dissertation submitted in partial satisfaction of the
requirements for the degree of
Doctor of Philosophy

in

Engineering

in the

Graduate Division

of the

Keio University, Yagami

Committee in charge:

Professor Tomoaki Ohtsuki, Chair
Professor Iwao Sasase
Professor Yukitoshi Sanada
Associate Professor Hiroshi Shigeno

March 2012

The dissertation of NORHARYATI BINTI HARUM, titled Impact of Channel Estimation Error and PAPR Reduction for Precoding Techniques in TDD-CDMA System, is approved:

Chair _____ Date _____

_____ Date _____

_____ Date _____

_____ Date _____

Keio University, Yagami

Impact of Channel Estimation Error and PAPR Reduction for Precoding Techniques in TDD-CDMA System

Contents

List of Figures

List of Tables

Acknowledgments

First of all, I would like to thank Professor Masao Nakagawa for guiding me on how to do research and for all the support since undergraduate course. Also, Professor Tomoaki Ohtsuki who supports me during my Ph.D. course. I am indebted to his diligence in constantly stimulating me towards the completion of this dissertation. Furthermore, I would also like to express my gratitude for the panel who examined this dissertation, Prof. Iwao Sasase, Prof. Yukitoshi Sanada, and Prof. Hiroshi Shigeno. Their critical reviews and constructive suggestions added an extra layer of polish to this dissertation.

I would also wish my deepest gratitude to Yayasan Pelajaran MARA for selecting me as one of Higher Education Project (HELP) students and gave me the opportunity to further my study from Bachelor, Master and Ph.D. course. Also, thanks to Universiti Teknikal Malaysia Melaka (UTeM) for supporting me during my Ph.D. course. I am grateful for the opportunity I was entrusted with, and being able to contribute back to the society through this research.

This dissertation has been a long journey. I will not be able to complete this journey with kind support from my colleagues, professor and family. I would also like to express my appreciation to every professor and staffs in the GCOE program, especially Ms. Maki Adachi, Ms. Yuko Izuta, and Ms. Chinatsu Ichikawa. As a member of Ohtsuki Laboratory, I would also like to take advantage of this opportunity to express my thanks towards my other colleagues for their support and encouragement. Last but not least, I wish to express my heartfelt thanks to my husband Mazwir Abdul Manan, my father Harum Embong, my mother Noriah Yazit and my beloved kids who have always been a great source of support and encouragement for me.

Abstract

In this dissertation, we focus on precoding techniques in time-division duplex code-division multiple-access (TDD-CDMA) system that can be realized by exploiting channel reciprocity. The study focuses on pre-rake and joint transmission (JT) techniques because of their simple algorithms compared to other precoding techniques. First, we analyze the impact of channel estimation error on the pre-rake technique, because the assumption of perfect channel knowledge is not practical for real mobile communications. Second, we propose a modified JT technique to reduce peak-to-average power ratio (PAPR) that results in a low cost mobile station and base station.

Chapter 1 presents an introduction of this thesis. First, we explain the background of wireless communications. We then discuss requirements for wireless mobile communication systems that include a low cost communications, a high spectral efficiency and a high data rate communication, with large capacity and coverage. This study focuses on low cost communications that can be realized by exploiting channel reciprocity feature in TDD-CDMA system, using precoding techniques; pre-rake and JT. TDD-CDMA is introduced with discussion of differences between TDD and frequency-division duplex (FDD), followed by the description of the TDD-CDMA systems. We then introduce channel reciprocity feature and precoding techniques that are the key technologies of this thesis. We finally present the motivation of our study and overview of each chapter to clarify problems and objectives of this study.

Chapter 2 presents our study on impact of channel estimation error in pre-rake TDD-

CDMA system. We investigate the impact of channel estimation error by computer simulation and numerical analysis. For comparison, we also present impact of channel estimation error on rake system. The channel estimation error consists of both amplitude and phase errors. The results show that the channel estimation error causes performance degradation, owing to large multiple-access interference caused by a high orthogonality loss among spreading codes of different users.

Chapter 3 presents the proposed modified JT technique to provide a low PAPR in TDD-CDMA system. The newly proposed JT technique selects a certain paths out of the total paths that processed in JT technique. Our proposed JT technique performs a lower PAPR than that in the conventional JT technique. To improve PAPR and BER performance, we combine the proposed JT with clipping technique. The results show that the combination of our proposed path selection technique with clipping technique provides a low PAPR without severe bit-error-rate (BER) degradation.

This dissertation is finally concluded in Chapter 4.

Chapter 1

Introduction

1.1 Recent Evolution of Wireless Mobile Communications

Nowadays, wireless communications have become increasingly important in our life, because the application is not only limited to voice transmission, but also video streaming, mobile internet and television broadcasting. The development of wireless communications gives big impact in economic field, since it can produce lots of business chances.

The wireless communications for cellular system was firstly developed in 1983, where the 1st generation (1G) system introduced analog communication with frequency-division multiple-access (FDMA) technology. Although the analog communication worked well, they had some drawbacks, and thus ideas to have digital communications systems were forming. The digital communication was firstly introduced in 2nd generation (2G) system in the beginning of 1990s. Figure 1.1 shows an evolution of wireless communications system from 2G to future 4th generation (4G) system. In 2G, global system for mobile (GSM), interim standard 95 (IS-95), digital advanced mobile phone service (D-AMPS) and personal digital cellular (PDC) were introduced. The GSM has been the most successful mobile cellular

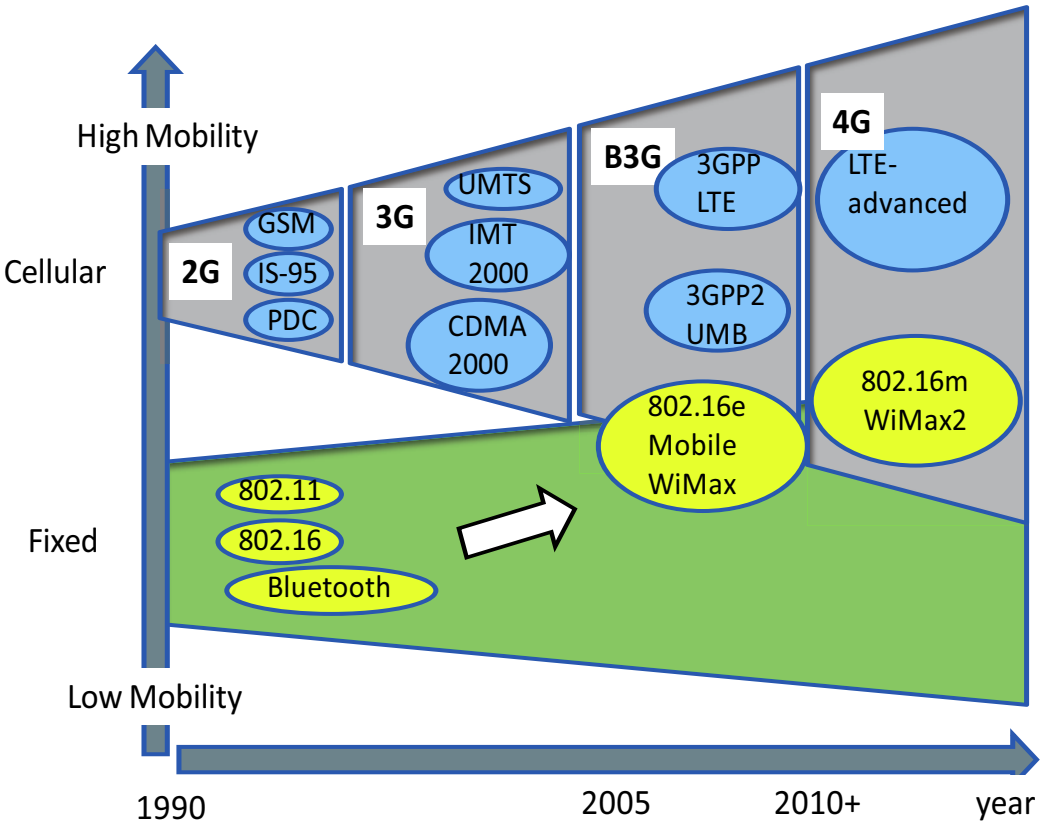

Figure 1.1: Evolution in Wireless Communications

system with users in more than 174 countries [1] [2] and in February 2004, more than one billion users are connected. The first work of GSM started in 1984 and deployed in 1991 in Europe, operated in 900 MHz frequency band. The GSM was also deployed in North America, operated in 1900 MHz frequency band. The 2G mobile systems have been focusing on voice and a low data rate service up to 14.4 Kbps such as short message service introduced in GSM.

The wireless communication systems are then developed with further enhancement in 3rd generation (3G) system with universal mobile telephone system (UMTS) standardized by 3rd generation partnership project (3GPP), international mobile telecommunication 2000 (IMT-2000) and code-division multiple-access 2000 (CDMA 2000) system standardized by

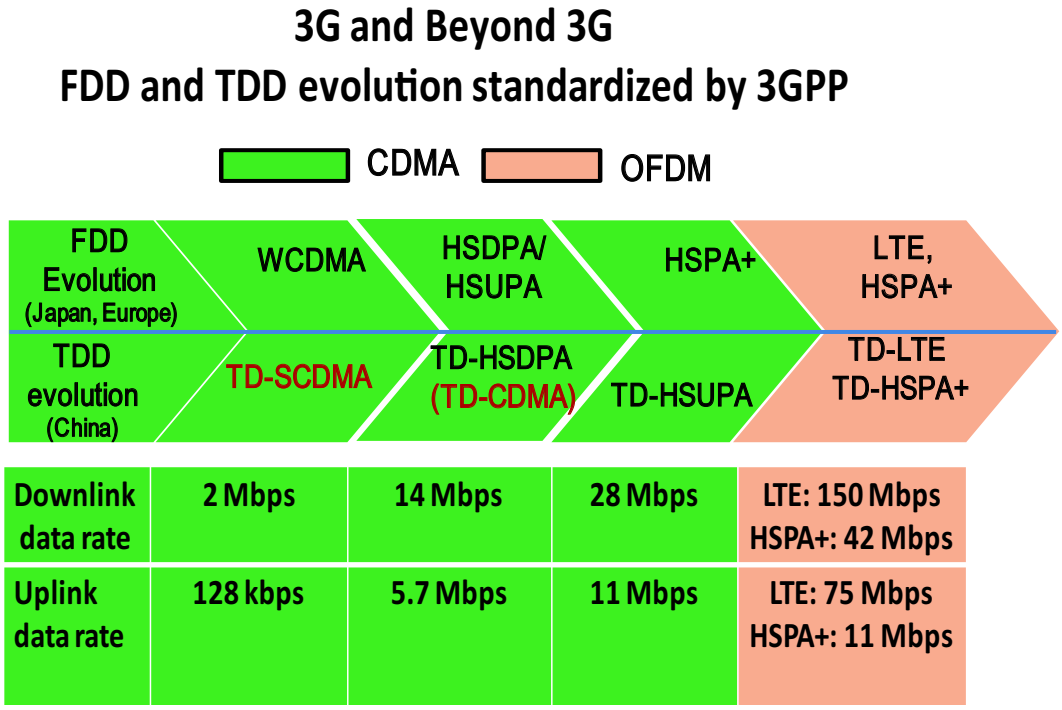

Figure 1.2: 3G and Beyond 3G by 3GPP

3GPP2. In 3G system, new applications that need high data rate such as video streaming and mobile internet have been introduced. To support the new multimedia services, the 3G system deployed to support data rates up to 384 Kbps for mobile users and 2 Mbps for fixed users. Since 2005, 3GPP introduces a new system long term evolution (LTE), which is standardized to support higher data rate than that in 3G system. The LTE is also called beyond 3G (B3G) system. The deployment of LTE started from 2010 and researches for LTE-advanced for 4G system is becoming a new hot topic in recent years.

Figure 1.2 shows the standards in 3G and B3G systems deployed by 3GPP. The 3GPP standardization is divided into two modes; Frequency-division duplex (FDD) and time-division duplex (TDD). The evolution of FDD started from wideband CDMA (WCDMA)

which has been used in Japan and Europe and then expanded to high speed downlink packet access (HSDPA) and high speed uplink packet access (HUSPA) with 28 Mbps of downlink (DL) data rate, following by high speed packet access (HSPA) evolution that can provide DL data rate up to 28 Mbps. To provide a higher data rate, LTE and evolved HSPA that can achieve 150 Mbps and 42 Mbps of DL data rate are then introduced. In LTE, orthogonal frequency-division multiplexing (OFDM) is introduced instead of CDMA to achieve higher data rate using a wider frequency band. On the other hand, the evolution of TDD started from time-division synchronous CDMA (TD-SCDMA). The TD-SCDMA has been developed by China communications standards association (CCSA) in China [3]. Also, it has been implemented in China since 2008. Parallel with FDD evolution, the TDD is expanded to HSDPA and HSUPA, known as time-division HSDPA (TD-HSDPA) or time-division CDMA (TD-CDMA) and time-division HSUPA (TD-HSUPA), respectively. To provide a higher data rate, time-division LTE (TD-LTE) and evolved TD-HSPA have been deployed. OFDM is also introduced in TDD evolution to provide a higher data rate. From Fig. 1.2, we can see that the FDD is evolved from WCDMA and TDD is evolved from TD-SCDMA. The TD-SCDMA will be expanded to multicarrier TD-SCDMA and TDD based LTE-advanced that might use OFDM in 4G system [4].

1.2 Requirements for Wireless Mobile Communications

As mentioned in section 1.1, the future mobile wireless communications are deployed with various standards to fulfill users' demands on mobile services. The most important point in wireless communications is spectral efficiency because only limited data can be transmitted to a certain number of users in a limited frequency bandwidth. In the future, different operators will deploy more standards, and thus limiting an available frequency band. The frequency band license is expensive and open frequency band should be avoided because of security problems. The lack of available frequency band requires a high spectral efficiency to

transmit the amount of data to the users within the limited bandwidth. Some technologies such as frequency reuse technique have been researched to increase spectral efficiency.

However, because of the growth of cellular phone's users and new applications such as mobile internet, video streaming and television broadcasting, the requirement of future wireless communications is not limited to high spectral efficiency but the following aspects should also be considered:

1. Data rate

   Nowadays many cellular applications are not only limited to voice transmission. Applications such as mobile internet, television broadcasting and video streaming are becoming the main interest of cellular's users. To support the applications, high data rate is required particularly for downlink transmission. Even though, current 3G system can support 2 Mbps for downlink transmission, higher data rates are expected for B3G system up to 100 Mbps. Higher data rate will be expected for future 4G system.

2. Capacity

   Capacity has been significantly improved after migration from 2G to 3G, where CDMA is used instead of FDMA. In CDMA, because users are divided by code, lack of frequency band can be solved. However, interferences between users caused by multipath fading limits the network capacity. For CDMA system, multiuser detection is one of the techniques to reduce the interference, which is also the key technology of this study.

3. Coverage

   Since many operators with more transmission schemes will be used in future mobile wireless communications, the lack of frequency band problem will occur. A low frequency band that only requires low cost antenna technologies has been used and only high frequency band will remain. The main problem of high frequency band usage is a coverage problem, where coverage becomes smaller for higher frequency band. Communication trend shows that migration from previous generation to current generation

causes out of coverage area in coverage edge in previous generation wireless communications. Nowadays, relay communications are widely discussed to solve the coverage problem.

4. Low cost communications

   Nowadays, wireless communications focus on not only high data rate technologies, but also technologies that can provide low error rate with low cost. Many companies struggle to produce low cost mobile devices to dominate cellular phone market, while operators struggle to have a low cost network and base station (BS) to provide low cost services. To provide the low cost communications, following aspects should be considered:

   - Transmission power

     An adequate transmission power is necessary to guarantee a high quality of service (QoS) data transmission. However, the transmission power must be kept as low as possible, owing to battery life problem. The transmission power is crucial for both mobile station (MS) and BS. A high transmission power in BS causes interferences to neighboring cells and limiting network capacity. The inadequate high power transmission can cause a high peak-to-average power ratio (PAPR) problem, which requires inefficient and expensive power amplifier in a transmitter [5]. This increases cost of device which is undesirable for MS. BS also requires an efficient power amplifier that can help operators to provide low cost services. The PAPR reduction technique is one of the topics in this study and will be discussed deeply later. Besides, radiation from the high transmit power can cause health problems [6]. The electromagnetic radiation problem should be taken seriously because nowadays the mobile users are limited to not only adults, but also kids.

   - Complexity

     The complexity of both transmitter and receiver is important since it determines

power consumption, size and cost. To reach the required high data rate, 100 Mbps in 4G system, future devices are expected to be built with many technologies, which requiring unlimited electronic circuits. This leads to production of a high cost devices. The simple device is mandatory for MS, and also important to BS. The applied technologies also cause delay in signal processing. For future mobile communication devices, an expected technology should not only focus on providing a high data rate transmission with small error rate, but a simple and low cost device [7]-[9]. Precoding technique is widely researched because of its ability to provide a good performance without causing complexity in receiver. In our study, we focus on two types of precoding techniques; pre-rake and joint transmission (JT) Techniques.

1.3 CDMA

CDMA is a multiple access technique where different users share the same frequency band at the same time. For more than a dozen years, the CDMA technology roadmap has provided operators with technology-leading performance capabilities and a time-to-market advantage. Thanks to CDMA's forward-and-backward compatible technology upgrades within the 1.25 MHz CDMA radio channel, CDMA operators have benefited from the favorable economics of an evolutionary in-band solution. As a result they have been able to deploy new technologies and value-added services throughout their entire network much faster than their competitors. The main technique of CDMA is spread spectrum technique, which use high rate signature pulses to enhance bandwidth required for higher data rate.

CDMA has been a good interface to support a high data rate services in 3G system. Though, since the CDMA performance is limited by multiple-access interference (MAI), it is predicted that the CDMA system will not be able to maintain users' growth in future mobile communications. Here, OFDM has been developed to provide a high data rate and

can support a network with a high number of users.

The next-generation of mobile communications systems based on CDMA and OFDM, as well as broadcast technologies, will be key enablers of the transition to the next dimension of wireless broadband capabilities and services. In particular, mobile broadband technologies such as HSPA+, LTE, and Mobile WiMAX (802.16m) will support multi-megabit-per-second data delivery to users, carrier-grade VoIP and other real-time and broadband intensive applications. The HSPA+ is based on CDMA system while Mobile WiMAX is based on OFDM system. For LTE, both CDMA-based and OFDMA-based standards are developed. For specific bandwidth-intensive applications such as multicasting and broadcasting, OFDM-based technologies such as digital video broadcasting-handheld (DVB-H), satellite-digital media broadcasting (S-DMB) and terrestrial-digital media broadcasting (T-DBM) have been commercialized since 2006.

For narrowband deployments (up to 5 MHz), CDMA technologies can achieve some of the highest data throughputs possible, while OFDM technologies can offer a simpler implementation within wider radio channels (more than 10 MHz). Here, the CDMA system can provide a high spectral efficiency system compared to that in OFDM system. However, the implementation of rake and joint detection (JD) cause complexity at receiver. Note that the rake receiver and JD are required in CDMA to combat multipath fading and reduce MAI. In this study, we perform a less complexity technology by focusing on pre-rake and JT, where the rake and JD technique are moved to transmitter.

On the other hand, the CDMA system is better than OFDM system in providing a lower PAPR. Note that a low PAPR allows an efficient and cheap power amplifier that is implemented in transmitter side. However, the CDMA has a lower PAPR than that in OFDM only for UL system. This is because, in UL, each user transmits only his data. In DL, CDMA signals may exhibit a PAR problem similar to an OFDM system [11], where the CDMA signals with 256 spreading factor resembles the PAPR of the OFDM signal with the FFT length 256. In this study, we focus on reducing PAPR of CDMA system using CDMA

specific technology, JT in chapter 2.

1.4 TDD

TDD systems have been attracted attention because their ability to provide a low cost and simple devices. Most standards focused on small cell and low power use TDD systems. For 2G systems, digital european cordless telephone (DECT) in Europe and personal handy phone System (PHS) in Japan use time-division multiple access (TDMA) [10]. For 3G systems, TD-CDMA and TD-SCDMA have been standardized as a part of 3GPP project. For the 4G systems, a combination of TDD with multicarrier CDMA is also predicted to support a high data rate and low cost services [12].

1.4.1 TDD and FDD differences

The main difference is that a pair frequency bands is needed for uplink (UL) and downlink (DL) transmission in FDD while UL and DL share the same frequency band in TDD system, as shown in Fig. 1.3. This allows TDD to have asymmetric time slots for data transmission between UL and DL. For example, 4 time slots are used for DL and 2 time slots are used for UL in Fig. 1.3 (b). Since the TDD uses the same frequency for uplink and downlink, the channel is reciprocal for the two links. The channel reciprocity feature can be used to implement some crucial functions such as power control, signal pre-emphasis and signal pre-shaping which can reduce complexity of the devices, resulting in less costly devices. A low complexity can be also realized in TDD, because only one set of electronics functions (oscillator and filter) is required at both MS and BS for both UL and DL.

The differences between FDD and TDD are solely physical layer manifestation, thus invisible to higher layer. Thus, there are no operational differences between the two modes in the system architecture. Table 1.1 shows TDD special features in LTE system. Note that the differences between FDD and TDD are to support various UL/DL allocations in TDD

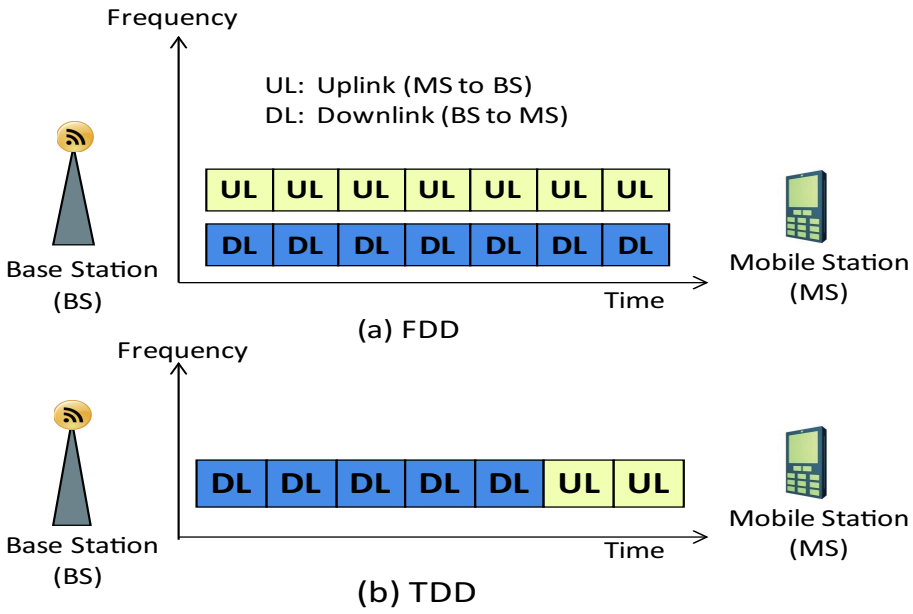

Figure 1.3: TD-CDMA frame structure

time slot and provide coexistence with other TDD systems, i.e. China TD-SCDMA system.

1.4.2 TDD-CDMA: TD-CDMA and TD-SCDMA

For 3G mobile communication system, standardizations are majorly developed by two different organizations; 3GPP and 3GPP2. The 3GPP has developed UMTS and IMT-2000, while 3GPP2 has developed CDMA2000. The UMTS system is then expanded in LTE and already standardized. In LTE by 3GPP, both FDD and TDD modes have been standardized. The TDD is standardized for CDMA systems and OFDM is standardized for OFDM systems.

The 3GPP TDD/ LTE TDD or time-division duplex CDMA (TDD-CDMA) has been divided into two modes: TD-CDMA which is called HCR (high chip rate) CDMA and TD-SCDMA which is called LCR (low chip rate) CDMA. The HCR mode utilizes 5 MHz bandwidth while LCR utilizes 1.6 MHz bandwidth. Both TDD-CDMA standards are described in [13] and in the corresponding standard 3GPP specification [14]. The TD-SCDMA is also standardized by CWTS (Chinese wireless telecommunications standard) organization

Table 1.1: TDD Special Features

Features	**TDD Implemetation**
Frame structure	A special sub-frame for switching from DL to UL and to provide coexistence with TD-SCDMA
Random access	Additional short random access format available in special sub-frame, multiple random access channels in a sub-frame
Scheduling	Multi-sub-frames scheduling for uplink
ACK/NACK	Bundling of acknowledgements or multiple acknowledgements on uplink control channel
HARQ process number	Variable number of HARQ processes depending on the UL/DL allocation

and has been implemented in China since 2008.

The key features from a physical layer point of view are given in Table 1.2 [13]. Spreading codes using in both TD-CDMA and TD-SCDMA are constructed from user specific orthogonal variable spreading factor (OVSF) codes, complex channelization codes and cell-specific scrambling multiplier (CSSM). A table in [15] lists 128 different scramble codes which consist of 16 chips. This means that TD-CDMA has short codes for a spreading factor = 16 since the symbol length is equal to the spreading code periodicity. In this thesis, short codes with spreading codes 16 is assumed for TD-SCDMA and spreading codes 64 is assumed for TD-CDMA.

Table 1.2 also shows differences between TD-CDMA and TD-SCDMA. For TD-SCDMA system, uplink and downlink are synchronized. Two time slots are used for the synchronization. Uplink synchronization is achieved by transmission timing adjustment feedback from BS to MS and by additional synchronization symbol in each time slot.

Frame and Slot Structure

For LTE system, there are two types of time slot frames; *Type* 1 is used for FDD system and *Type* 2 for TDD system [4][16].

Table 1.2: Physical layer parameters of TDD-CDMA systems

	TD-CDMA	**TD-SCDMA**
Chip rate	3.84 Mcps	1.28 Mcps
Carrier Spacing	5 MHz	1.6 MHz
Modulation	QPSK, 16-QAM	QPSK, 8-PSK, 16-QAM
Spreading code	0VSF + CCSM	
Spreading factor	1, 2, 4, 8, 16, 32, 64	
Pulse shaping	Root raised cosine, r = 0.22	
Interleaving	10, 20, 40, 80 ms	
Coding	Convolutional (rate = 1/2, 1/3), no coding	
Radio frame length	10 ms	
Time slots per radio frame	15	14 + 2 sync-frame
Slot length	2560 chips (667 μs)	864 chips (675 μs)

Figure 1.4 shows frame structure of *Type* 2 [17]. Each radio frame contains ten sub-frames with length 1 ms each. Sub-frame 0 and 5 contain synchronization signal and broadcast information necessary for the MS to perform synchronization and obtain system information for downlink sub-frames. Sub-frame 1 is a special sub-frame that is also known as switching point between downlink and uplink. The special sub-frame contains three fields; Downlink pilot time slot (DwPTS), guard period (GP), and uplink pilot time slot (UpPTS). The GP includes the sum of switching times from DL to UL and UL to DL. The switching from UL and DL can be achieved by appropriate timing advance at MS. Two switching point periodicities are supported for TDD-CDMA which are 5 ms and 10 ms. For 5 ms periodicity, two switching points exist at sub-frame 1 and sub-frame 6. For the 10 ms periodicity, switching point is only at sub-frame 1 and sub-frame 6 is a downlink sub-frame. Table 1.3 shows UL and DL configuration defined by 3GPP for TDD systems.

Figure 1.5 shows a frame structure of TD-CDMA system. Each radio frame has a duration of 10 ms and is subdivided into 15 time slots (TS) of $2560 \times T_c$ duration each. A time slot corresponds to 2560 chips. Note that one sub-frame in Fig. 1.4 contains 2 time slots of Fig. 1.5. From 2560 chips, 2 $\times$1104 chips are assigned for data transmission, 256 chips for

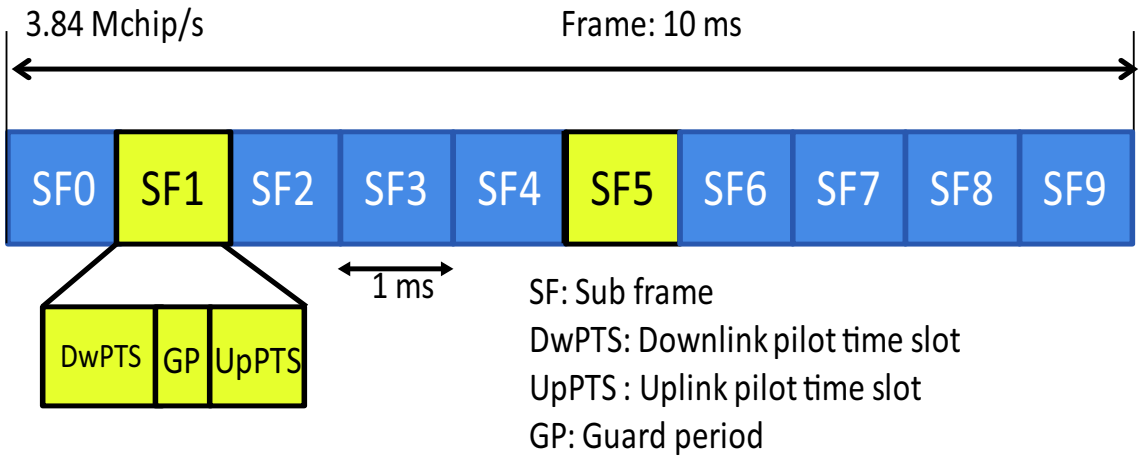

Figure 1.4: Frame structure for *Type* 2 of TD-CDMA system

Table 1.3: Uplink-Downlink allocation (DL: Downlink, UL: Uplink, S: Special)

UL/DL Configuration	**Period (ms)**	**Sub-frame**									
		0	1	2	3	4	5	6	7	8	9
0	5	DL	S	UL	UL	UL	DL	S	UL	UL	UL
1		DL	S	UL	UL	DL	DL	S	UL	UL	DL
2		DL	S	UL	DL	DL	DL	S	UL	DL	DL
3	10	DL	S	UL	UL	UL	DL	DL	DL	DL	DL
4		DL	S	UL	UL	DL	DL	DL	DL	DL	DL
5		DL	S	UL	DL	DL	DL	DL	DL	DL	DL
6	5	DL	S	UL	UL	UL	DL	S	UL	UL	DL

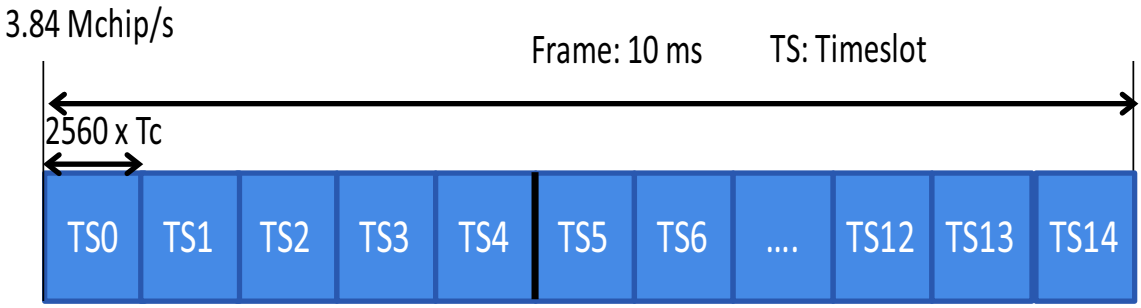

Figure 1.5: TD-CDMA frame structure

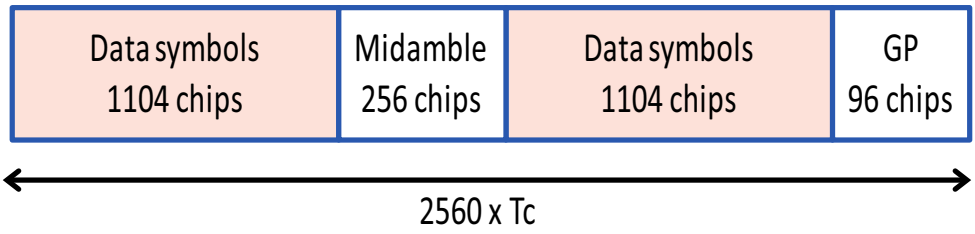

Figure 1.6: The structure of data time slot of TD-CDMA

midamble and 96 chips for GP, as shown in Fig. 1.6

Figure 1.7 shows frame structure of TD-SCDMA system. Each radio frame with 5ms length contains ten time slots with $864 \times T_c$; Seven time slots can be used for data transmission while three time slots is used for switching from UL to DL and DL to UL. Similar with TD-CDMA system the time slot for switching point contains three fields; DwPTS, GP, and UpPTS. From 864 chips, 2×352 chips are assigned for data transmission, 144 chips for midamble and 16 chips for GP, as shown in Fig. 1.8.

As discussed above, one of the TDD particular features is coexistence between different TDD systems. Figure 1.10 shows switching point alignment between TD-CDMA and TD-SCDMA system.

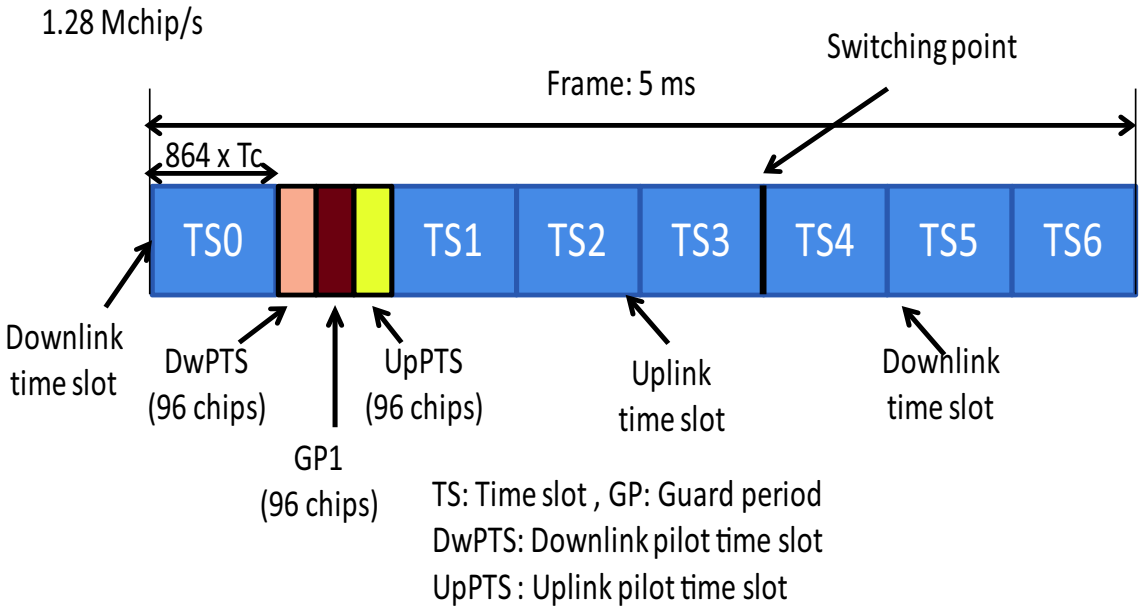

Figure 1.7: TD-SCDMA frame structure

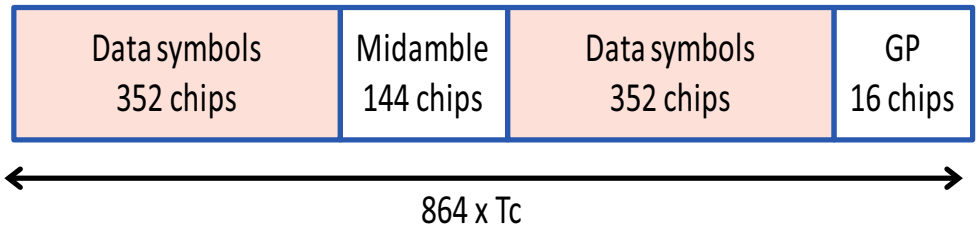

Figure 1.8: The structure of data time slot of TD-SCDMA

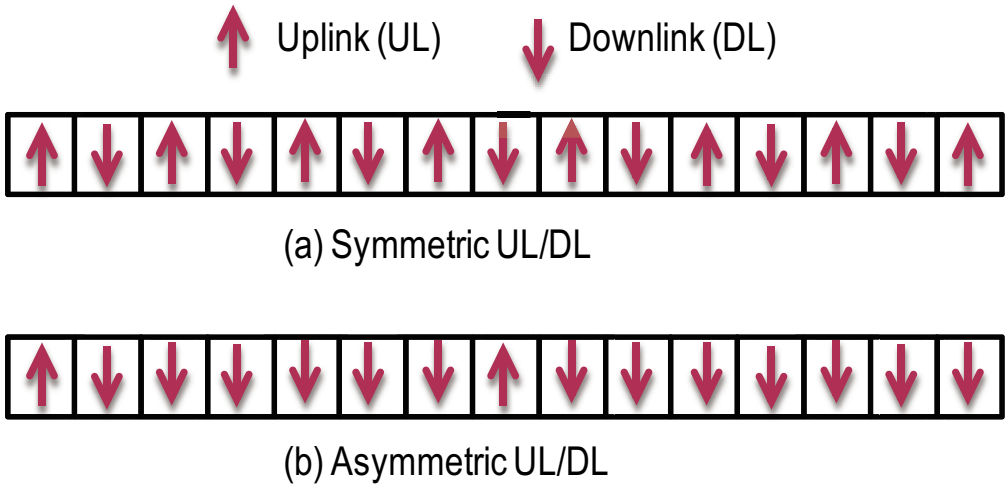

Figure 1.9: Frame structure with different UL/DL configuration, (a) symmetric (b) asymmetric

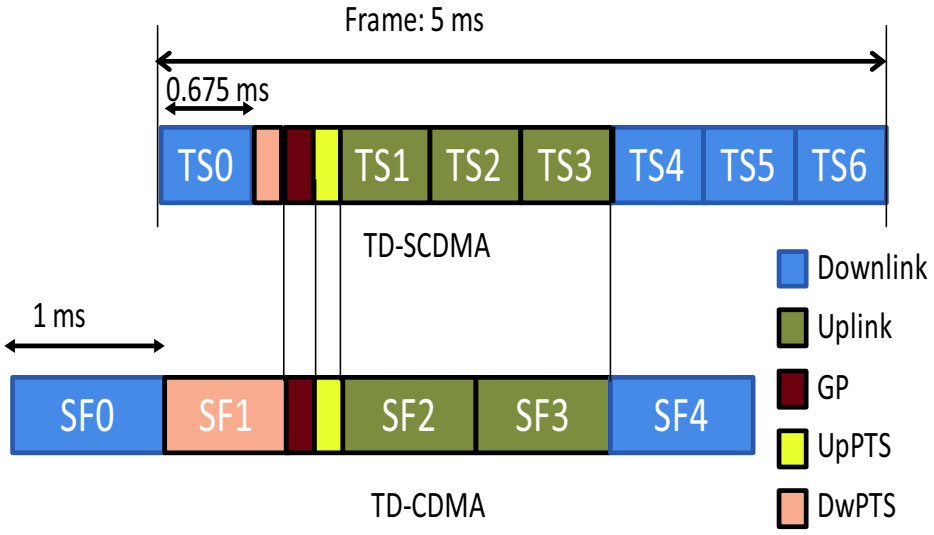

Figure 1.10: Coexistence between TD-CDMA and TD-SCDMA

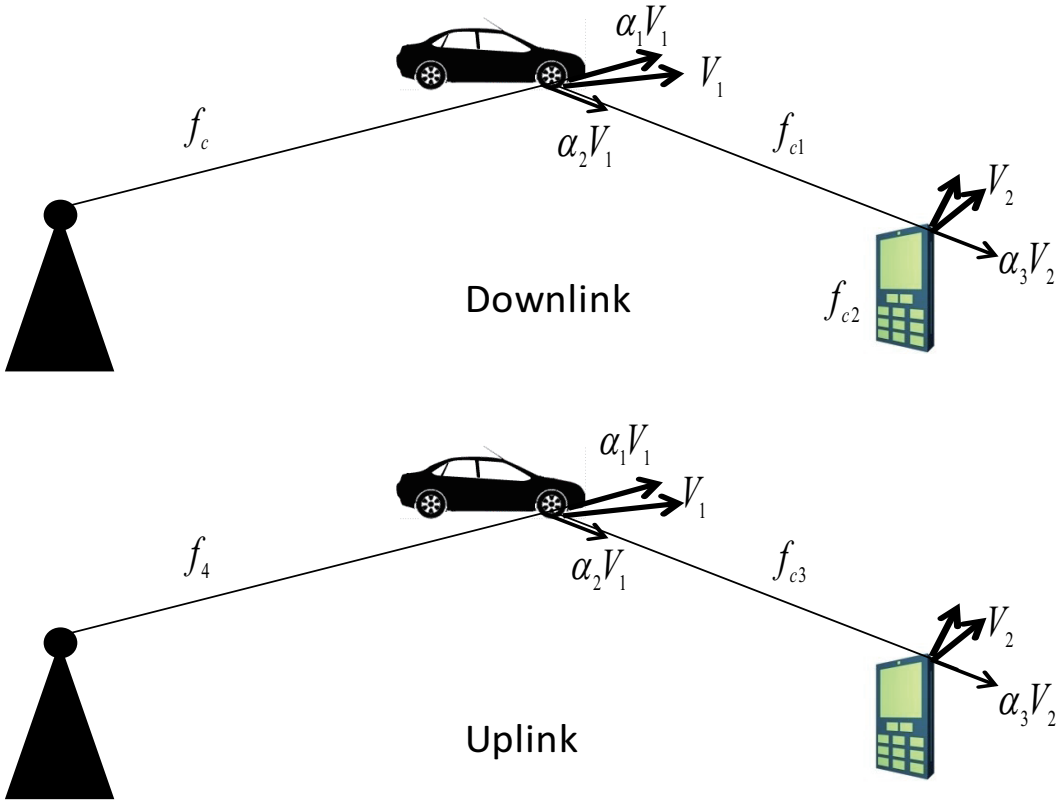

Figure 1.11: Fading reciprocity with a moving reflector

1.4.3 Channel Reciprocity

In TDD system, the same frequency is used in UL and DL. Thus, the channel condition of UL and DL are same. This feature is called channel reciprocity that can be used to estimate DL channel from received UL channel information. As shown in Fig. 1.8, each TDD-slot contains midamble with pilot symbols for channel estimation. In the UL, the channel is estimated using the pilot symbols for UL signal detection.

Mobile communication channels are characterized by multipath signal arrival and fading. The received signal is the sum of many reflections of the transmitted signal from building, cars, and the ground. Each received signal component has a different carrier phase shift, signal strength and propagation delay. For transmitted signal $s(t)$, the received signal $r(t)$

can be defined as:

$$r(t) = \sum_{k=1}^{K} b_k s(t - \delta_k) e^{j\theta_k} + n(t), \tag{1.1}$$

where b_k is the signal gain factor, δ_k is the propagation delay, and θ_k is the carrier phase shift for path k. The components in (1.1) are the same for UL and DL, except for noise part. Since the TDD uses the same antennas for transmission and reception, the same number of paths can be assumed in UL and DL. This results to the same fading characteristics between UL and DL if the time offset between UL and DL is small.

Fig. 1.11 shows the shift in center frequency due to movement of MS and any possible signal's reflector. The Doppler shifts for UL and DL are identical for TDD communication channel. Fig. 1.11 also shows an example of fading reciprocity with a moving reflector. The f_c represents DL carrier frequency and V_1 represents the speed of moving reflector. The new frequency f_{c1} between moving reflector and MS can be written as:

$$f_{c1} = f_c + \frac{(\alpha_2 - \alpha_1) V_1 f_c}{c}, \tag{1.2}$$

where $\alpha_1 V_1$ is the component of reflector speed in the same direction of transmitted signal, and $\alpha_2 V_2$ is the component of reflected direction. The received signal at the moving MS with a carrier frequency f_{c2} can be written as

$$f_{c2} = f_{c1} + \frac{\alpha_3 V_2}{c}, \tag{1.3}$$

where $\alpha_3 V_2$ is the speed component in the same direction as received signal. Using (1.2), f_{c2} can be rewritten as

$$f_{c2} = f_c + \frac{(\alpha_2 - \alpha_1) V_1 f_c}{c} + \frac{\alpha_3 V_2 f_c}{c} + \frac{\alpha_3 V_2 (\alpha_2 - \alpha_1) V_1 f_c}{c^2}. \tag{1.4}$$

For UL transmission, the signal transmitted from MS has a Doppler shifted carrier frequency, defined as:

$$f_{c3} = f_{c1} + \frac{\alpha_3 V_2}{c}. \tag{1.5}$$

The reflected signal from moving reflector also has its own carrier frequency, f_4, written as

$$f_{c4} = f_{c3} + \frac{(\alpha_2 - \alpha_1) V_1 f_{c3}}{c}. \tag{1.6}$$

Using (1.5), (1.6) can be rewritten as

$$f_{c4} = f_c + \frac{(\alpha_2 - \alpha_1) V_1 f_c}{c} + \frac{\alpha_3 V_2 f_c}{c} + \frac{\alpha_3 V_2 (\alpha_2 - \alpha_1) V_1 f_c}{c^2}. \tag{1.7}$$

We can see that (1.4) is equal to (1.7), shows that the Doppler shift for UL and DL for TDD system is equal. For the case of stationery reflector, both α_1 and α_2 are zero, which yields

$$f_{c2} = f_{c4} = f_c + \frac{\alpha_3 V_2 f_c}{c}. \tag{1.8}$$

However, the estimated channel is then used for DL communications, under assumption that the time offset between UL and DL is sufficiently small. Therefore, it is desirable to minimize the distance between UL channel estimation and DL channel estimation.

In TDD, UL and DL slots can be changed depending on requirements. This is important in wireless communications because applications such as mobile TV and mobile internet require more slots for DL transmission. However, if more time slots are assigned to the DL, the time span between UL channel measurement and the end of DL transmission increases. In this case, the estimated UL channel is inadequate for DL because of the time-varying characteristic of the wireless channel.

Table 1.4: Time estimation (T_{est}) from UL channel estimation to the end of the DL transmission

Standard	$T_{\text{slot}}(\mu\text{s})$	$\beta_{\text{DL/UL}}$	T_{est}(ms)
TDD-CDMA	667	1	1
TDD-CDMA	667	14	9.67
TD-SCDMA	675	6	4.39

Table 1.5: Doppler frequency, speed and coherence time for $f_c = 2$ GHz

Speed km/h	Doppler frequency $f_{\text{D,max}}$ (Hz)	T_{coh} (ms)
3	5.6	32
10	18.5	9.7
50	92.6	1.9
120	222.2	0.8

The time span between channel estimation in UL and DL transmission is defined as

$$T_{\text{est}} = T_{\text{slot}} \left(\frac{1}{2} + \beta_{\text{DL/UL}} \right), \tag{1.9}$$

where $\beta_{\text{DL/UL}}$ is the downlink-uplink ratio and T_{slot} is the slot duration. Figure 1.9 shows TDD frames with different UL and DL configuration while Table 1.4 shows example of T_{est}.

The coherence time indicates the time duration over which the channel impulse response is essentially invariant. The time coherence is defined as [19]

$$T_{\text{coh}} = \frac{9}{16\pi f_{\text{D,max}}} = \frac{9\lambda}{16\pi v} \tag{1.10}$$

where λ represents wave length and $f_{\text{D,max}}$ represents maximum Doppler frequency.

To find a suitability of using asymmetric TDD, i.e. $\beta_{\text{DL/UL}} > 1$, we summarize the relation between mobile speed and time coherence in Table 1.5. Note that the values in Table 1.5 are calculated for $f_c = 2$ GHz. The wave length λ can be calculated using $\lambda = \frac{c}{f_c} = 0.15$

cm with c represents the light speed. The maximum Doppler frequency can be defined as $f_{\mathrm{D,max}} = \frac{v}{\lambda}$. From T_{est} in Table 1.4 and T_{coh} in Table 1.5, we can conclude that a high $\beta_{\mathrm{DL/UL}}$ is suitable for pedestrian speed. For 50 km/h speed and above, only a symmetric DL/UL traffic, i.e. $\beta_{\mathrm{DL/UL}} = 1$ can guarantee a reliable UL channel to be used for DL. For a high speed case, the channel reciprocity can be used if an advanced channel prediction algorithms is employed.

1.4.4 Precoding in TDD

Rake and Pre-rake

The rake receiver has been proposed to combat fading [18][19]. In rake combining process, the received signal is firstly passed through the matched filter before processed in the rake receiver.

The rake combining technique is a form of maximum ratio combining (MRC) method, proposed to combat multipath fading. Figure 1.12 shows a rake combining receiver, derived in [20]. The optimum weighing factor a_k in Fig. 1.12 is derived to be proportional to the individual path strengths b_k; $a_k \propto b_k^*$, where b_k^* is the complex conjugate of the estimated path strength. Symbol k represents number of paths with $k = 1, ..., K$. The paths of the signals are summed with a uniform phase to maximize the summed signal power and minimize the summed noise power. Figure 1.13 shows the time domain response of the product of the channel impulse response and rake combiner. The desired output is at time $t = (K-1)T_c$, which is the main peak of Fig. 1.13 (c) and proportional to $\sum_{k=0}^{K-1} a_k b_k$ [20]. The rake combiner uses transversal filter and a channel estimator that requires significant signal processing and power consumption which increases portable MS size.

In cellular mobile communications, it is desirable to reduce the complexity, size and cost of MS as minimum as possible, and concentrate on all the complexities at the BS. These can be achieved by using pre-rake combining method which was first proposed in [21]. The

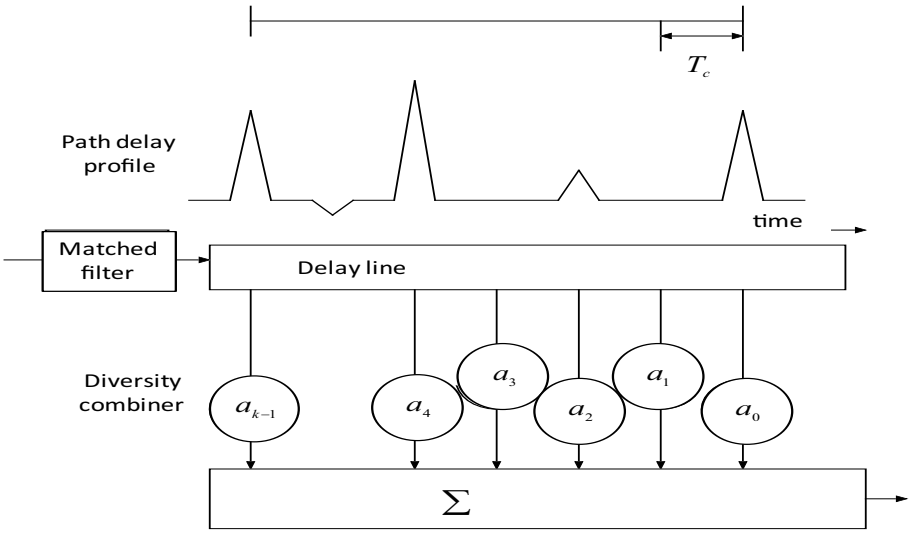

Figure 1.12: Diversity combining receiver

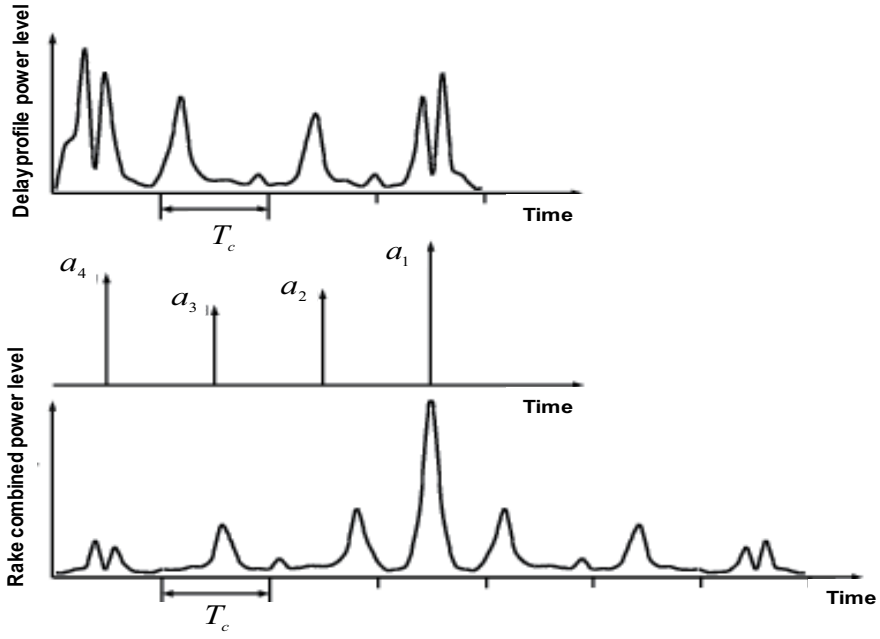

Figure 1.13: Concept of rake combiner process

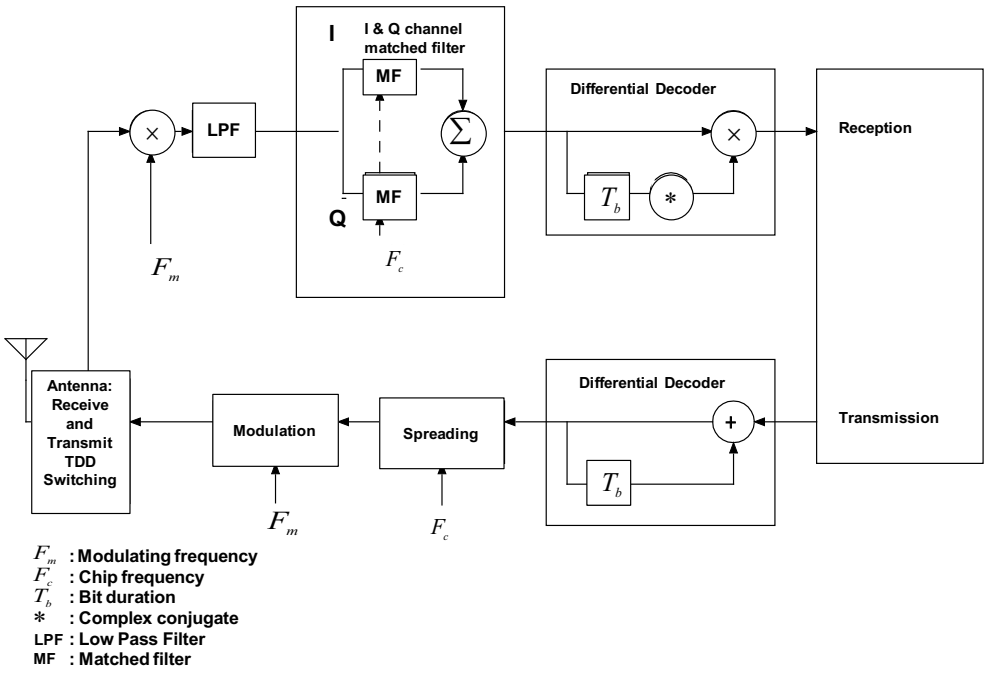

Figure 1.14: The block diagram for the MS of pre-rake system in TDD transmission

technique is based on precoding of the transmitted signal, using knowledge of the channel estimation response before transmission. The block diagrams of the MS and BS of a pre-rake system are shown in Fig. 1.14 and Fig. 1.15, respectively. We can see that in pre-rake system, the rake combining is done in transmitter side of BS. Also, only one antenna is used for transmission and reception at BS and MS. Thus, a low complexity device is allowed in TDD system compared to that in FDD system.

In this technique, the transmitter (i.e. BS) needs to estimate the future channel impulse response by using present channel impulse response measured from the received signal in BS. Combining process and block diagram of rake and pre-rake are shown in Fig. 1.16 and Fig. 1.17, respectively.

The conventional transmitted signal without pre-rake for user k with binary phase-shift keying (BPSK) modulation is given by

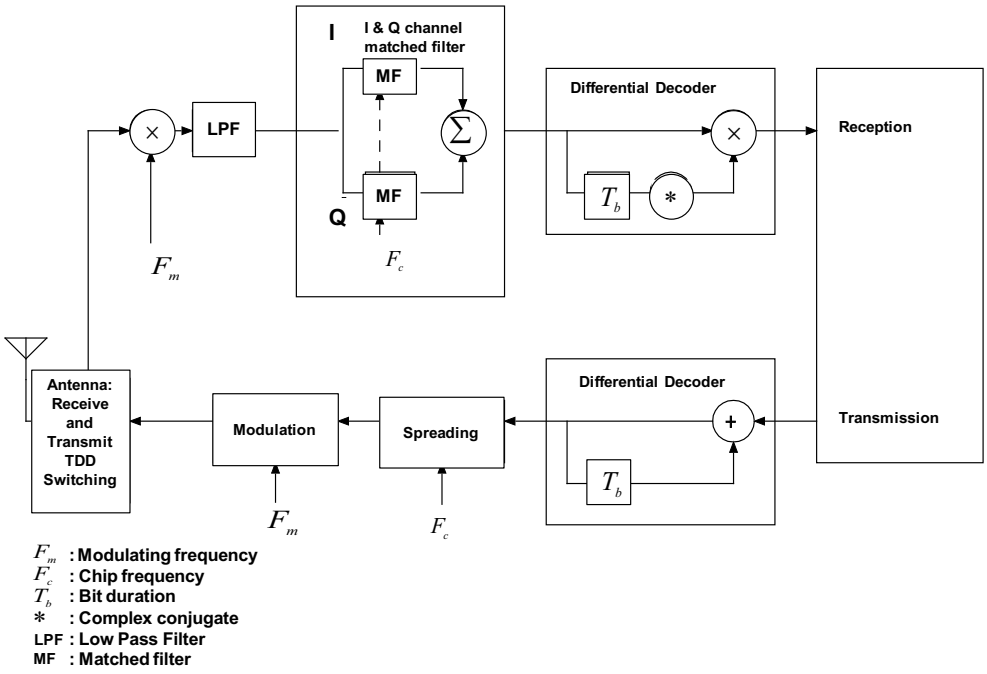

Figure 1.15: The block diagram for the BS of pre-rake system in TDD transmission

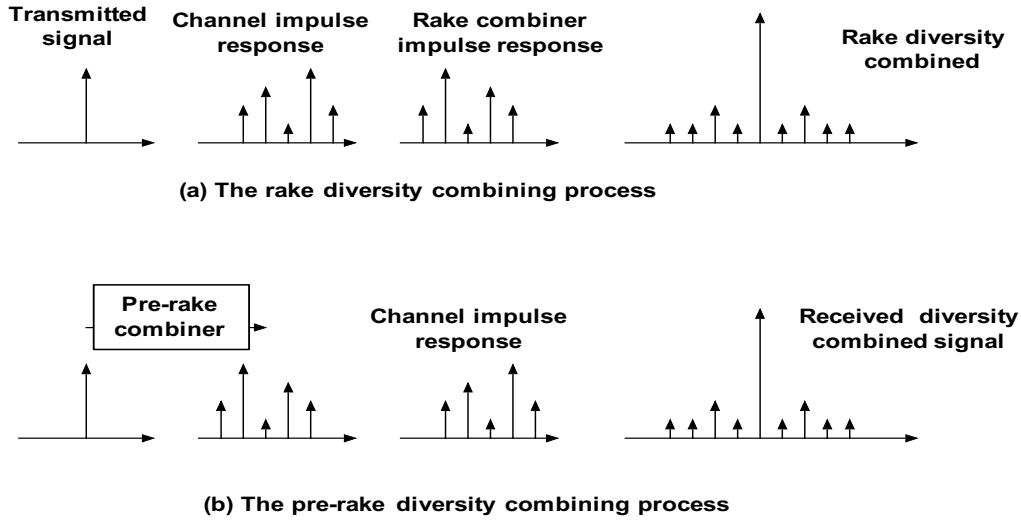

Figure 1.16: Rake and pre-rake combining process

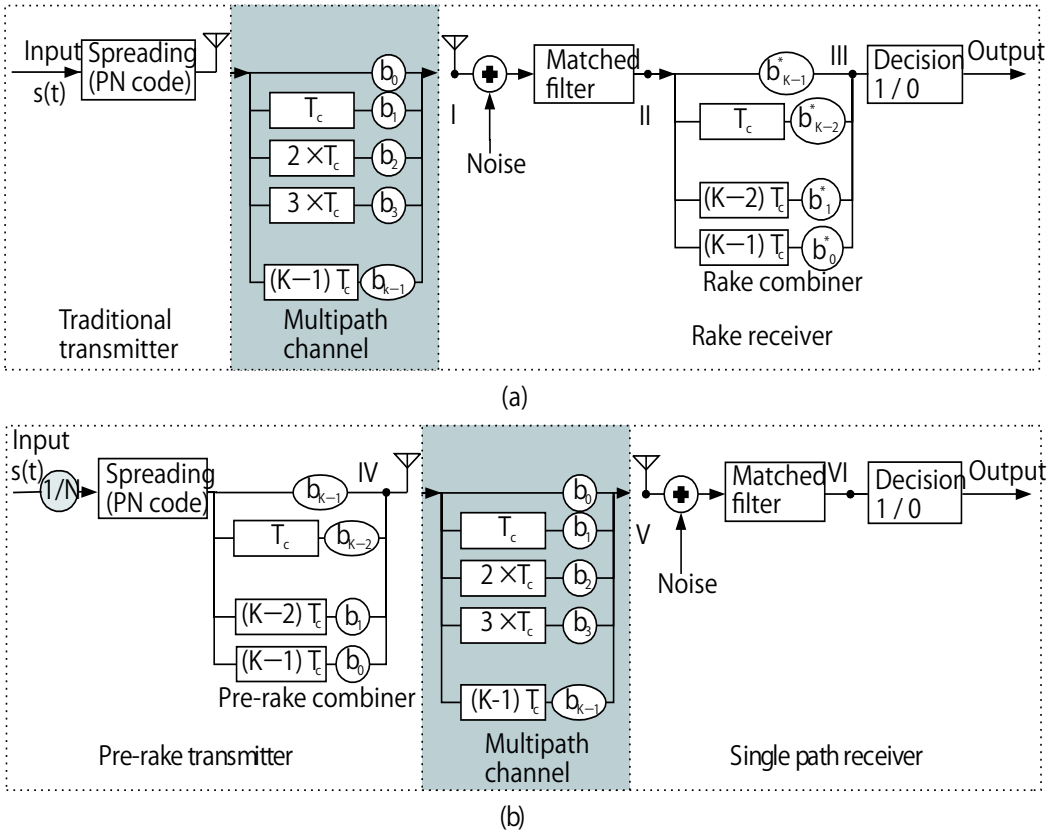

Figure 1.17: Block diagram of (a) rake and (b) pre-rake combining

$$s_k(t) = \sqrt{2P} b_k(t) a_k(t) \exp(j\omega t) \tag{1.11}$$

where P is transmit power, ω is the carrier frequency, $b_k(t)$ is the data stream for user k with ± 1 value, consisting of a train of i.i.d. data bits with duration T which take the values of ± 1 with equal probability. The current bit is denoted by b_k^0 while next or previous bit is denoted by adding or subtracting the superscript by one. $a_k(t)$ is the pseudo-random noise (PN) code of user k with ± 1 chip of duration T_c and code length $N = T/T_c$. The bit and chip waveforms are rectangular. For the pre-rake system with perfect channel estimation, the transmitted signal for BPSK modulation is given by

$$s_k(t) = \sqrt{\frac{2P}{U_k}} \sum_{l=0}^{L-1} \beta_{k,L-l-1} b_k[t - lT_c] a_k[t - lT_c] \exp[j\omega(t - lT_c) - j\gamma_{k,L-l-1}], \quad (1.12)$$

where U_k is a normalizing factor to keep the instantaneous transmitted power constant, and given by

$$U_k = \sum_{n=0}^{L-1} \beta_{k,n}^2. \quad (1.13)$$

Multiuser Detection and Multiuser Transmission

Even the multiuser detection is not the main topic in this thesis, it is closely related to the main idea of this thesis, known as multiuser transmission. A several of multiuser detection techniques have been proposed to reduce MAI [22]-[25].

The motivation of multiuser detection comes from inter-symbol interference (ISI) and MAI existence in whitening matched filter [25]. The whitening matched filter (WMF) consists of prewhitening filter and a matched filter, simply illustrated in Fig. 1.18. Assuming that $\mathbf{d}$ is a data vector and $\mathbf{A}$ is a modulator matrix consisting channel impulse responses and spreading sequences [25], the received signal $\mathbf{e}$ can be expressed as:

$$\mathbf{e} = \mathbf{A}\mathbf{d}. \quad (1.14)$$

From (1.14), the detected data $\hat{\mathbf{d}}$ after WMF process can be written as:

$$\begin{aligned} \hat{\mathbf{d}} &= \mathbf{A}^H\mathbf{A}\mathbf{d} + \mathbf{A}^H\mathbf{n} \\ &= \mathrm{diag}(\mathbf{A}^H\mathbf{A})\mathbf{d} + \overline{\mathrm{diag}}(\mathbf{A}^H\mathbf{A})\mathbf{d} + \mathbf{A}^H\mathbf{n} \end{aligned} \quad (1.15)$$

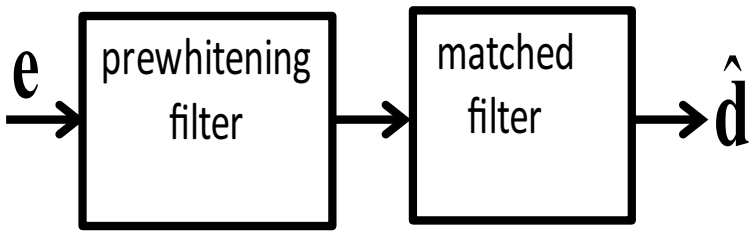

Figure 1.18: Structure of whitening matched filter

where the first term represents desired signal, second term represents ISI and MAI and third term represents noise. The diag($\mathbf{X}$) represents the diagonal elements of the matrix $\mathbf{X}$ and $\overline{\text{diag}} = \mathbf{X} - \text{diag}(\mathbf{X})$ represents a matrix with zero diagonal elements containing all elements except for the diagonal elements of $\mathbf{X}$. The $\mathbf{X}^H$ represents conjugate transpose of matrix $\mathbf{X}$. From (1.15), we can see that the estimated data that passed through the WMF consists of ISI and MAI. That means that the WMF is only suitable for a case that ISI and MAI component are negligible like a single user system and a system that having large spreading factors, i.e. for a case that spreading factor is larger than the number of paths. Thus, multiuser detectors have been studied to eliminate both ISI and MAI.

The following linear data detector techniques are the simplest technique of the multiuser detection:

- **Zero-Forcing Block Linear Equalizer**

  The zero forcing block linear equalizer (ZF-BLE) is the simplest multiuser detection technique with a simple calculation. The ZF-BLE technique is also known as JD technique, which is related to main topic of this study, JT.

  Figure 1.19 shows a structure of ZF-BLE, consists of WMF, whitening filter and interference eliminator. The data detected after ZF-BLE can be written as:

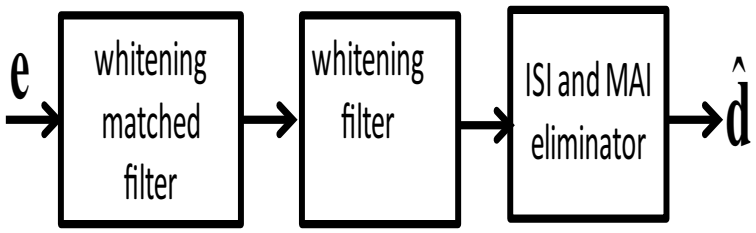

Figure 1.19: Structure of zero forcing block linear equalizer

$$\begin{aligned} \hat{\mathbf{d}} &= (\mathbf{A}^H\mathbf{A})^{-1}\mathbf{A}^H\mathbf{e} \\ &= \mathbf{d} + (\mathbf{A}^H\mathbf{A})^{-1}\mathbf{A}^H\mathbf{n}. \end{aligned} \tag{1.16}$$

The first term represents the desired detected data while the second term represents the noise term. We can see that the ISI and MAI are perfectly eliminated when using the ZF-BLE. The technique is stated as zero forcing since it totally eliminates the MAI and ISI. Here, the ZF-BLE requires the nonsingular matrix ($\mathbf{A}^H\mathbf{A}$), which sometimes cannot be guaranteed. However, the ZF-BLE only provides a good performance under small noise case. This can be seen in second terms of (1.16), where the noise cannot be eliminated.

- **Minimum Mean-Square-Error Block Linear Equalizer**

  The minimum mean-square-error block linear equalizer (MMSE-BLE) is an extension of ZF-BLE, with additional function of Wiener estimator. The structure of MMSE-BLE is shown in Fig. 1.20. The MMSE can reduce ZF-BLE performance degradation for a large noise case. The estimated data of MMSE-ZFE can be written as:

$$\begin{aligned} \hat{\mathbf{d}} &= \mathrm{diag}\mathbf{W}_0.\mathbf{d} + \overline{\mathrm{diag}}\mathbf{W}_0.\mathbf{d} \\ &\quad +(\mathbf{A}^H\mathbf{A} + \alpha.\mathbf{I})^{-1}\mathbf{A}^H\mathbf{n}, \end{aligned} \tag{1.17}$$

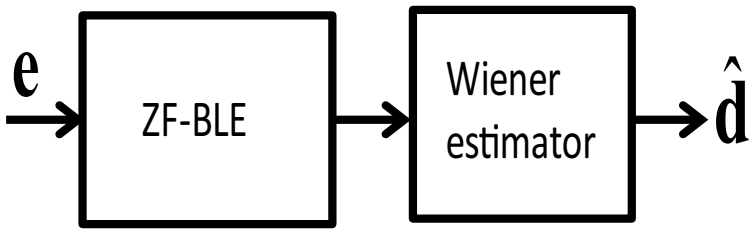

Figure 1.20: Structure of minimum mean-square-error block linear equalizer

where $\mathbf{W}_0$ represents a Wiener estimator and α represents signal-to-noise power-ratio (SNR). The $\mathbf{I}$ represents identity matrix with ones on the main diagonal and zeros elsewhere. The first term is a desired symbol, the second term is MAI and ISI, and the third term is noise. By the factor $\mathbf{W}_0$ the desired signal and the ISI, MAI, noise are decorrelated. From (1.17), it can be seen that for $\alpha^2 \rightarrow 0$ approaches ZFE-BLE of (1.16) and $\alpha^2 \rightarrow \infty$ approaches WMF of (1.15). Here, the $\alpha^2 \rightarrow 0$ means that the signal has a large noise and $\rightarrow \infty$ means that the signal contains only small noise.

Multiuser transmission has the same concept with multiuser detection. In multiuser transmission, the multiuser detection is moved from receiver to transmitter side. The multiuser transmission can be applied because for the system that has priori channel knowledge in transmitter side. This can be done only in TDD system with channel reciprocity feature.

The zero forcing multiuser transmission has been proposed as transmitter precoding in [26][27], where the transmitter structure is predefined by a linear symbol pre-distortion followed by spreader without a pre-rake. In 3GPP standardization, the zero-forcing multiuser transmission (ZF MuT) is known as in Joint Predistortion, published by Bosch [28]. The ZF MuT is then discussed in detail using different name, JT which is inverse of multiuser detection technique known as JD. The studies using JT are published in [29][30]. In this study, we focus on JT technique, which is described in detail in chapter 3. We decided to focus our study on JT because of the capability to reduce complexity of both receiver and transmitter, since the implementation of the ZF-BLE does not require complicated function.

Table 1.6: Difference between multiuser detection and multiuser transmission

	Multiuser detection Receiver processing	**Multiuser transmission Transmitter processing**
Suitable link	Uplink	Downlink
Channel estimation	Pilot symbol	TDD channel reciprocity
Received sequence	Known	Unknown
Transmit sequence	Unknown	Known

Table 1.7: Detectors for multiuser detection and multiuser transmission

Detector	**Multiuser Detection**	**Multiuser Transmission**
Matched filter maximize SNR	Rake	Pre-rake
Linear ZF Eliminate ISI and MAI	Joint Detection	Joint Transmission
Linear MMSE Minimize MSE	Wiener filter	Wiener filter

Table 1.6 summarizes the different between multiuser detection and multiuser transmission while Table 1.7 represents detectors in both multiuser detection and multiuser transmission with their advantages. In this study, we focus on impact of channel estimation error in pre-rake and PAPR reduction using JT technique.

Both pre-rake and JT, which originated from rake and JD, are the CDMA specific technologies. In our study, we only focus on TDD-CDMA system using TD-CDMA parameter for pre-rake and TD-SCDMA for JT. For pre-rake we investigate impact of channel estimation error while for JT, we investigate PAPR of JT-TDD-CDMA and propose a PAPR reduction technique using JT. However, the pre-rake combination can be used in OFDM system in each carrier, under assumption that the impulse responses of a channel are known at transmitter side and constant during one OFDM packet for perfect channel estimation case. The implementation of pre-rake can increase multipath diversity effect. On the other hand, it had been proved that implementation of JT can reduce transmit power [31], as same as in

CDMA system. The JT changes transmit power, thus affects PAPR of OFDM transmission. In CDMA, JT can reduce PAPR in single path case, while multipath in JT can cause a high PAPR. The JT can reduce PAPR of OFDM system since the OFDM system can mitigate multipath channel by having a longer symbol period and using cyclic prefix function.

1.5 Motivation of This Study

It has been discussed in section 1.2 that the future wireless communication requires spectral efficiency, a high data rate, a high capacity, coverage expansion and low cost communications. It also has been discussed in section 1.1 that TDD system provides a high spectral efficiency compared with FDD system, because the TDD only requires a frequency band for both uplink and downlink transmission. The TDD system can also be considered as a high spectral efficiency system, because it allows asymmetric transmission between uplink and downlink. In future, data traffic growth is estimated owing to a new application, social networking website such as twitter and face book. The usages of the social websites require more downlink data transmission. This can be fulfilled by using TDD asymmetric feature.

Furthermore, the TDD system also has potential to provide a low cost device using its main feature, channel reciprocity. The concept of channel reciprocity has been discussed in section 1.4.3, where the estimated uplink channel can be used for downlink transmission for a small time offset between uplink and downlink. The channel reciprocity allows adaptive operation [13][32] which can reduce cost of devices.

Another technology that can be done by exploiting the channel reciprocity feature is precoding technique, which has been discussed in section 1.4.4. In this study, we focus on precoding techniques; pre-rake and JT owing to the following reasons:

- Capability to provide a low cost device.
- Provide interference cancellation without causing significant processing delay, i.e. simple algorithm.

However, the pre-rake can provide a good BER as in rake only for perfect channel estimation case. In practice, the channel measurements are corrupted owing to measurement errors and the presence of interferences and noise.

On the other hand, it has been proved that the JT technique can mitigate interference without causing complexity in BS for downlink system. However, the implementation of JT causes complexity to small and low cost BS (e.g. relay station). In 4G system, it has been predicted that a large number of relay stations will be implemented to combat coverage problem. Thus, we propose a JT technique with low complexity feature. One of the methods to reduce complexity is to use an efficient power amplifier, which requires a low PAPR. The process of JT before transmission affects PAPR owing to the change of transmission signal compared to the transmission signal in JD.

Regarding to the fact that the channel cannot be perfectly estimated and the fact that it is important to reduce complexity in both MS and relay station, we focus our study in following aspects

- Effect of channel estimation error in pre-rake system using numerical analysis.
- PAPR reduction using modified JT method with BER numerical analysis.

1.6 Organization and Overview of each Chapter

This thesis is divided into four chapters and summarized in Fig. 1.23.

Overview of chapter 2: This chapter discusses our performance analysis of pre-rake in TDD-CDMA under imperfect channel estimation. The overview of chapter 2 is summarized in Fig. 1.21. The background of the research is firstly discussed in section 2.1. The pre-rake is proposed to mitigate multipath fading effects without causing complexity at MS by exploiting TDD reciprocity feature. However, the estimated uplink channel cannot be used as a perfect channel for a large time offset between UL and DL. This causes channel estimation error which is not considered in most of the previous researches. We perform numerical analysis

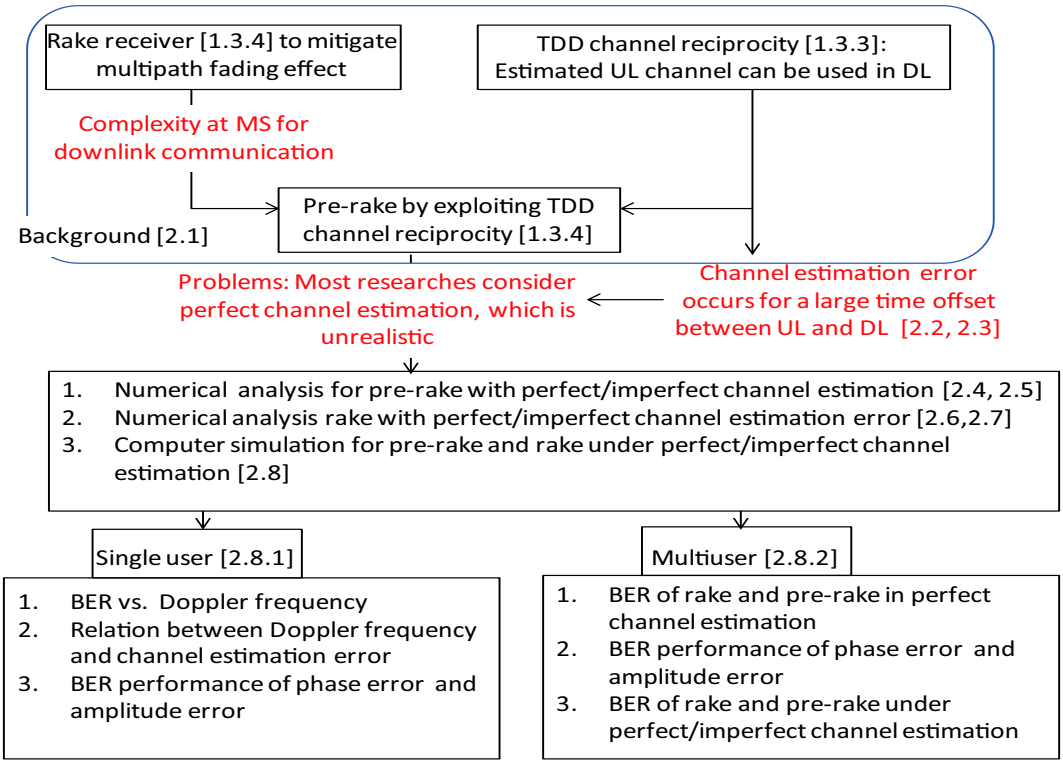

Figure 1.21: Overview of chapter 2

of pre-rake TDD-CDMA under imperfect channel. The multipath channel model and the channel estimation error model is shown in and section 2.3, respectively. We calculate the probability of error for perfect channel and imperfect channel of pre-rake TDD-CDMA system in section 2.4 and section 2.5, respectively. For the sake of comparison we also calculate the probability of error of rake system under perfect channel estimation and imperfect channel estimation in section 2.6 and section 2.7, respectively. Probability of error calculated in sections 2.4-2.5 is compared with computer simulation results in section 2.8.Performance comparison between rake and pre-rake under imperfect channel estimation is also presented in section 2.8. Chapter 2 is concluded in section 2.9. We found that the imperfect channel estimation error cause BER degradation in pre-rake system. We also found that the effect of channel estimation error is larger in pre-rake than in rake system.

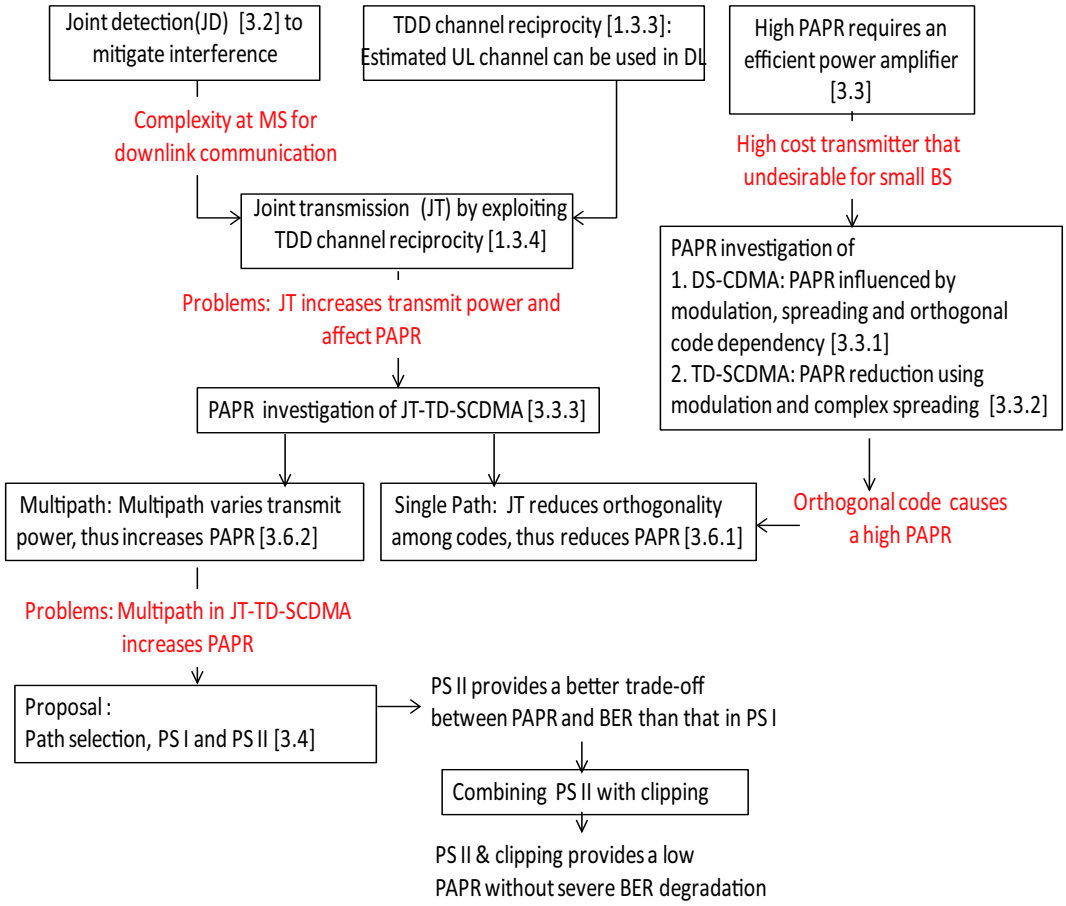

Figure 1.22: Overview of chapter 3

Overview of chapter 3: In chapter 3, our proposal of PAPR reduction technique in JT TD-SCDMA is presented. The background of the research is firstly discussed in section 3.1. PAPR problem must be kept as low as possible to allow low cost power amplifier in transmitter side. The PAPR problem should be considered in downlink transmission because implementation of the small BS is predicted in the future. On the other hand, JT technique is used to mitigate interference instead of JD, to avoid complexity at MS. The basic concept and data detection method of conventional JD and JT are discussed in section 3.2. Section 3.3 discusses PAPR concept with calculation and concept of PAPR for DS-CDMA, TD-SCDMA and JT-TD-SCDMA are described in section 3.3.1, section 3.3.2 and section

3.3.3, respectively. The PAPR of DS-CDMA is influenced by modulation techniques, spreading techniques and orthogonal code dependency. For conventional TD-SCDMA, PAPR is reduced using QPSK modulation and complex spreading. This means that the TD-SCDMA still has a possibility to have a high PAPR owing to orthogonal code dependency. Section 3.3.3 describes PAPR of JT-TD-SCDMA system which is then divided into single path and multipath, to clarify the different behavior of PAPR in single and multipath. Here, the PAPR reduction for single path JT-TD-SCDMA is explained. Also, the reason of a high PAPR in multipath JT-TD-SCDMA is also discussed. The proposed path selection techniques to reduce PAPR in multipath JT-TD-SCDMA are discussed in section 3.4. The data detection, SNR and probability analysis of the proposed techniques are presented in section 3.5. The PAPR evaluation and comparison between the numerical analysis and computer simulation results of proposed techniques are presented in section 3.6. The proposed path selection, PS II provides a good trade-off between PAPR and BER compared to that in PS I. We then combine the proposed PS II and clipping technique. Chapter 3 is concluded in section 3.7. From computer simulation we found that the combination of PS II and clipping provides a low PAPR without a severe BER degradation.

This dissertation is finally concluded in chapter 4. The contributions of our studies described in chapter 2 and chapter 3 are summarized in Table 1.8.

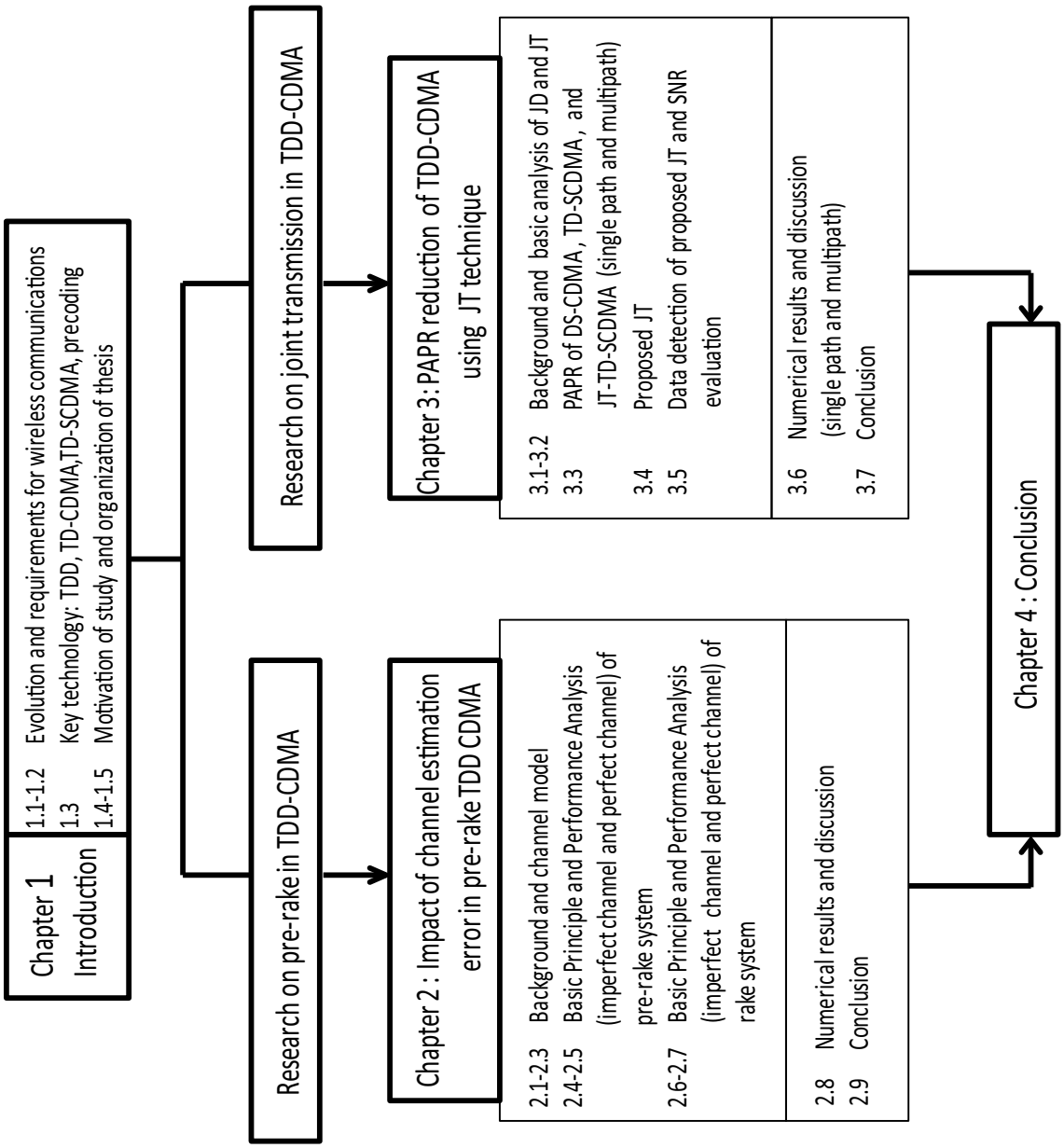

Figure 1.23: The overall structure of this dissertation.

Table 1.8: Contributions of This Study

Impact of Channel Estimation Error in Pre-rake TDD-CDMA [chapter 2]	
Related previous studies	Contribution of this study
• Performance analysis of pre-rake in TDD-CDMA [21],[33]. • Problems and issues left in previous studies. – The analysis considered perfect channel estimation, which is impossible owing to present of interferences and noise.	• Analyzed performance of pre-rake in TDD-CDMA under imperfect channel estimation and clarified that: – A high Doppler frequency increases channel estimation errors, thus increases the BER degradation of pre-rake system. – pre-rake with imperfect channel does not improve when number of path increases which is contra to that in perfect channel estimation. – The effect of channel estimation error is larger in pre-rake than that in rake.
PAPR Reduction using Joint Transmission Technique [chapter 3]	
Related previous studies	Contribution of this study
• JT is used instead of JD to reduce interferences without causing complexity at MS [29], [30]. • Problems and issues left in previous studies – JT changes transmit power from that in JD, affects PAPR. – The implementation of JT causes complexity at BS which is not suitable for small BS such as relay station	• Investigated PAPR of JT and clarified that: – Implementation of JT in single path channel can reduce PAPR – Multipath channel increases PAPR compared to that in single path channel • Proposed a technique that can reduce PAPR with BER analysis – Provides a low PAPR with BER degradation. • Combined the proposed technique with clipping technique – Provides a low PAPR without severe BER degradation. • PAPR reduction by proposed technique allows more efficient PA, which reduces complexity at BS.

Chapter 2

Channel Estimation Error in Pre-rake TDD CDMA

This chapter performs impact of imperfect channel estimation on pre-rake TDD-CDMA system. Background of this chapter is firstly introduced in section 2.1. Section 2.2 briefly presents the multipath channel model used in this study. In section 2.3, the error model used for realizing imperfect channel estimation is defined. Section 2.4 and section 2.5 present performance analysis of pre-rake system for perfect channel estimation error and imperfect channel estimation error, respectively. For comparison, performance analysis for rake system under perfect channel estimation error is presented in section 2.6, followed by imperfect channel estimation in section 2.7. The results of numerical analysis and computer simulations are compared, and discussed in section 2.8. This chapter is finally concluded in section 2.9.

2.1 Background

Direct sequence code-division multiple access (DS-CDMA) was widely researched and used as 3G standards in WCDMA and IMT 2000. Most of the DS-CDMA mobile communications systems use rake combining technique to improve the communication quality through its

ability to achieve multipath diversity gain. However, rake receivers require significant signal processing for setting the weighing factor and combination function. These cause complexity and more power consumption that increase the cost of MS.

TDD-CDMA is increasingly becoming the focus of research for the fourth generation mobile communications systems. In TDD, since the same frequency channel is used in both uplink and downlink, the channel characteristics are highly correlated for the two links.

Pre-rake combining method firstly proposed in [21] to minimize complexity, size and cost of MS and still preserves the diversity gain. In this technique, rake combining function is performed before transmission in BS. As the channel characteristics are reciprocal for the downlink and uplink in TDD, the channel state is available and can be used on pre-rake combining. It has been proved that the pre-rake system performance is equal to that of the rake system for single user system [21], and outperforms the rake system for multi-user system [33].

As explained above, channel estimation is one of the most important aspects of pre-rake combining technique. However, previous works have not taken into consideration the effect of imperfect channel estimation, except for some preliminary results [36]. The effect of imperfect channel estimation can be very important in the high rate transmission envisaged for the fourth generation cellular mobile communication system. In this study, we extend the study of pre-rake TDD CDMA in [33], and present a comprehensive investigation on the effect of imperfect channel estimation on the pre-rake system performance. For this, we evaluate the system performance through both numerical analysis and computer simulations.

2.2 Multipath Channel Model

In this study, we consider the simplified tapped delay line multipath channel model of [18]. The uplink channels are assumed to be statistically independent for all users. In addition, with uplink power control, the uplink channels are assumed to be statistically identical, even

if MS is at different distance from the BS. The complex low-pass impulse response of the channel user k^{th} is given by

$$h_k(t) = \sum_{l=0}^{(L-1)} g_{k,l}\delta(t - lT_c), \tag{2.1}$$

where L is the number of resolvable paths, $g_{k,l} = \beta_{k,l}e^{j\gamma_{k,l}}$ is the complex gain with amplitude $\beta_{k,l}$ and phase $\gamma_{k,l}$ of l^{th} path of the k^{th} user. The complex gains $g_{k,l}$ are independent identically distributed (i.i.d.) Rayleigh random variables (r.v.'s) for all k and l, the angles $\gamma_{k,l}$ are i.i.d. uniformly distributed in [0,2π], and T_c is the chip duration of PN). Without loss of generality we can take the normalization $E[\beta_{k,l}^2] = 1$ under slow fading conditions. Also, we assume that $h_k(t)$ does not change during two successive up and down time slots.

2.3 Error Model

As explained above, in TDD systems the channel is estimated by BS upon reception in the uplink period, and this estimation is used for the pre-rake combining in the downlink. However, the wireless channel is usually time-variant in mobile communication systems. In other words, even if the ideal channel estimation can be performed in the reception, it is unlikely that the channel impulse response will be exactly known before transmission. The error in the channel estimation depends on how fast the channel changes and SNR level. The channel changes can be measured by using Doppler spread of the channel, known as Doppler frequency f_d.

$$f_d = \frac{V}{\lambda_c}, \tag{2.2}$$

where V is the mobile velocity and λ_c is the carrier wavelength. The error in channel estimation increases when the Doppler frequency f_d increases.

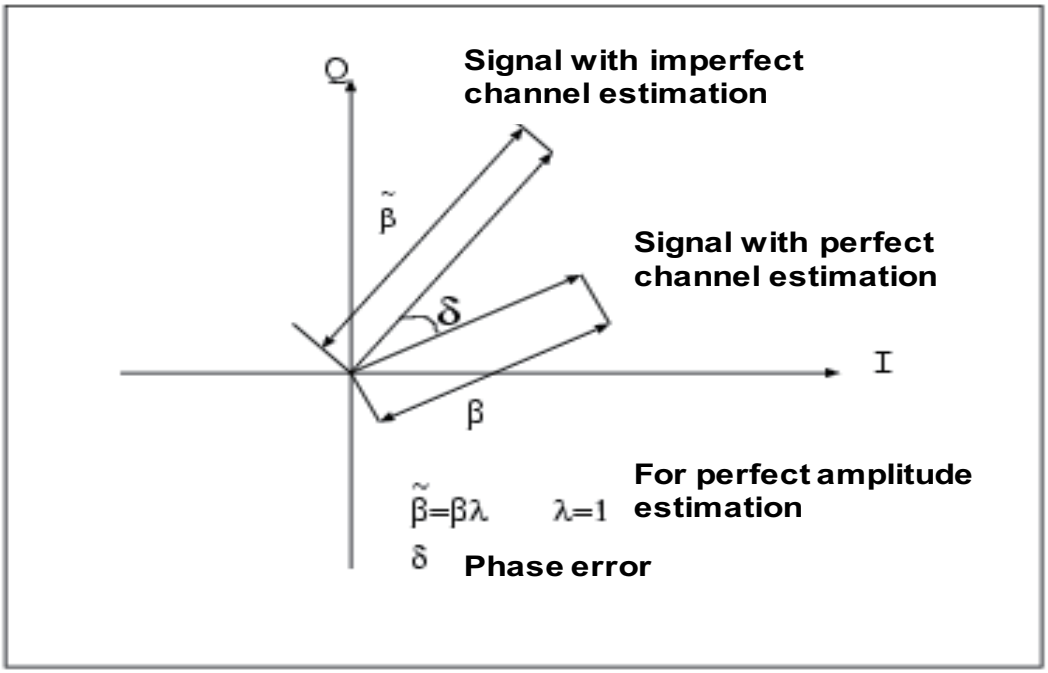

Figure 2.1: Error model in channel estimation

The error model in channel estimation is illustrated in Fig. 2.3. If error in channel estimation is considered, (1.12) in section 1.4.4 will turn to be

$$\begin{aligned} s_k(t) &= \sqrt{\frac{2P}{\tilde{U}_k}} \sum_{l=0}^{L-1} |\tilde{\beta}_{k,L-l-1}| b_k(t - \tilde{\tau}_{k,L-1} + \tilde{\tau}_{k,L-l-1}) \\ &\quad .a_k(t - \tilde{\tau}_{k,L-1} + \tilde{\tau}_{k,L-l-1}) \\ &\quad .\exp(j\omega(t - \tilde{\tau}_{k,L-1} + \tilde{\tau}_{k,L-l-1}) - j\tilde{\gamma}_{k,L-l-1}), \end{aligned} \tag{2.3}$$

where $\tilde{\tau}_{k,l} = lT_c + \tilde{X}_{k,l}$. $\tilde{X}_{k,l}$ is the estimate of the error encountered during the estimation of path number 1 for user number k. All $\tilde{X}_{k,l}$ are i.i.d. r.v's. uniform in $[-\rho T_c, \rho T_c]$, where $\rho \leq 0.5$, $\tilde{\beta}_{k,l}$ is the estimate of the complex Gaussian r.v's. $\beta_{k,l} e^{j\gamma_{k,l}}$ and is given by

$$\tilde{\beta}_{k,l} = |\tilde{\beta}_{k,l}|e^{j\tilde{\gamma_{k,l}}} = |\beta_{k,l}.\lambda_{k,l}|.e^{j\tilde{\gamma_{k,l}}}, \tag{2.4}$$

where λ is treated as a real r.v's, a log normal function [37] with a 0-dB mean and variable variance σ_λ^2, $\tilde{\gamma} = \gamma + \delta$, $\delta_{k,l}$ is treated as uniform in $[-\delta, \delta]$ and represents the estimate of the error encountered during the estimation of gain and phase of 1st path for kth. λ and $\delta_{k,l}$ are assumed to be i.i.d. and $\tilde{U}_k = \sum_{i=0}^{L-1} |\tilde{\beta}_{k,i}|^2$. In this study, we have not considered the effect of error encountered during the path delay estimation $\{\rho = 0\}$ as the effect is considered to be small. Thus, (2.3) will turn to be

$$\begin{aligned} s_k(t) &= \sqrt{\frac{2P}{\tilde{U}_k}} \sum_{l=0}^{L-1} |\tilde{\beta}_{k,L-l-1}| b_k(t - lT_c) \\ &\quad a_k(t - lTc)\exp(j\omega(t - lT_c) - j\tilde{\gamma}_{k,L-l-1}). \end{aligned} \tag{2.5}$$

2.4 Performance Analysis of Pre-rake with Perfect Channel Estimation

The conventional transmitted signal without pre-rake for user k with BPSK modulation is given by

$$s_k(t) = \sqrt{2P} b_k(t) a_k(t) \exp(j\omega t), \tag{2.6}$$

where P is transmit power, ω is the carrier frequency, $b_k(t)$ is the data stream for user k with ± 1 value, consisting of a train of i.i.d. data bits with duration T, $a_k(t)$ is the PN code of user k with ± 1 chips of duration T_c and code length $N = T/T_c$. For the pre-rake system (perfect channel estimation), the downlink transmitted signal will be

$$\begin{aligned} s_k(t) &= \sqrt{\frac{2P}{U_k}} \sum_{l=0}^{L-1} \beta_{k,L-l-1} b_k[t-(\tau_{k,L-1}-\tau_{k,L-l-1})] a_k[t-(\tau_{k,L-1}-\tau_{k,L-l-1})] \\ &\quad \exp[j\omega(t-(\tau_{k,L-1}-\tau_{k,L-l-1}))-j\gamma_{k,L-l-1}] \\ &= \sqrt{\frac{2P}{U_k}} \sum_{l=0}^{L-1} \beta_{k,L-l-1} b_k[t-lT_c] a_k[t-lT_c] \exp[j\omega(t-lT_c)-j\gamma_{k,L-l-1}], \end{aligned} \tag{2.7}$$

where U_k is a normalizing factor to keep the instantaneous transmitted power constant, and given by

$$U_k = \sum_{n=0}^{L-1} \beta_{k,n}^2. \tag{2.8}$$

Assuming a CDMA system with K users, the received signal at user i during downlink time-slot is given by

$$r_i(t) = n(t) + Re \sum_{k=1}^{K} \sum_{j=0}^{L-1} \beta_{i,j} s_k(t-jT_c) \exp(j\gamma_{i,j}), \tag{2.9}$$

where $n(t)$ is the zero-mean additive white Gaussian noise (AWGN) with two-sided power spectral density $N_0/2$.

Without loss of generality, we assume that user 1 is the desired user. The output of matched-filter of user 1 is given by

$$\begin{aligned} Z &= \int_{(L-1)T_c}^{(L-1)T_c+T} r_1(t) a_1[t-(L-1)T_c] \\ &\quad .\cos[\omega t - \omega T_c(L-1)] dt \\ &= D + S + A + \eta, \end{aligned} \tag{2.10}$$

where D is desired part for the current bit, S is self interference, A is multiple access interference (MAI) and η is a zero mean Gaussian r.v. with variance $N_o T/4$.

By substituting $k = 1$ and $l = L - 1 - j$, we can write the desired part of $r_1(t)$ in (2.9) as:

$$D = \sqrt{\frac{P}{2}} b_1^o T \sqrt{U}_1. \tag{2.11}$$

For interference, we employ the Gaussian approximation [38], which is well known in providing good results for multiuser system and readily shown that they are independent with zero mean. Hence, we only interested in their variances. The variances of S and A are evaluated conditioned on $\beta_{1,j}$.

2.4.1 Self Interference

Self interference exists even in a single-user system and is caused by multipath. From (2.10), S is found by substituting $k = 1$ and $j \neq L - l - 1$. For $m = L - l - 1$, S is given by

$$\begin{aligned} S &= \sqrt{\frac{P}{2U_1}} \sum_{j=0}^{L-1} \sum_{m=0,\neq j}^{L-1} \beta_{1,j}\beta_{1,m} \cos[\omega T_c(j-m) + \gamma_{1,m} - \gamma_{1,j}] \\ &\quad . \int_0^T b_1[t-(j-m)T_c] a_1[t-(j-m)T_c] a_1(t) dt. \end{aligned} \tag{2.12}$$

The following identity is used for summating (2.12):

$$\sum_{j=0}^{L-1} \sum_{m=0,\neq j}^{L-1} f(j,m) = \sum_{j=0}^{L-2} \sum_{m=j+1}^{L-1} f(j,m) + f(m,j). \tag{2.13}$$

From [38], we have

$$\int_0^T b_1[t-\tau] a_1[t-\tau] a_1(t) dt = [b_k^{\pm} R_{k,i} + b_k^0 \hat{R_{k,i}}] \tag{2.14}$$

where i represents desired user and k represents the remain users. Also we have

$$\begin{aligned} R_{k,i}(\tau) &= \int_0^\tau a_k(t-\tau)a_i(t-\tau)d\tau \\ &= C_{k,i}(l-N)T_c + [C_{k,i}(l+1-N) - C_{k,i}(l-N)](\tau - lT_c), \end{aligned} \tag{2.15}$$

and

$$\begin{aligned} \hat{R}_{k,i}(\tau) &= \int_0^\tau a_k(t-\tau)a_i(t-\tau)d\tau \\ &= C_{k,i}(l)T_c + [C_{k,i}(l+1) - C_{k,i}(l)].(\tau - lT_c). \end{aligned} \tag{2.16}$$

For synchronous downlink systems, the second term of (2.15) and (2.16)is going to be zero. Therefore, we have

$$\begin{aligned} &\int_0^T b_1[t-(j-m)T_c]a_1[t-(j-m)T_c]a_1(t)dt \\ &= \begin{cases} T_c[b_k^{-1}C_{k,1}(m-N) + b_k^0 C_{k,1}(m)] & m \geq 0 \\ T_c[b_k^0 C_{k,1}(m) + b_k^1 C_{k,1}(N+m)] & m < 0 \end{cases} \end{aligned} \tag{2.17}$$

where $C_k(m)$ is the discrete a periodic cross correlation function defined in [38] and [33]. Substituting $C_{i,i}$ by $C_i(m)$ and using $C_i(m) = C_i(-m)$ we get

$$\begin{aligned} S &= T_c\sqrt{\frac{P}{2U_1}}\sum_{j=0}^{L-2}\sum_{j=m+1}^{L-1}\beta_{1,j}\beta_{1,m}\cos[\omega T_c(j-m) + \gamma_{1,m} - \gamma_{1,j}] \\ &\quad .[b_1^{-1}C_1(N-m+j) + b_1^1(N-m+j) + 2b_1^0 C_1(m-j)]. \end{aligned} \tag{2.18}$$

Taking the second moment of S,

$$\begin{aligned} E[S^2|(\beta_{i,j}),(\beta_{i,j})] &= \frac{PT_c^2}{2U_1}\sum_{j=0}^{L-2}\sum_{m=j+1}^{L-1}\beta_{1,j}^2\beta_{1,m}^2 \\ &\quad [C_1^2(N-m+j)+2(C_1^2(m-j)] \\ &= \frac{PT_c^2}{2U_1}[2N\chi-\mu], \end{aligned} \tag{2.19}$$

where

$$\chi = \sum_{j=0}^{L-2}\sum_{m=j+1}^{L-1}\beta_{1,j}^2\beta_{1,m}^2$$

and

$$\mu = \sum_{j=0}^{L-2}\sum_{m=j+1}^{L-1}\beta_{1,j}^2\beta_{1,m}^2(m-j)$$

.

2.4.2 Multiple Access Interference

MAI part is a major difference between pre-rake and rake system. In the pre-rake, the signal of each user is pre-raked according to its uplink channel impulse response. Hence, in the downlink only the desired user's signal is maximal ratio combined, while other users' are not. In the rake system, the desired and multiple-access signals are combined. Thus, the effect of MAI is larger in rake system than that in pre-rake system. MAI can be found by substituting $k \neq 1$ in (2.10), and can be written as:

$$\begin{aligned} A &= \sqrt{\frac{P}{2}}\sum_{k=2}^{K}\sum_{j=0}^{L-1}\sum_{m=0}^{L-1}\frac{\beta_{1,j}\beta_{k,m}}{\sqrt{U}_k}\cos[\omega T_c(j-m)+\gamma_{k,m}-\gamma_{1,j}] \\ &\quad \int_0^T b_k[t-(j-m)T_c]a_k[t-(j-m)T_c]a_1(t)dt. \end{aligned} \tag{2.20}$$

For $m = j$, (2.20) can be written as

$$A|_{m=j} = T_c\sqrt{\frac{P}{2}}\sum_{k=2}^{K}\sum_{j=0}^{L-1}\frac{\beta_{1,j}\beta_{k,j}}{\sqrt{U}_k}\cos[\gamma_{k,j}-\gamma_{1,j}]b_k^0C_{k1}^0. \tag{2.21}$$

For $m \neq j$, (2.20) can be written as

$$\begin{aligned} A|_{m\neq j} &= T_c\sqrt{\frac{P}{2}}\sum_{k=2}^{K}\sum_{j=0}^{L-2}\sum_{m=j+1}^{L-1}\frac{1}{\sqrt{U}_k}\{\beta_{1,j}\beta_{k,m}\cos[\omega T_c(j-m)+\gamma_{k,m}-\gamma_{1,j}] \\ &\quad .[b_k^0 C_{k,1}(j-m)+b_k^1 C_{k,1}(N+j-m)]+\beta_{1,m}\beta_{k,j}\cos[\omega T_c(m-j)+\gamma_{k,j}-\gamma_{1,m}] \\ &\quad .[b_k^{-1} C_{k,1}(m-j-N)+b_k^0 C_{k,1}(m-j)]\}. \end{aligned} \tag{2.22}$$

Using (2.13) and(2.17), the second moment of A is given by

$$E[A^2|\{\beta_{i,j}\}),\{\beta_{i,j}\}] = \frac{PT_c^2}{4}N\frac{\beta_{k,j}^2}{U_k}\sum_{k=2}^{K}\{\sum_{j=0}^{L-1}\beta_{1,j}^2+\sum_{j=0}^{L-2}\sum_{m=j+1}^{L-1}[\beta_{1,j}^2+\beta_{1,m}^2], \tag{2.23}$$

where

$$E[\frac{\beta_{k,j}^2}{U_k}] = \frac{1}{L}$$

After some manipulations, (2.23) can be written as:

$$E[A^2|\{\beta_{i,j}\}),\{\beta_{i,j}\}] = \frac{U_1 PNT_c^2(K-1)(L-1+W)}{4L}, \tag{2.24}$$

where W is a pointer with $W = 0$ for orthogonal codes and $W = 1$ for unorthogonal codes.

2.4.3 Probability of Error

We can find that the probability of error is given by

$$P(e|\{\beta_{1,n}\}) = 0.5erfc(\sqrt{Y}), \tag{2.25}$$

where Y is the signal noise ratio(SNR), given by
$Y = D^2/2\text{Var}(Z)$, where $\text{Var}(Z)$ is the variance of Z, and given by

$$\text{Var}(Z) = \text{Var}(A) + \text{Var}(S) + \text{Var}(\eta). \tag{2.26}$$

After some manipulations, Y is found to be

$$Y = \left[\frac{L}{\gamma_b U_1} + \frac{4\chi}{NU_1^2} - \frac{2\mu}{N^2U_1^2} + \frac{(K-1)(L-1+W)}{NL}\right]^{-1}, \tag{2.27}$$

where $\gamma_b = PTL/N_0$ is the average received signal to AWGN ratio. The probability density function (pdf) is very difficult to obtain. Thus, the value of $P(e)$ is evaluated by using Monte Carlo simulation [39]. At each iteration L Rayleigh r.v.'s are computer generated, U_1, χ, and μ are evaluated and Y is found and substituted in (2.25). For each value, (2.25) is averaged over a large number of iterations.

2.5 Performance Analysis of Pre-rake with Imperfect Channel Estimation

In pre-rake system, considering imperfect channel estimation, instead of (2.7) the downlink transmitted signal will turn to be

$$\begin{aligned} s_k(t) &= \sqrt{\frac{2P}{\tilde{U}_k}} RE\{\sum_{l=0}^{L-1} \tilde{\beta}_{k,L-l-1} b_k(t - \tilde{\tau}_{k,L-1} + \tilde{\tau}_{k,L-l-1}) \\ &\quad a_k(t - \tilde{\tau}_{k,L-1} + \tilde{\tau}_{k,L-l-1}) \exp(j\omega(t - \tilde{\tau}_{k,L-1} + \tilde{\tau}_{k,L-l-1}))\}, \end{aligned} \tag{2.28}$$

where $\tau_{k,l} = lT_c$, $\tilde{\tau}_{k,l} = \tau_{k,l} + \tilde{X}_{k,l}$. $\tilde{X}_{k,l}$ is the estimate of the error encountered during the estimation of 1st path for kth. All $\tilde{X}_{k,l}$ are i.i.d, r.v., uniform in $[-\rho T_c, \rho T_c]$, where $\rho \leq 0.5$, $\tilde{\beta}_{k,l}$ is the estimate of the complex Gaussian r.v. $\beta_{k,l} e^{j\gamma_{k,l}}$ and is given by

$$\tilde{\beta}_{k,l} = |\tilde{\beta}_{k,l}|e^{\gamma\tilde{k},l} = |\beta_{k,l}.\lambda|.e^{\gamma\tilde{k},l}, \tag{2.29}$$

where λ is treated as a complex Gaussian r.v., a log normal function with a 0-dB mean and variable variance σ_λ^2, $\delta_{k,l}$ is treated as uniform in $[-\delta T_c, \delta T_c]$ and represents the estimate of the error encountered during the estimation of gain and phase of 1st path for kth user. λ and $\delta_{k,l}$ are assumed to be i.i.d. and $\tilde{U}_k = \sum_{i=0}^{L-1} |\tilde{\beta}_{k,i}|^2$. In this study, we have not considered the effect of error encountered during the path delay estimation $\{\rho = 0\}$ as the effect is not too much. Thus, (2.28) will turn to be

$$s_k(t) = \sqrt{\frac{2P}{\tilde{U}_k}} \sum_{l=0}^{L-1} RE\{\tilde{\beta}_{k,L-l-1} b_k(t - lT_c) a_k(t - lTc) \exp(j\omega(t - lT_c) - \tilde{\gamma}_{k,L-l-1})\}. \tag{2.30}$$

Substituting (2.30) into (2.9), output of the MF can be divided into desired part and interferences part as in (2.10). Desired part is given by $k = 1$, $l = L - 1 - j$ parts of $r_1(t)$ in (2.10), and can be written as

$$D = \sqrt{\frac{P}{2\tilde{U}_1}} b_1^o T \tilde{\Lambda}, \tag{2.31}$$

where $\tilde{\Lambda} = \sum_{j=0}^{L-1} \beta_{1,j}|\tilde{\beta}_{1,j}|\cos(\delta) - \rho \sum_{j=0}^{L-2} \beta_{1,j}|\tilde{\beta}_{1,j}|\cos(\delta)$. We note that in the case of perfect channel estimation, $\rho = 0$ and $\sigma_\epsilon^2 = 0$. Again, we have to note that ρ is assumed to be 0 in this study as considering that the effect of the error during path delay estimation is not too much and can be neglected. From (2.31), it can be seen that the desired part decreases due to channel estimation error.

2.5.1 Self Interference

From (2.10), S is found by substituting $k = 1$ and $l \neq L - 1 - j$. Substituting $m = L-1-j$, S is given by

$$
\begin{aligned}
S &= T_c\sqrt{\frac{P}{2\tilde{U}_1}}\sum_{j=0}^{L-2}\sum_{j=m+1}^{L-1}\beta_{1,j}|\tilde{\beta}_{1,m}|\cos[\omega T_c(j-m)+\tilde{\gamma}_{1,m}-\gamma_{1,j}] \\
&\quad .[b_1^{-1}C_1(N-m+j)+b_1^1(N-m+j)+2b_1^0C_1(m-j)]. \qquad (2.32)
\end{aligned}
$$

The second moment of S is given by

$$
\begin{aligned}
E[S^2|(\beta_{1,j}),(\tilde{\beta}_{1,j})] &= \frac{PT_c^2}{2\tilde{U}_1}\sum_{j=0}^{L-2}\sum_{m=j+1}^{L-1}\beta_{1,j}^2|\tilde{\beta}_{1,m}^2|[C_1^2(N-m+j)+2(C_1^2(m-j)] \\
&= \frac{PT_c^2}{2\tilde{U}_1}[2N\tilde{\chi}-\tilde{\mu}], \qquad (2.33)
\end{aligned}
$$

where

$$\tilde{\chi}=\sum_{j=0}^{L-2}\sum_{m=j+1}^{L-1}\beta_{1,j}^2|\tilde{\beta}_{1,m}^2|,$$

and

$$\tilde{\mu}=\sum_{j=0}^{L-2}\sum_{m=j+1}^{L-1}\beta_{1,j}^2|\tilde{\beta}_{1,m}^2|(m-j),$$

.

2.5.2 Multiple Access Interference

MAI for imperfect channel estimation can be found by substituting $\{k \neq 1\}$ in (2.10), and can be written as

$$
\begin{aligned}
A &= \sqrt{\frac{P}{2}}\sum_{k=2}^{K}\sum_{j=0}^{L-1}\sum_{m=0}^{L-1}\frac{\beta_{1,j}|\tilde{\beta}_{k,m}|}{\sqrt{\tilde{U}_k}}\cos[\omega T_c(j-m)+\tilde{\gamma}_{k,m}-\gamma_{1,j}] \\
&\quad \int_0^T b_k[t-(j-m)T_c]a_k[t-(j-m)T_c]a_1(t)dt. \qquad (2.34)
\end{aligned}
$$

After some manipulations as analysis of pre-rake with perfect channel estimation, the second moment of A is found to be

$$E[A^2|\{\beta_{1,j}\}),\{\tilde{\beta}_{1,j}\}] = \frac{\tilde{U}_1 PNT_c^2(K-1)(L-1+W)}{4L}, \tag{2.35}$$

where W is a pointer with $W = 0$ for orthogonal codes and $W = 1$ for unorthogonal codes. It is clear that when orthogonal code is used as a spreading sequence $\{W = 0\}$, the MAI part increases due to the increase of the paths.

2.5.3 Probability of Error

The value of Y in (2.25) is given by

$$Y_{im} = \left[\frac{L\tilde{U}_1}{\tilde{\gamma}_b\tilde{\Lambda}^2} + \frac{4\tilde{\chi}}{N\tilde{\Lambda}^2} - \frac{2\tilde{\mu}}{N^2\tilde{\Lambda}^2} + \frac{\tilde{U}_1^2(K-1)(L-1+W)}{NL\tilde{\Lambda}^2}\right]^{-1}, \tag{2.36}$$

where $\tilde{\gamma_b} = PTL/N_0$ is the average received signal to AWGN ratio for imperfect channel estimation. Again, the Monte Carlo simulation is used to evaluate $\tilde{\Lambda}$, $\tilde{\chi}$ and $\tilde{\mu}$. At each iteration, L Rayleigh r.v.'s for $\beta_{1,j}$, L Rayleigh r.v.'s for $\tilde{\beta}_{1,j}$, L uniform distributed r.v.'s for $\delta_{1,j}$ are computer generated, $\tilde{U}_1$ are evaluated, then Y is found and substituted in (2.25). For each value, (2.25) is averaged over a large number of iterations. From (2.36), it is clear that the channel estimation error decreases the desired part and increases the interference parts.

2.6 Performance Analysis of Rake System with Perfect Channel Estimation

For the sake of comparison, we also evaluate the bit-error-rate (BER) performance of rake receiver here by using the same assumptions as in pre-rake, written in section 2.4. We

assumed that the rake receiver is equipped with L rake fingers, each tuned to one of the channel paths. Each finger gets self interference and multiple access interference. Without pre-rake, the transmitted signal substituted in (2.9) (the received signal at user 1) is given by (2.6) instead of (2.7). Thus, with MRC the output of MF is given by

$$\begin{aligned} Z &= \sum_{n=0}^{L-1} \beta_{1,n} \int_{nT_c}^{nT_c+T} r_1(t) a_1[t - nT_c] \cos[\omega t - \omega n T_c + \gamma_n] dt \\ &= D + S + A + \eta, \end{aligned} \tag{2.37}$$

where η is a zero mean Gaussian r.v. with variance $N_0 T U_1/4$ [18], D is desired user, S is self interference and A is multiple access interference. D is found by substitute $k = 1$ and $j = n$ in $r(t)$. Thus, D is given by

$$D = \sqrt{\frac{P}{2}} b_1^o T U_1. \tag{2.38}$$

2.6.1 Interference Parts

Self interference S is found by substitute $k = 1$ and $n \neq j$ and given by

$$\begin{aligned} S &= T_c \sqrt{\frac{P}{2}} \sum_{j=0}^{L-2} \sum_{j=n+1}^{L-1} \beta_{1,j} \beta_{1,n} \cos[\omega T_c (j-n) + \gamma_{1,n} - \gamma_{1,j}] \\ &\quad .[b_1^{-1} C_1(N - n + j) + b_1^1 (N - n + j) + 2 b_1^0 C_1(n - j)], \end{aligned} \tag{2.39}$$

From (2.12) and (2.39), we can see that the self interference parts of pre-rake and rake is similar except for U_1 in pre-rake. The second moment of S is given by

$$\begin{aligned} E[S^2|(\beta_{i,j}), (\beta_{i,j})] &= \frac{P T_c^2}{2} \sum_{j=0}^{L-2} \sum_{n=j+1}^{L-1} \beta_{1,j}^2 \beta_{1,n}^2 \\ &\quad [C_1^2(N - n + j) + 2(C_1^2(n - j)] \\ &= \frac{P T_c^2}{2} [2N\chi - \mu], \end{aligned} \tag{2.40}$$

where χ and μ is given in analysis of pre-rake with perfect channel estimation in section 2.4.

For MAI, it has been proved that MAI of rake receiver is higher than that in the pre-rake system. In the pre-rake system, the signal of each user is pre-raked according to its channel impulse response. Thus, only the desired signal is combined in MS. While in the rake system, the desired and the MAI are combined. The MAI of rake system is given by

$$\begin{aligned} A &= \sqrt{\frac{P}{2}} \sum_{k=2}^{K} \sum_{n=0}^{L-1} \sum_{j=0}^{L-1} \beta_{1,n}\beta_{1,j} \cos[\omega T_c(j-n) + \gamma_{1,n} - \gamma_{1,j}] \\ &\quad \int_0^T b_k[t-(j-n)T_c] a_k[t-(j-n)T_c] a_1(t) dt. \end{aligned} \tag{2.41}$$

After some manipulations, the second moment of A is given by

$$E[A^2|\{\beta_{i,j}\}), \{\beta_{i,j}\}] = \frac{PNT_c^2(K-1)({WU_1}^2+\chi)}{2}, \tag{2.42}$$

where W is a pointer for spreading codes as explained before.

Then, we substitute variance of A, S and η into Y in (2.25).

$$Y = \left[\frac{L}{\gamma_b U_1} + \frac{4\chi}{NU_1^2} - \frac{2\mu}{N^2 U_1^2} + \frac{2(K-1)({WU_1}^2+\chi)}{N{U_1}^2} \right]^{-1} \tag{2.43}$$

where $\gamma_b = PTL/N_0$ is the average received SNR for rake system with perfect channel estimation.

2.7 Performance of Rake System with Imperfect Channel Estimation

Again, for the sake of comparison we also evaluate the performance of rake system with imperfect channel estimation by using the same assumption as that in pre-rake. The output of the rake receiver of user 1 for imperfect channel estimation is given by

$$\begin{aligned} Z &= \sum_{n=0}^{L-1} \tilde{\beta}_{1,n} \int_{nT_c}^{nT_c+T} r_1(t) a_1[t - nT_c] \cos[\omega t - \omega n T_c + \tilde{\gamma}_n] dt \\ &= D + S + A + \eta, \end{aligned} \tag{2.44}$$

where η is a zero mean Gaussian r.v. with variance $N_0 T \tilde{U}_1/4$. By substituting $k = 1$ and $n = j$, the desired part D is given by

$$D = \sqrt{\frac{P}{2}} b_1^o T \tilde{\Lambda}, \tag{2.45}$$

where $\tilde{\Lambda} = \sum_{j=0}^{L-1} \beta_{1,j} \tilde{\beta}_{1,j} \cos(\delta) - \rho \sum_{j=0}^{L-1} \beta_{1,j} \tilde{\beta}_{1,j} \cos(\delta)$. We note that in the case of perfect channel estimation, $\rho = 0$ and $\sigma_\epsilon^2 = 0$. Again, as we do not consider the error during the path delay estimation, ρ is going to be zero.

2.7.1 Interference Parts

By substituting $k = 1$ and $j \neq n$, self interference S for imperfect channel estimation case is given by

$$\begin{aligned} S &= T_c \sqrt{\frac{P}{2}} \sum_{j=0}^{L-2} \sum_{j=n+1}^{L-1} \beta_{1,j} \tilde{\beta}_{1,n} \cos[\omega T_c (j - n) + \tilde{\gamma}_{1,n} - \gamma_{1,j}] \\ &\quad .[b_1^{-1} C_1(N - n + j) + b_1^1 (N - n + j) + 2 b_1^0 C_1(n - j)]. \end{aligned} \tag{2.46}$$

After some manipulations, the second moment of S is given by

$$
\begin{aligned}
E[S^2|(\beta_{i,j}),(\tilde{\beta}_{i,j})] &= \frac{PT_c^2}{2}\sum_{j=0}^{L-2}\sum_{n=j+1}^{L-1}\beta_{1,j}^2\tilde{\beta}_{1,n}^2[C_1^2(N-n+j)+2(C_1^2(n-j)] \\
&= \frac{PT_c^2}{2}[2N\tilde{\chi}-\tilde{\mu}], \qquad (2.47)
\end{aligned}
$$

where $\tilde{\chi}$ and $\tilde{\mu}$ are given in analysis of pre-rake with imperfect channel estimation in section 2.5. We can see that from (2.47), as in the case of perfect channel estimation , the self interference part of rake with imperfect channel estimation is similar to that in pre-rake with imperfect channel estimation error except for $\tilde{U}_1$.

The MAI of rake system considering imperfect channel estimation is given by

$$
\begin{aligned}
A &= \sqrt{\frac{P}{2}}\sum_{k=2}^{K}\sum_{n=0}^{L-1}\sum_{j=0}^{L-1}\tilde{\beta}_{1,n}\beta_{1,j} \\
&\quad \cos[\omega T_c(j-n)+\tilde{\gamma}_{1,n}-\gamma_{1,j}] \\
&\quad \int_0^T b_k[t-(j-n)T_c]a_k[t-(j-n)T_c]a_1(t)dt. \qquad (2.48)
\end{aligned}
$$

After some manipulations, the second moment of A is given by

$$
E[A^2|\{\beta_{i,j}\}),\{\tilde{\beta}_{i,j}\}] = \frac{PNT_c^2(K-1)(W\tilde{U}_1^2+\tilde{\chi})}{2} \qquad (2.49)
$$

where W is a pointer for spreading codes as explained before.

Then, we substitute variance of A, S and η into Y in (2.25), and calculate a new Y_im under imperfect channel estimation as

$$
Y_{im} = \left[\frac{L\tilde{U}_1}{\tilde{\gamma_b}\tilde{\Lambda}^2}+\frac{4\tilde{\chi}}{N\tilde{\Lambda}^2}-\frac{2\mu}{N^2\tilde{\Lambda}^2}+\frac{2(K-1)(W\tilde{U}_1^2+\tilde{\chi})}{N\tilde{\Lambda}^2}\right]^{-1}. \qquad (2.50)
$$

where $\tilde{\gamma_b} = PTL/N_0$ is the average received SNR for rake system with imperfect channel estimation.

2.8 Numerical Result and Discussion

Probability of errors, $P(e)$ are evaluated both for single-user system and multi-user system. For numerical analysis, we evaluate BER by using Monte Carlo simulation [39] as the pdf of the r.v.'s $U_1, \tilde{U_1}, \Lambda, \chi, \tilde{\chi}, \mu$ are very difficult to obtain. At each iteration, L Rayleigh r.v.'s for $\{\beta_{1,j}\}$, L Rayleigh r.v.'s for $\{\tilde{\beta}_{1,j}\}$, L uniform distributed r.v.'s for $\{\delta_{1,j}\}$ are computer generated. Then, $U_1, \tilde{U_1}, \Lambda, \chi, \tilde{\chi}, \mu, \tilde{\mu}$ are evaluated , then Y is found and substituted in (2.25). For each value, $P(e)$ is averaged over a sufficiently large number of iterations.

For computer simulation, the parameters in Table 2.1 are used. In this study, channel estimation error effect was simulated with different value of Doppler frequency (5, 50, 100 Hz). Then, the effect of the error is theoretically analyzed. Since it is difficult to generate the error in the theoretical analysis, we first compared simulation results with analysis results for single-user system to find the relation between error (phase and amplitude) and Doppler frequency value. Then, the value of phase error and amplitude error for each Doppler frequency value are used in analysis performance for multi-user system. The relation between Doppler frequency with phase error and amplitude error is shown in Table 2.2.

2.8.1 Single-user System

It has been proved that pre-rake performs similar BER performance to that in rake system when perfect channel estimation and single-user cases are considered [21]. Thus, for single-user case, we only evaluate the effect of channel estimation error in pre-rake system in this study.

In Fig. 2.2, the BER performance of pre-rake system with different Doppler frequency is presented. We can see that the error of channel estimation increases as the Doppler frequency

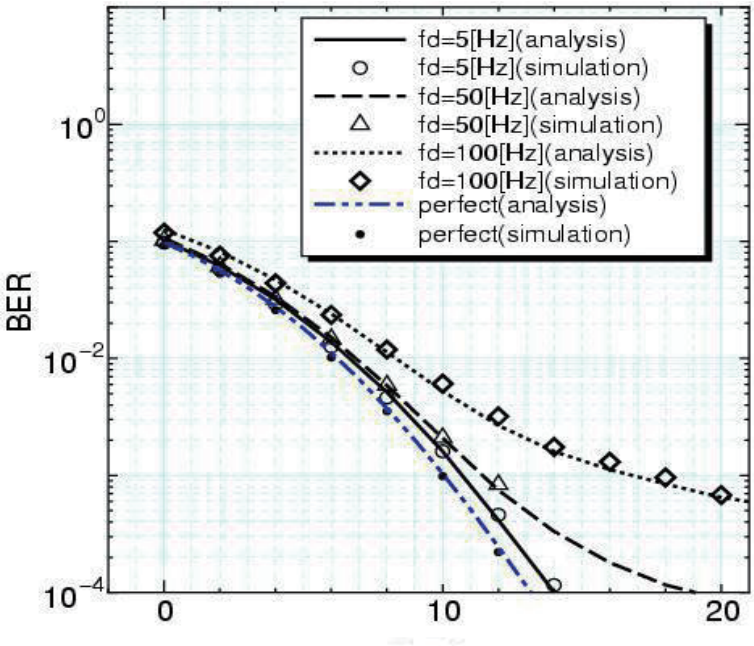

Figure 2.2: BER vs. Eb/No in pre-rake system performance with different Doppler frequency

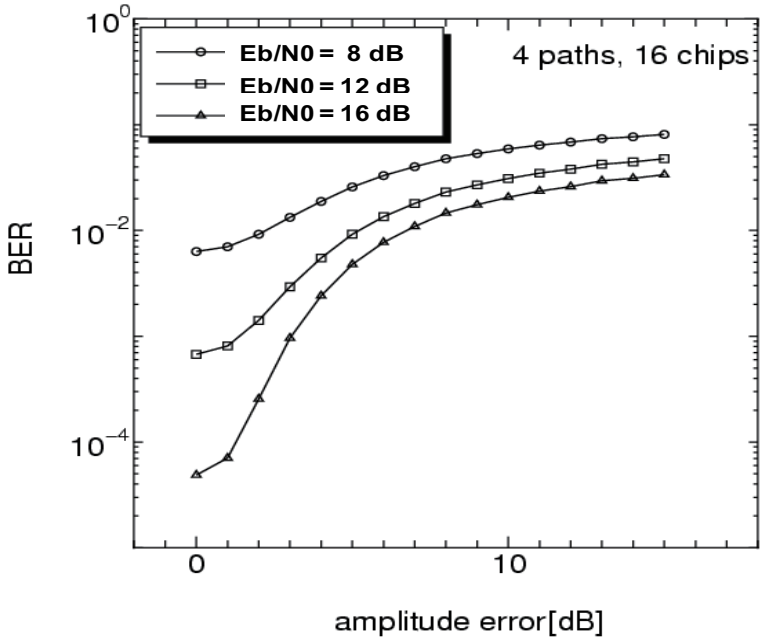

Figure 2.3: BER vs. amplitude error in channel estimation for single-user case

Table 2.1: Parameter

Bit Rate	512000 [bit/sec]
Spreading code	16
Modulation	BPSK
Doppler frequency	5, 50, 100 Hz
Number of paths	2, 4
Packet length	100 [bit/packet]
Power delay profile	Exponential decay profile
Frame length	10ms
Number of slots	15
Time slot length	0.667 ms

Table 2.2: Relation between Doppler frequency and error

Doppler Freq. [Hz]	Amp Error [dB]	Phase Error [degree]
5	0.3	5
50	1.0	10
100	3.0	25

increases, as the correlation between the fading values of consecutive slots decrease due to time-variant channel in mobile communication systems. Also, we can see that the simulation results match numerical analysis results.

Figure 2.3 and Fig. 2.4 show the effect of amplitude and phase error encountered during channel estimation in single-user pre-rake system. We can see that the performance drastically degrades at large E_b/N0 (16 dB) due to increased noise. The large noise breaks channel reciprocity, where the estimated UL channel condition varies, and not valid to be used in DL. Note that, the channel reciprocity of UL and DL can be used for a low noise case only, as described in section 1.4.3.

In Fig. 2.5 the relation between BER and the number of paths, for the two cases, perfect and imperfect channel estimation is presented. From Fig. 2.5 we note that for the perfect channel estimation, the performance of single-user pre-rake system improves as the number of paths increases due to the diversity effect. For pre-rake with imperfect channel estimation

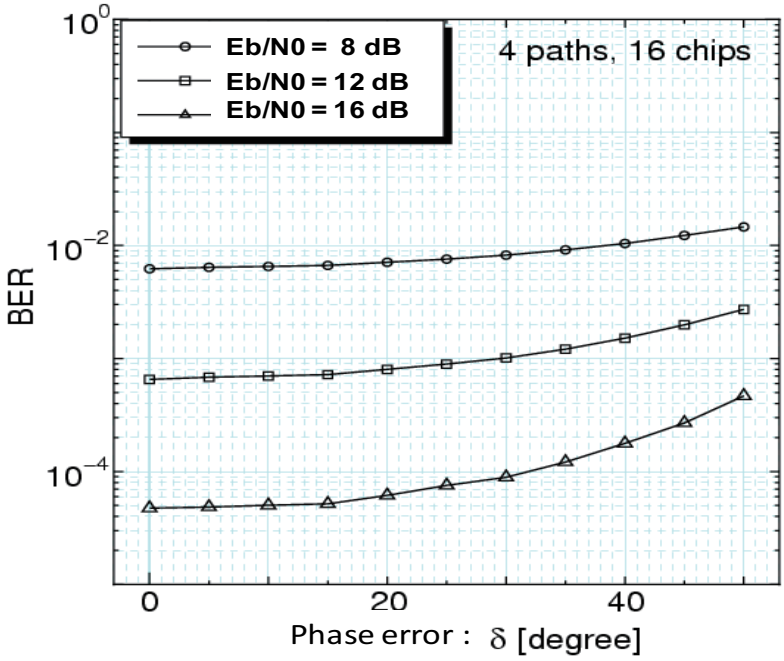

Figure 2.4: BER vs. phase error in channel estimation for single-user case

system, the BER performance does not improve due to decreasing power level of desired signal part shown in (2.31), which increases self-interference.

2.8.2 Multi-user System

A TDD CDMA system with 20 users and code length $N = 64$ is considered in multi-user case. The results of multi-user system are shown in Figs. 2.6 - 2.11. Figure 2.6 shows the BER performance of pre-rake and rake system with perfect channel estimation. Clearly, when random codes are used, the pre-rake system greatly outperforms the rake system since the latter enhances the interference parts as well. When orthogonal codes are used, the BER performance improves for both systems compared to that in random codes. However, when orthogonal code is used, the rake system performing better than rake system due to high orthogonality loss in pre-rake system.

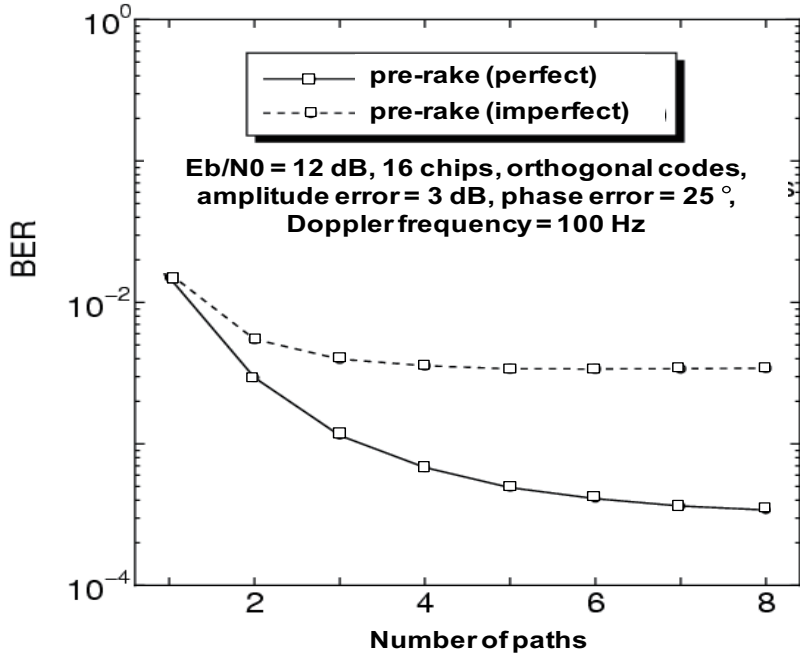

Figure 2.5: BER vs. number of paths

Fig. 2.7 and Fig. 2.8 show the effect of amplitude and phase error during the channel estimation in multi-user system. We can see that when orthogonal codes are used, the effect of amplitude error is larger in pre-rake system than that in rake system. From Fig. 2.8, it can be seen that the effect of phase error (more than 50 degree) is significant when orthogonal sequences are used as spreading sequence in both rake and pre-rake systems. This is because, high orthogonality loss occurs due to increased phase error.

Fig.2.9 shows the performance of rake and pre-rake systems with orthogonal codes as the spreading sequence under perfect and imperfect channel estimation. Again, we can see that the effect of channel estimation error in pre-rake multi-user system is larger than that in rake multi-user system due to increased interference parts. In pre-rake combining as shown in Fig. 2.10, the desired signal and interference signals (MAI) are multiplied with their own channel. Hence, only the desired signal is affected by channel estimation error, which increases orthogonality loss. In rake combining, both desired signal and interference signals

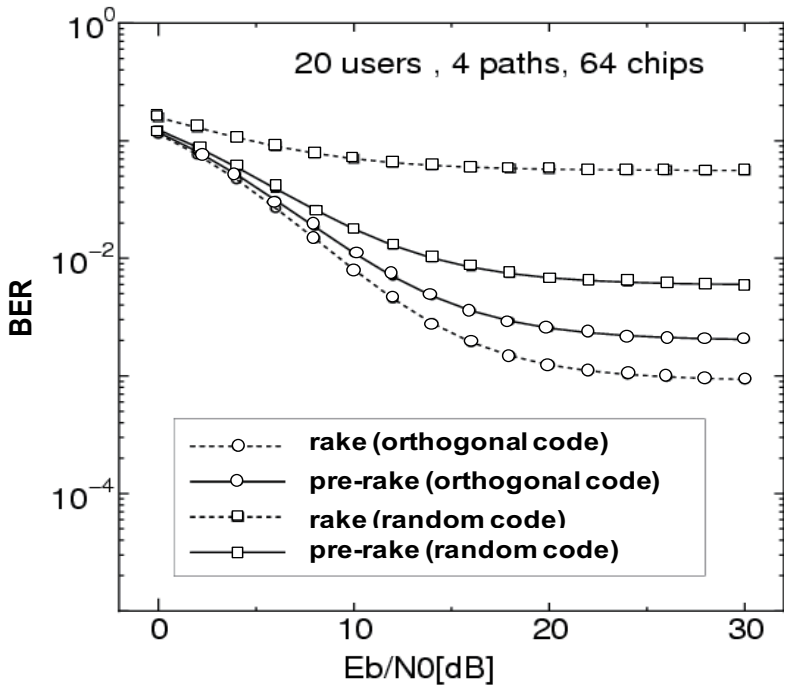

Figure 2.6: BER vs. Eb/No performance for perfect channel estimation system for multi-user system

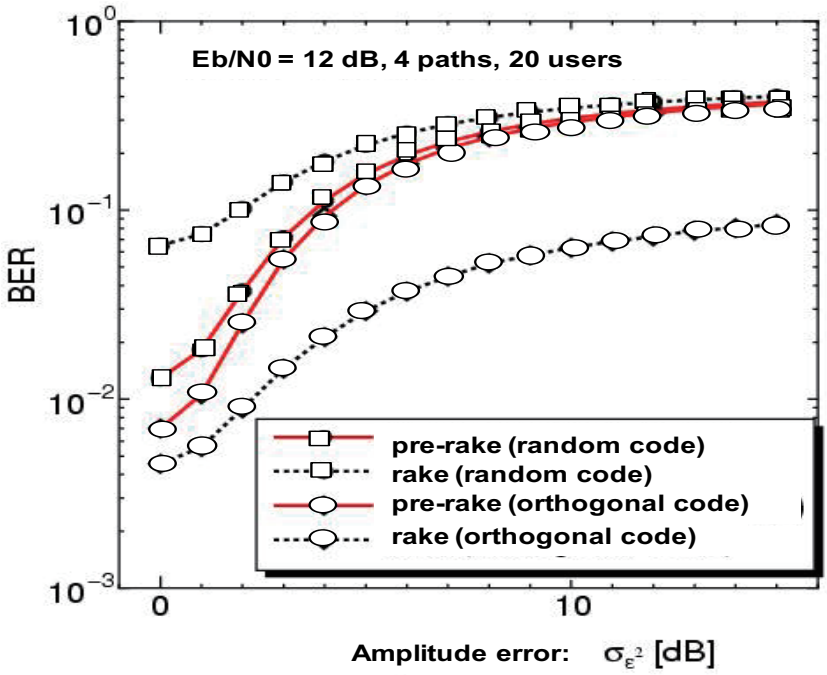

Figure 2.7: BER vs. amplitude error for multi-user system

are multiplied with the same channel. Thus, both are affected by channel estimation error. This phenomenon causes performance degradation in pre-rake combining larger than in rake combining.

Figure 2.11 shows the BER performance of pre-rake and rake systems under perfect and imperfect channel estimation with increased number of paths. We can see that in pre-rake with perfect channel estimation, as the number of paths increases the performance improves at first, then it starts to degrade due to increased interference from large number of paths of all users. For pre-rake with imperfect channel estimation, it can be seen that the diversity gain cannot be achieved at all as the error increases MAI and self-interference. Also, we can see that the channel estimation error degrades BER performance of pre-rake than that in rake system when orthogonal codes are used.

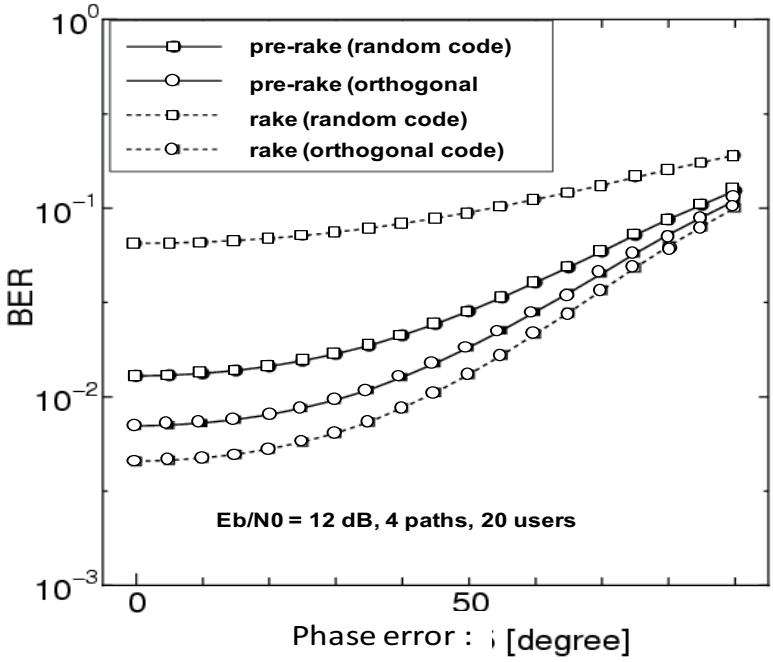

Figure 2.8: BER vs. phase error for multi-user system

2.9 Conclusion

Most of previous works of pre-rake TDD CDMA have not taken into consideration the effect of imperfect channel estimation. In this study, the performance of pre-rake TDD CDMA under imperfect channel estimation has been evaluated. It has been confirmed that the errors in channel estimation drastically degrade the system performance particularly in multi-user system. Thus, the error in channel estimation should not be neglected in pre-rake performance evaluation.

However, many researches related to pre-rake such as combination between pre-rake and rake in [34], combination of pre-rake and JT in [35], only considered perfect channel estimation. Most of the techniques provide improvement in BER performance that might be inaccurate when imperfect channel estimation is considered. These researches should be investigated under imperfect channel estimation to provide more accurate results.

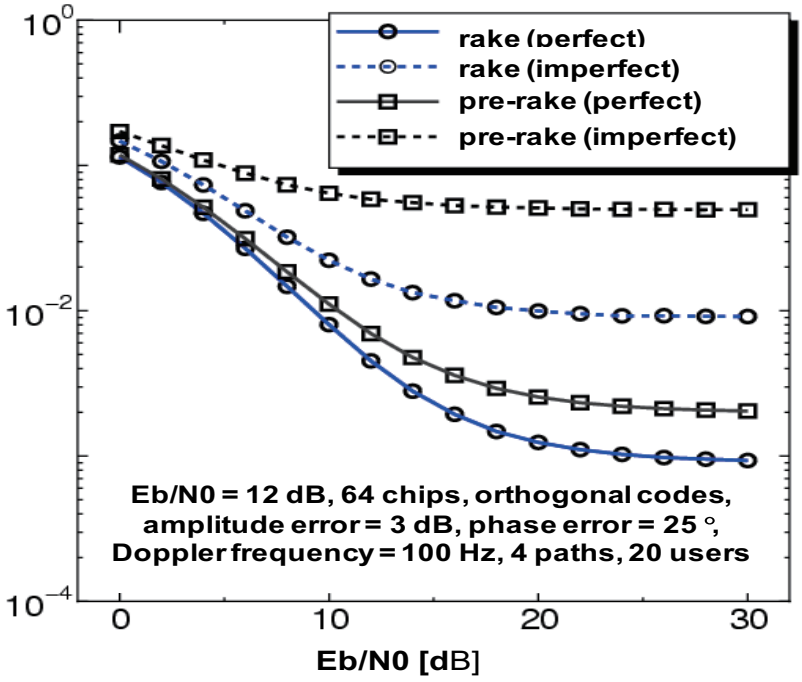

Figure 2.9: BER vs. Eb/No for multi-user system

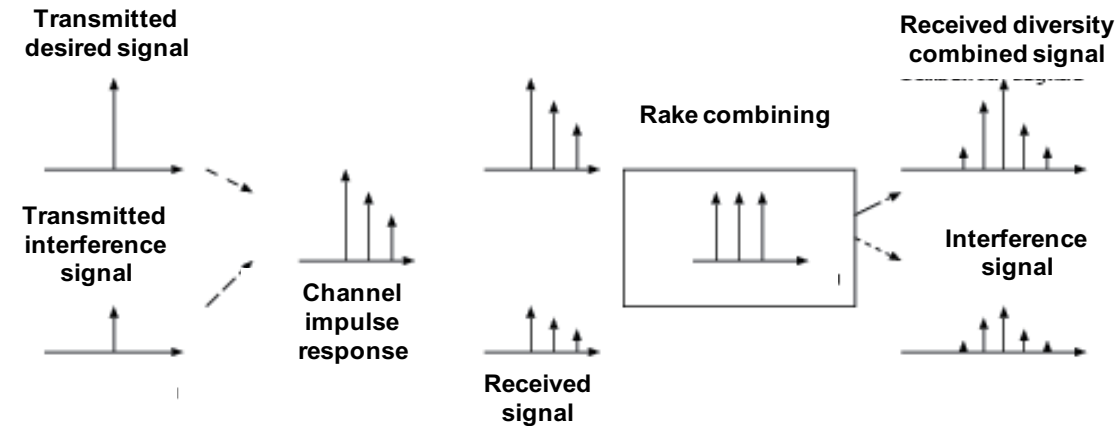

(a) The rake diversity combining process with channel estimation error

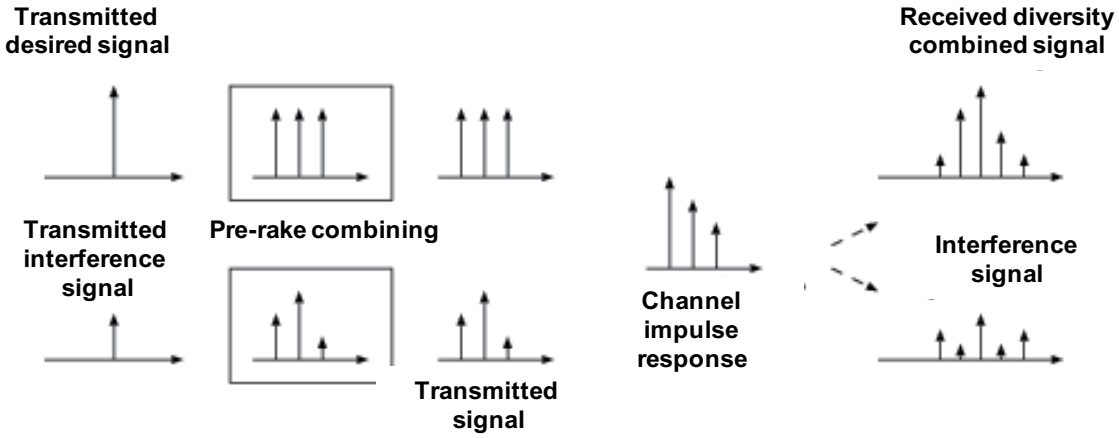

(b) The pre-rake diversity combining process with channel estimation error

Figure 2.10: The effect of channel estimation error in pre-rake and rake combining process for multi-user system

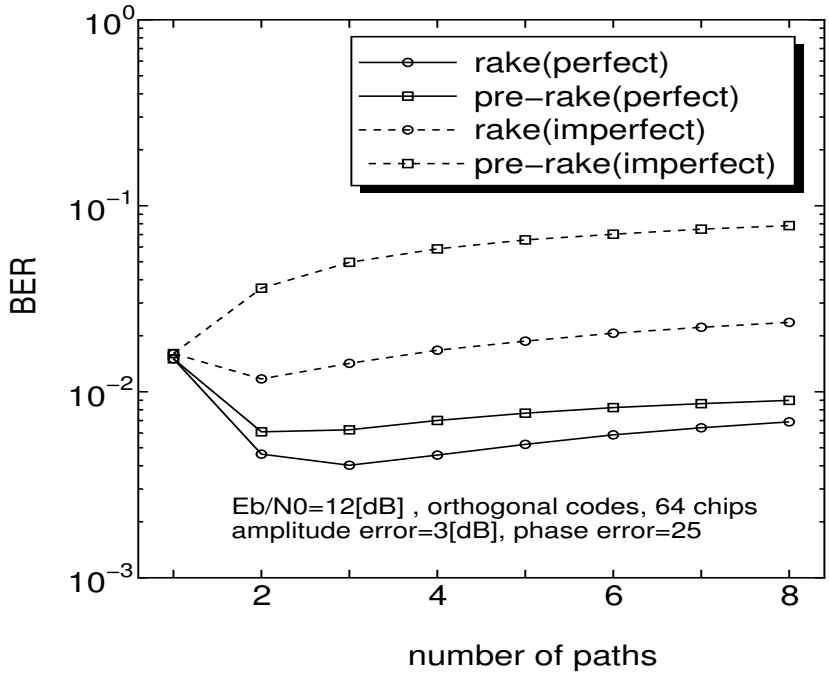

Figure 2.11: BER vs. number of paths for multi-user system

Chapter 3

PAPR Reduction using Joint Transmission Technique

This chapter performs proposal of PAPR reduction technique using modified JT in TDD-CDMA system. Background of this chapter is firstly introduced in section 3.1. Section 3.2 discusses conventional JT and JD techniques. In section 3.3, PAPR about CDMA, DS-CDMA and TD-SCDMA is discussed. Discussion for PAPR of JT-TD-SCDMA in section 3.3.3 is divided into two subsection; single path and multipath because of their different behavior, where multipath causes a high PAPR in JT-TD-SCDMA. The proposal to reduce PAPR for the multipath JT-TD-SCDMA is described in section 3.4. The, we present SNR and BER evaluation for proposed techniques in section 3.5. The results of numerical analysis and computer simulations are compared, and discussed in section 3.6. This chapter is finally concluded in section 3.7.

3.1 Background

TDD-CDMA is based on time slotted CDMA, where UL and DL are divided by time. TD-SCDMA, one of the TDD interfaces, has been selected by 3GPP for 3G mobile radio systems

[14][40] and used as Chinese 3G interface since 2008. In current TD-SCDMA, JD has been used to reduce ISI and MAI. In JD, MS needs a channel estimator to estimate channel impulse responses (CIRs) used for the process. This causes complexity in MS due to the significant calculation overhead imposed by JD processing. The complexity in MS can be avoided by using TDD channel state feature. In TDD, as UL and DL are divided by time, where channel condition does not vary too much, CIRs estimated in UL can be used in DL. Note that it is under assumption that the time offset between UL and DL is sufficiently small. Using this feature, JT has been proposed in [29][30] to reduce ISI and MAI without causing complexity at MS. The concept of JT is all of the JD functions in MS are moved to BS and done before transmission. Only a simple filter is needed at MS for data detection.

On the other hand, PAPR is an important factor in realizing a low cost communication system. Higher PAPR will require an expensive power amplifier with a good linearity characteristic. A lot of PAPR studies of CDMA system concentrate on UL system to realize low cost of MS [41][42]. However, in the future network such as IMT-advanced, a small BS known as relay station (RS) may be implemented [12]. Thus, it is also important to have a small PAPR for DL transmitter at RS. The implementations of JT causes large transmit signal power compared to that of conventional JD in [29]. This phenomenon may affect PAPR. As CIRs are used before transmission in JT, multipath condition might also affect the transmitted signal, and PAPR performance.

In this study, we investigate PAPR of JT-TD-SCDMA system for both a single and multipath conditions. We further propose a new approach of JT technique that maintains low PAPR of the TD-SCDMA system. The new technique is done by selecting certain paths instead of all the paths in CIRs for JT processing. The path selection is done using two different methods; one by taking certain paths from all the paths and the other by taking paths having path gains above a certain threshold value. We also combine the proposed path selection technique with clipping, a common PAPR reduction technique. We evaluate PAPR and BER of conventional JT and all the proposed techniques by computer simulation.

We show that the proposed path selection techniques perform lower PAPR and better BER performance than those in the conventional JT processing. We also show that the combination of path selection technique and clipping performs low PAPR performance without severe BER degradation compared to those in the clipping technique.

In this study, simulation parameters are based on current TD-SCDMA system. The equivalent low pass representation of signals and channel transfer functions are chosen. Complex quantities are underlined, and vectors and matrices are shown in boldface. The element in the ith row and jth column of a matrix is denoted by $[.]_{i,j}$. The symbol $(.)^T$ and $(.)^{*T}$ designate transposition and conjugate transposition, respectively.

3.2 Joint Detection vs. Joint Transmission

Joint Detection

JD which is also known as multiuser detection is widely investigated owing to its ability to eliminate both ISI and MAI. To present JD technique using equations, we use Fig. 3.1 to show discrete-time baseband model of a block transmission CDMA system.

A system with K users access the same channel at the same time and frequency band with linear data modulation is considered. Each user transmits a data symbol sequence

$$\mathbf{d}^{(k)} = (d_1^{(k)}, d_2^{(k)}, ..., d_N^{(k)}),\ k = 1...K, \tag{3.1}$$

consisting of N elements at symbol interval T_s. The N values should not be the same for all users K because each users might consumes different data rates. Each data symbls $d_n^{(k)}, n = 1...N$ of user k is reapeated Q times. This requires Q-dimensional vector of the sinature sequence that needed for spreading process, defined as follows:

$$\mathbf{c}^{(k)} = (c_1^{(k)}, c_2^{(k)}, ..., c_Q S^{(k)}),\ k = 1...K, \tag{3.2}$$

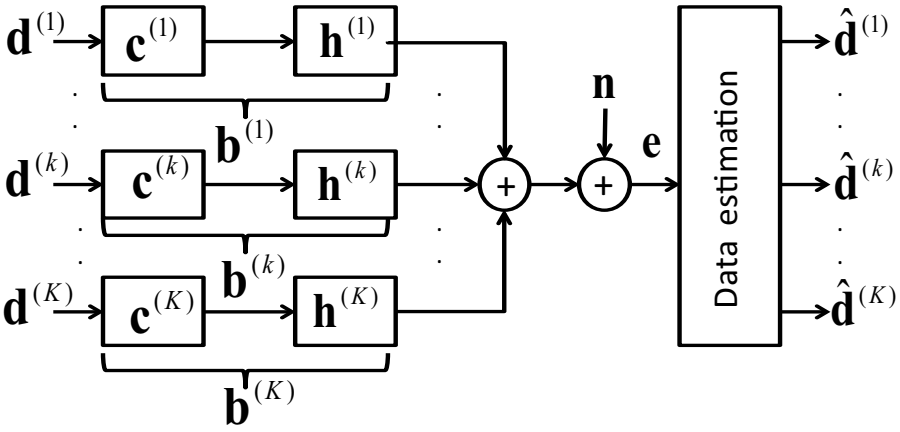

Figure 3.1: Discrete-time baseband model of a block transmission CDMA system

where Q is a number of chip or spreading factor at chip interval $T_c = T_s/Q$. Here, each K channels is characterized by its impulse response defined in W length of vector

$$\mathbf{h}^{(k)} = (h_1^{(k)}, h_2^{(k)}, ..., h_W^{(k)}),\ k = 1...K, \tag{3.3}$$

where W represents the number of paths at chip interval T_c.

The combined channel impulse response with spreading sequences is defined as

$$\mathbf{b}^{(k)} = (b_1^{(k)}, b_2^{(k)}, ..., b_{Q+W-1}^{(k)}) = \mathbf{c}^{(k)} * \mathbf{h}^{(k)},\ k = 1...K, \tag{3.4}$$

The received sequence e is obtained at the chip rate. It is a sum of K sequences, each of length $N.Q + W - 1$, that are supposed to arrive synchronously, with an additive stationary noise sequence

$$\mathbf{n} = (n_1, n_2, ..., n_{N.Q+W-1}), \tag{3.5}$$

with zero mean and covariance matrix $\mathbf{R} = E(\mathbf{n}.\mathbf{n}^H)$ [43].

The received sequence $\mathbf{e}$ can be written as

$$\mathbf{e} = (e_1, e_2, ..., e_{N.Q+W-1}) = \mathbf{A}\mathbf{d} + \mathbf{n}, \tag{3.6}$$

where vector $\mathbf{d}$ consists of a total transmitted data for K users defined as

$$\mathbf{d} = (\mathbf{d}^{(1)} \dots \mathbf{d}^{(K)}) = (d_1 .... d_{KN}) \tag{3.7}$$

and $\mathbf{A}$ represents a system matrix fro JD defined as

$$\mathbf{A} = (A_{i,j}); i = 1...N.Q + W - 1,\ j = 1...K.N, \tag{3.8}$$

$$A_{Q(n-1)+l,n+N(k-1)} = \begin{cases} b_l^{(k)}, & \text{for } k = 1 \dots K, n = 1 \dots N, \\ & \quad l = 1 \dots Q + W - 1 \\ 0, & \text{else} \end{cases} . \tag{3.9}$$

The received data $\mathbf{e}$ has to be processed in a detector to obtain decisions on the transmitted data symbols sequences $\mathbf{d}^{(k)}, k = 1...K$. Using Zero forcing (ZF) block linear equalizer, the detected data can be shown as [25]

$$\hat{\mathbf{d}} = (\mathbf{A}.\mathbf{A}^H)^{-1}\mathbf{A}^H\mathbf{e}. \tag{3.10}$$

Substuting (3.6) into (3.10), the detected data $\hat{\mathbf{d}}$ is only consists of desired data $\mathbf{d}$ and noise $\mathbf{n}$. This means by applying ZF JD, the MAI and ISI can be perfectly eliminated. However, theperformance of ZF JD degrades when a large noise exists.

In JD, the data detection from K users is done in receiver, which cause complexity and delay at receiver. This is undesirable for downlink transmission because low cost MS must be realized for future wireless communication s system.

Joint Transmission

In JT, all of the process in JD is moved to the transmitter. The MAI and ISI elimination is done in transmitter before transmission. This can realize a low cost MS for downlink system, where all the JD function in MS is moved to the BS.

The transmit signal of a single-input single-output (SISO) antenna can be defined as

$$\hat{\mathbf{s}} = (s_1^{(k)}.....s_{Q.N})^T. \tag{3.11}$$

of length QN.

With the channel impulse responses $\mathbf{h}^{(k)}$ defined as (3.3) in previous subsection, the $[QN + W - 1] \times [QN]$ matrices

$$\begin{aligned} \mathbf{H}^{(k)} &= (H_{i,j}^{(k)}), i = 1, \ldots, QN + W - 1 \\ & j = 1, \ldots, QN, k = 1, \ldots, K. \end{aligned} \tag{3.12}$$

$$H_{i,j}^{(k)} = \begin{cases} h_{i-j+1}^{(k)}, & \text{for } 1 \leq i - j + 1 \leq W \\ 0, & \text{else} \end{cases}. \tag{3.13}$$

The CIRs matrices $\underline{\mathbf{H}}$ in (3.12) for all users can be stacked as $K[QN + W - 1] \times [QN]$ matrix as

$$\mathbf{H} = (\mathbf{H}^{(1)^T}...\mathbf{H}^{(K)^T})^T. \tag{3.14}$$

Using transmitted signal $\mathbf{s}$ in (3.11), the received signal of length $QN + W - 1$ at k user can be defined as

$$\mathbf{e}^{(k)} = \mathbf{H}^{(k)}\mathbf{s}. \tag{3.15}$$

The total reiceived signal of K users can be stacked into $K(QN+W-1)$ vector as

$$\mathbf{e} = (\mathbf{e}^{(1)^T} \dots \mathbf{e}^{(K)^T})^T. \tag{3.16}$$

The received signal $\mathbf{e}$ corresponds to the reception of one TDMA burst. By using (3.14) and (3.11), the total recieved signal of (3.16) can be written as

$$\mathbf{e} = \mathbf{H}\mathbf{s}. \tag{3.17}$$

Note that the correlation between channel duration is sufficiently large than TDMA burst duration, which should be considered when designing a system.

To show data detecion process, we perform transmitted signal using transmitted data in (3.1) as follow:

$$\mathbf{s} = \mathbf{M}\mathbf{d}, \tag{3.18}$$

where $\mathbf{M}$ is a modulator matrix and has to be known at transmitter to perform modulation. Note that the JT process and calculation is done in the matrix $\mathbf{M}$, which is described latter.

To perform data detection in MS, a matrix $\mathbf{D}^{(k)}$ with $[KN] \times [QN+W-1]$ size is multiplied with the partial received signal $\mathbf{e}^{(k)}$. The matrix $\mathbf{D}^{(k)}$ consits of spreading sequences. The matrix $\mathbf{D}^{(k)}$ is assumed to be known in both BS and MS. The desired data after detection process can be defined as:

$$\hat{\mathbf{d}}^{(k)} = \mathbf{D}^{(k)}\mathbf{e}^{(k)}. \tag{3.19}$$

The detected data must consist of desired data without MAI and ISI as same as JD to avoid performance degradation because of the change. Substituting (3.18) into (3.19),the detected data can be written as

$$\hat{\mathbf{d}}^{(k)} = \mathbf{D}^{(k)}\mathbf{H}^{(k)}\mathbf{s}. \tag{3.20}$$

Here the partial detector matrix $\mathbf{D}^{(k)}$ can be stacked into a total detector matrix with $[KN] \times [K(QN + W - 1)]$ size as

$$\mathbf{D} = \text{blockdiag}[\mathbf{D}^{(1)} \dots \mathbf{D}^{(K)}], \tag{3.21}$$

where blockdiag($\mathbf{A}$) represents block diagonal matrix for matrix $\mathbf{A}$, defined as

$$\underline{\mathbf{A}} = \begin{pmatrix} \underline{\mathrm{A}}_1 & 0 & \dots & 0 \\ 0 & \underline{\mathrm{A}}_2 & \dots & 0 \\ \vdots & \vdots & \ddots & \vdots \\ 0 & 0 & \dots & \underline{\mathrm{A}}_n \end{pmatrix}, \tag{3.22}$$

where $\underline{\mathrm{A}}_n$ is a square matrix, with $[n] \times [n]$ size.

Following shows matrix $\mathbf{D}$ for $K = 2$, $Q = 4$, $N = 3$, $W = 2$,

$$\underline{\mathbf{D}} = \begin{pmatrix} D^{(1)}_{1,1} & D^{(1)}_{2,1} & D^{(1)}_{3,1} & 0 & 0 & 0 \\ D^{(1)}_{1,2} & D^{(1)}_{2,2} & D^{(1)}_{3,2} & 0 & 0 & 0 \\ \vdots & \vdots & \vdots & \vdots & \vdots & \vdots \\ D^{(1)}_{1,QN+W-1} & D^{(1)}_{2,QN+W-1} & D^{(1)}_{3,QN+W-1} & 0 & 0 & 0 \\ 0 & 0 & 0 & D^{(2)}_{1,1} & D^{(2)}_{2,1} & D^{(2)}_{3,1} \\ 0 & 0 & 0 & D^{(2)}_{1,2} & D^{(2)}_{2,2} & D^{(2)}_{3,2} \\ \vdots & \vdots & \vdots & \vdots & \vdots & \vdots \\ 0 & 0 & 0 & D^{(2)}_{1,QN+W-1} & D^{(2)}_{2,QN+W-1} & D^{(2)}_{3,QN+W-1} \end{pmatrix}, \tag{3.23}$$

where $D_{n,l}^{(k)}, k = 1 \dots K, n = 1 \dots N, l = 1 \dots QN + W - 1$.

Here, from matrix $\mathbf{D}$ that consists of spreading sequences and $\mathbf{H}$ that consist of channel impulse responses, a system matrix $\mathbf{B}$ can be defined as

$$\mathbf{B} = \mathbf{DH}. \tag{3.24}$$

From (3.20), $\mathbf{d}$ can also be defined as

$$\mathbf{d} = \mathbf{Bs}. \tag{3.25}$$

By substituting (3.18) into (3.25), the desired data can also be written as

$$\mathbf{d} = \mathbf{BMd}, \tag{3.26}$$

where $\mathbf{M}$ is a modulator matrix and should be determined to derive a detected data without MAI and ISI.

There are three cases to determine $\mathbf{M}$, depends on number of user K and spreading factor Q as follows

$$\underline{\mathbf{s}} = \underline{\mathbf{B}}^{*T}(\underline{\mathbf{BB}}^{*T})^{-1}\underline{\mathbf{d}} \quad \text{for} \quad K < Q. \tag{3.27}$$

$$\mathbf{s} = (\mathbf{B})^{-1}\mathbf{d}, \quad \text{for} \quad K = Q, \tag{3.28}$$

$$\mathbf{s} = (\mathbf{BB}^{*T})^{-1}\mathbf{B}^{*T}\mathbf{d}, \quad \text{for} \quad K > Q. \tag{3.29}$$

3.3 Peak-to-Average Power-Ratio

PAPR is one of the main topic in wireless communication because it affects structure of transmitter. A high PAPR of transmitted signal needs an efficient and expensive power amplifier to avoid signal distortion. The signal distortion occurs owing to power amplifier unlinearity characteristic. The power amplifier that operates in linear reduces power amplifier efficiency, hence, increase power consumption. This is undesirable in wireless communication because it increases cost of devices and reduce battery lifetime. Amplifier efficiency can be increased by using signaling format with a low PAPR.

Most researches in PAPR focus on OFDM system, because the multicarrier transmission causes a high PAPR [44], [45]. Many PAPR reduction techniques are also proposed for OFDM transmission. Some techniques including clipping [46], clipping and filtering [47], coding [48] and selected mapping [49] are proposed for PAPR reduction.

The PAPR of any continuous-time signal $u(t)$ is defined as the ratio of the peak envelope power to the average envelope power, can be expressed as

$$PAPR = \frac{\max(|u(t)|^2)}{P_{\text{av}}}, \tag{3.30}$$

where $P_{\text{av}} = (1/T)\int_0^T |u(t)|^2 dt$ is the average envelope power of $u(t)$ and T is a symbol length.

3.3.1 DS-CDMA

In this study, we focus on PAPR for DS-CDMA system. Even the PAPR for DS-CDMA system is lower than that in OFDM system, the PAPR problem should be considered, because the PAPR should be kept as low as possible to realize low cost device. In DS-CDMA, three main factors can influence PAPR value of transmitted signal as follows:

- Orthogonal Code Dependency

The complex envelope of a CDMA downlink signal can be expressed as:

$$u(t) = \sum_{l=1}^{L} (\lambda_l PN_I(l) + j\lambda_l PN_Q(l)) p(t - lT_c) \tag{3.31}$$

where L is the number of chips per bit duration, T_b, λ_l is defined as the digital transmission sequence given by

$$\lambda_l = \sum_{k=0}^{K-1} d_k w_k(l) \tag{3.32}$$

where k is the number of users of K users, d_k represents data bit for user k, $w_k(l)$ represents lth chip of orthogonal code assigned to user k, PN_I and PN_Q are pseudo-random short codes, and $p(t)$ is the transmission pulse shape. λ_l depends on the orthogonal code and the applied data bit d_l. Due to the band-limited nature of channel, the pulse width of p_t will generally span over several chip that causes inter-chip interference. Due to the fact that different users share the same PN sequence, a certain combination of orthogonal codes and data bits could result a particular digital transmit sequence λ_l that has a higher peak power compared with the others.

Figures 3.2 and 3.3 show digital transmit sequences for a bad and good combination of orthogonal codes and data bits, resepectively. Figure 3.2 represents digital transmit sequences for orthogonal code set $= w_0, w_{32}, w_{16}, w_{48}, d_k(1) = 1, 1, 1, 1$ while Fig. 3.3 represents $= w_0, w_1, w_{33}, w_{49}, d_k(1) = 1, 1, 1, 1$. In Fig. 3.2, consecutive peaks at $l = 14, 15, 16$ causes overlapping among transmit pulse $p(t)$, causing a high peak.

On the other hand, a smaller peak can be seen in Fig. 3.3, because the combination of orthogonal codes and data bits do not cause consecutive peak.

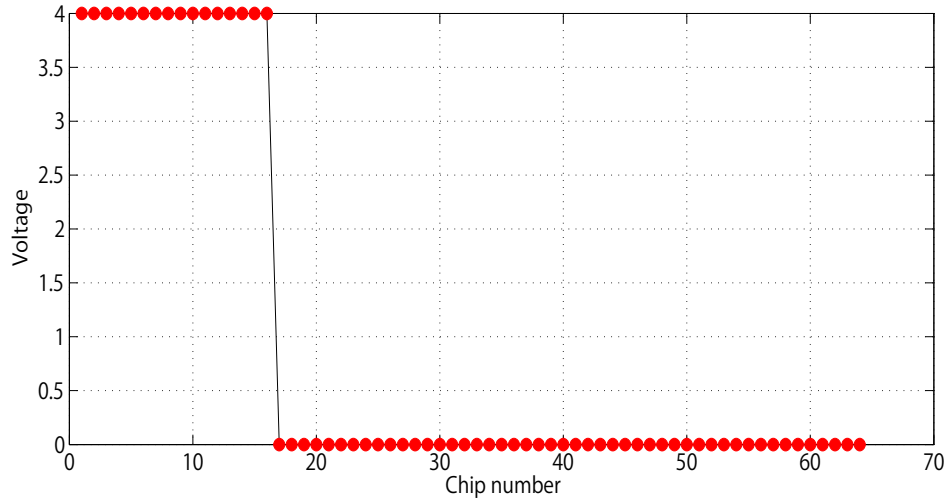

Figure 3.2: Transmit digital sequence of 4 users: bad orthogonal code combination

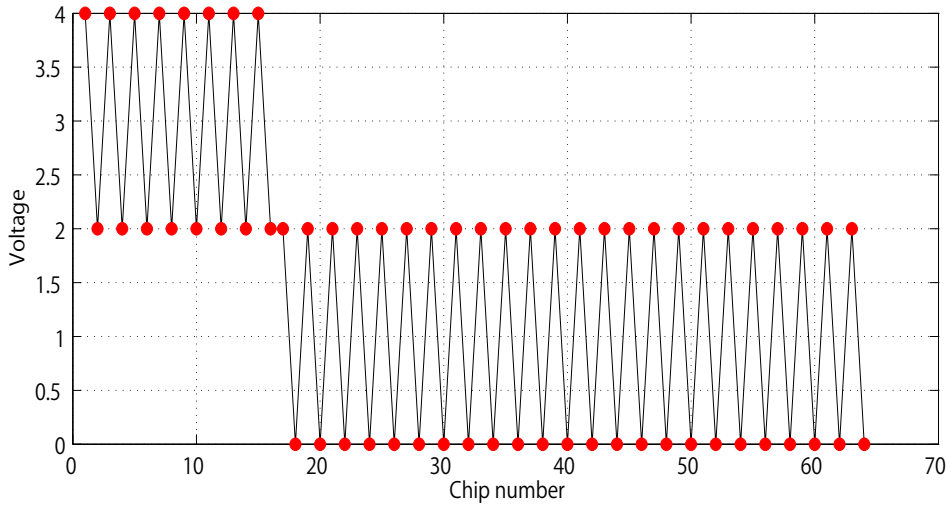

Figure 3.3: Transmit digital sequence of 4 users: good orthogonal code combination

- Modulation Scheme

  The complex envelope of DS-CDMA for downlink is defined as:

$$s(t) = \sum_{l}^{L} (\lambda_l^I + j\lambda_l^Q)(PN_I(l) + PN_Q(l))p(t - T_c), \tag{3.33}$$

  where

$$\begin{aligned} \lambda_l^I &= \sum_{k=0}^{K} d_k^I w_k(l) \\ \lambda_l^Q &= \sum_{k=0}^{K} d_k^Q w_k(l) \end{aligned} \tag{3.34}$$

  We consider BPSK and QPSK to show that modulation scheme affects PAPR value. For BPSK, I and Q phase of transmitted signal are defined as:

$$\begin{aligned} s_I &= \sum_{l} \lambda_l PN_I(l)p(t - T_c) \\ s_Q &= \sum_{l} \lambda_l PN_Q(l)p(t - T_c). \end{aligned} \tag{3.35}$$

  Here, as the PN_I and PN_Q are independent pseudo-random binary sequences $+1, -1$, they just toggle the sign of the peaks. Peak position is influenced by digital transmission sequence λ_l. From (3.35), we can see that the same λ_l affects trasmission signal of I phase and Q phase. This means that the I phase and Q phase are highly correlated.

  For QPSK is applied the I and Q phase of transmitted signal are defined as:

$$\begin{aligned} s_I &= \sum_{l} \lambda_l^I PN_I(l)p(t - T_c) \\ s_Q &= \sum_{l} \lambda_l^Q PN_Q(l)p(t - T_c). \end{aligned} \tag{3.36}$$

We can see that the different transmit digital sequence λ_l^I and λ_l^I are multiplied in QPSK scheme. From (3.34), λ_l^I is determined by data bits d_k^I and λ_l^Q is determined by data bits d_k^Q. This means that the magnitude of I and Q phase become uncorrelated when QPSK is applied.

Here, the transmission power is calculated as $\sqrt{s_I^2 + s_Q^2}$. A large peak occurs when both I and Q phase are in large magnitude. Highly correlated I and Q phase signals causes high peak power. Thus, the QPSK signaling performs a lower PAPR than that in BSPK signaling. Note that (3.36) is done using real spreading to investigate the QPSK effect. The effect of spreading scheme in PAPR will be discussed in the next subsection.

- Spreading scheme

  In DS-CDMA system, spreading scheme can be divided into real spreading and complex spreading. In real spreading, data bits are multiplied with a real orthogonal codes set. In complex spreading, channelization code spesific multiplier (CCSM) is multiplied after spreading process, to realize both I and Q phase spreading. As described in previous subsection, PAPR becomes high if both I and Q phase in a large magnitude. It has been desribed in [42] that unbalance between I and Q phase causes a high PAPR. Using the complex spreading IQ imbalance can be avoided and a low PAPR can be achieved.

3.3.2 TD-SCDMA

For the conventional TD-SCDMA system, when K users are active, transmitted signal for the qth chip is expressed as

$$s(t) = \sum_{k=1}^{K} \sum_{q=1}^{Q} \sum_{n=1}^{N} d_{k,n} c_k(q) e^{j\omega t}, \tag{3.37}$$

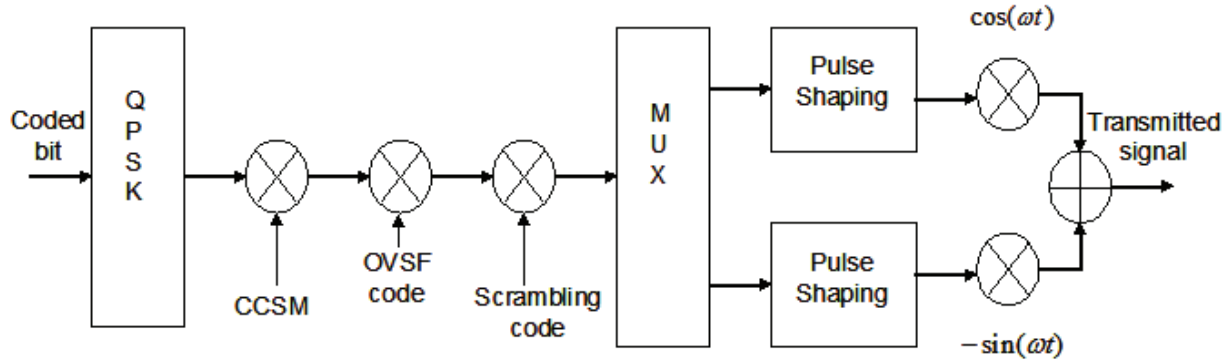

Figure 3.4: Transmitter block diagram of TD-SCDMA system

where Q is the number of chips in one symbol, i.e. spreading factor, N is the total number of data transmitted by one user, d is binary complex data, c represents complex spreading codes, and ω is a carrier frequency. From (3.30) and (3.37), PAPR for TD-SCDMA system can be expressed as

$$PAPR = \frac{\max(|s(t)|^2)}{P_{\text{av}}}, \tag{3.38}$$

where $P_{\text{av}} = (1/T)\sum_{t=0}^{T}|s(t)|^2$ is the average envelope power of $s(t)$ and T represents the number of chips within a symbol period. Note that PAPR is calculated within a symbol period.

Figure 3.4 shows a transmitter block diagram for TD-SCDMA system. In TD-SCDMA, complex QPSK symbols of multicode MS are multiplied by a channelization code specific multiplier (CCSM) consisting of 16 complex numbers, $\{(i+j),(i-j),(-i+j),(-i-j)\}$. Then the signal is spread with channelization codes, also known as the orthogonal-variable-spreading-factor (OVSF) codes. After spreading, the chip rate signals are further multiplied with scrambling codes. Finally, the real and imaginary parts of the chip sequence are passed through root raised cosine (RRC) filters and up-converted to the desired carrier frequency.

PAPR of CDMA system is influenced by three main factors; modulation technique,

spreading technique, and orthogonal code dependency. Studies of PAPR proved that QPSK modulation technique can perform lower PAPR than BSPK [42]. Also, it has been proved that complex spreading can reduce PAPR. This is because, when the complex spreading is done, spreading codes consisting of complex binary codes $[\pm 1, \pm j]$ are multiplied with transmitted data, I signal and Q signal being uncorrelated in magnitude. Note that overall peak of the complex envelope is given by $\sqrt{s_I^2 + s_Q^2}$. The symbol s_I and s_Q represent a real part and imaginary part of transmitted signal s, respectively. A large peak will occur only when both I and Q signals are large in magnitude. By using complex spreading, I and Q signals can be spread independently and phenomenon of large magnitude for both I and Q signals can be mitigated. In orthogonal code dependency aspect, certain combination of orthogonal codes and data bits could result in high peak compared with other combinations.

In current TD-SCDMA system, PAPR reduction is done by implementation of QPSK modulation and complex spreading by assigning CCSM into OVSF spreading code. However, as orthogonal code is used in the TD-SCDMA signal, a combination of certain orthogonal codes with data bits causes a high peak, leading to high PAPR value.

3.3.3 Joint Transmission TD-SCDMA

Figure 3.5 shows transmission scheme for conventional JD and JT. In Fig. 3.5, $\underline{\mathbf{d}}$, $\underline{\mathbf{s}}$, $\underline{\mathbf{e}}$, $\underline{\mathbf{n}}$, and $\underline{\hat{\mathbf{d}}}$ represent a transmitted data vector from BS to MS, a transmitted signal vector, a received signal vector, a noise vector, and a detected data vector in MS, respectively. $\underline{\mathbf{M}}$ refers to modulator matrix at BS, and $\underline{\mathbf{D}}$ is a demodulator matrix, both contain different components for JD and JT.

In JT, as derived in [29], total transmitted signal from BS to MSs, is defined vector $\underline{\mathbf{s}}$

$$\underline{\mathbf{s}} = \underline{\mathbf{B}}^{*T}(\underline{\mathbf{B}}\underline{\mathbf{B}}^{*T})^{-1}\underline{\mathbf{d}}, \tag{3.39}$$

of length QN, where

$$\underline{\mathbf{s}} = (s_1, s_2, ..., s_{QN}). \tag{3.40}$$

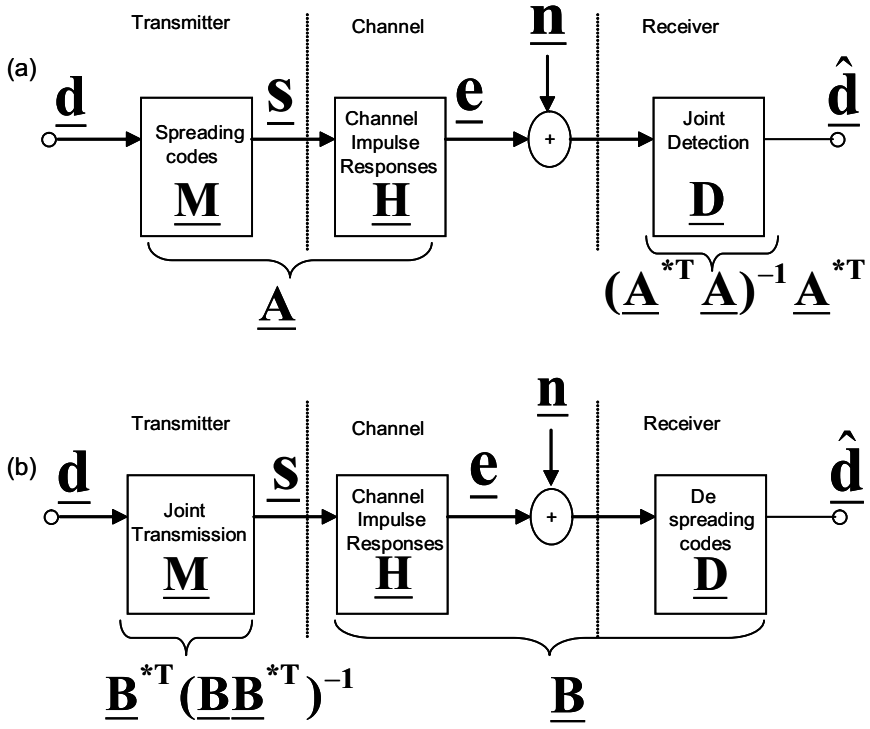

Figure 3.5: Transmission schemes for (a) JD (b) JT

Q is a total number of chips within a symbol, and $\underline{\mathbf{d}}$ is the total transmitted data from BS to MS of K users and can be calculated as

$$\underline{\mathbf{d}} = (\underline{\mathbf{d}}^{(1)^T} ... \underline{\mathbf{d}}^{(K)^T}) = (d_1, ..., d_{KN})^T. \tag{3.41}$$

The elements $\underline{\mathbf{d}}^{(k)}$, $k = 1, ..., K$ of the data vector $\underline{\mathbf{d}}$ are assumed to be independent and identically distributed (i.i.d.) with unit variance of real and imaginary parts. For the covariance matrix, it follows:

$$\underline{\mathbf{R}}_{\underline{\mathbf{d}}} = \mathrm{E}\{\underline{\mathbf{d}}\underline{\mathbf{d}}^{*T}\} = 2\underline{\mathbf{I}}, \tag{3.42}$$

where $\underline{\mathbf{I}}$ is an identity matrix. In this paper, QPSK modulation is assumed, i.e., the element $\underline{\mathbf{d}}^{(k)}$ of the data vector $\underline{\mathbf{d}}$ are taken from alphabet $\{(i+j), (i-j), (-i+j), (-i-j)\}$.

Note that $\underline{\mathbf{s}}$ in (3.39) is only for a system that having the number of users smaller than

spreading factor case $[K < Q]$. For other cases, the transmitted vector $\underline{\mathbf{s}}$ can be defined as [29]

$$\underline{\mathbf{s}} = (\underline{\mathbf{B}})^{-1}\underline{\mathbf{d}}, \quad \text{for} \quad K = Q, \tag{3.43}$$

and

$$\underline{\mathbf{s}} = (\underline{\mathbf{B}}\underline{\mathbf{B}}^{*T})^{-1}\underline{\mathbf{B}}^{*T}\underline{\mathbf{d}}, \quad \text{for} \quad K > Q. \tag{3.44}$$

For simplicity, a SISO (single-input single-output) antenna system is assumed. $\underline{\mathbf{B}}$ is a JT system matrix consisting of spreading code matrix $\underline{\mathbf{C}}$ and CIRs matrix $\underline{\mathbf{H}}$, expressed as

$$\underline{\mathbf{B}} = \underline{\mathbf{C}}^{*T}\underline{\mathbf{H}}. \tag{3.45}$$

$\underline{\mathbf{C}}^{*T}$ is a $[KN] \times [K(QN + W - 1)]$, shown as $\underline{\mathbf{D}}$ in Fig. 3.5. The matrix $\underline{\mathbf{D}}$ contains total spreading codes for K users and can be calculated as

$$\underline{\mathbf{C}}^{*T} \quad = \quad \text{blockdiag}[\underline{\mathbf{C}}^{(1)} \dots \underline{\mathbf{C}}^{(K)}], \tag{3.46}$$

where blockdiag[.] represents a block matrix, where the off-diagonal blocks are zero matrices, and the main diagonal matrices are square matrices. Spreading codes for kth user can be described as

$$\begin{aligned} \underline{\mathbf{C}}^{(k)} \quad &= \quad (C_{i,j}^{(k)}),\ i = 1, \dots, QN + W - 1 \\ &\qquad j = 1, \dots, N,\ k = 1, \dots, K. \end{aligned}$$

$$C_{i,j}^{(k)} = \begin{cases} c_{i-Q(j-1)}^{(k)}, & \text{for } 1 \le i - Q(j-1) \le Q \\ 0, & \text{else} \end{cases}. \tag{3.47}$$

At the BS CIRs of kth user of length W can be defined as

$$\underline{\mathbf{h}}^{(k)} = (h_1^{(k)}, ..., h_W^{(k)}). \tag{3.48}$$

With the CIRs, a total CIRs of $[QN+W-1]\times[QN]$ matrices for all users can be expressed as

$$\underline{\mathbf{H}}^{(k)} = (H_{i,j}^{(k)}), i = 1,\ldots,QN+W-1$$
$$j = 1,\ldots,QN, k = 1,\ldots,K. \tag{3.49}$$

$$H_{i,j}^{(k)} = \begin{cases} h_{i-j+1}^{(k)}, & \text{for } 1 \le i-j+1 \le W \\ 0, & \text{else} \end{cases}. \tag{3.50}$$

The CIRs matrices $\underline{\mathbf{H}}$ in (3.45) for all users can be stacked as $K[QN+W-1]\times[QN]$ matrix as

$$\underline{\mathbf{H}} = (\underline{\mathbf{H}}^{(1)^T}...\underline{\mathbf{H}}^{(K)^T})^T. \tag{3.51}$$

By using (3.38) and (3.39), PAPR for N data of JT TD-SCDMA can be calculated as a vector

$$\underline{\mathbf{PAPR}} = \begin{pmatrix} \frac{\max|s_i^2|}{\frac{1}{Q}\sum_{i=1}^{Q}|s_i^2|} \\ \frac{\max|s_i^2|}{\frac{1}{Q}\sum_{i=Q+1}^{2Q}|s_i^2|} \\ . \\ . \\ \frac{\max|s_i^2|}{\frac{1}{Q}\sum_{i=Q(N-1)+1}^{QN}|s_i^2|} \end{pmatrix}. \tag{3.52}$$

of length N. The $\max|s_i^2|$ represents peak power of transmitted signal s_i, $i = 1,...,QN$, and calculated within spreading factor Q. The denominator $\frac{1}{Q}\sum_{i=1}^{Q}|s_i^2|$ represents average

power of transmitted signal s_i within spreading factor Q. As the PAPR is calculated within spreading factor, the PAPR for transmitted signal s of length QN can be derived as a vector of length N as shown in (3.52).

Single Path Behavior

In a single path environment, the elements of the matrix $\underline{\mathbf{B}}$ can be expressed as

$$\underline{\mathbf{B}} = \underline{\mathbf{C}}^{*T}\underline{\mathbf{H}} \begin{pmatrix} \underline{\mathbf{B}}^{(1)} & \mathbf{0}_{1,4} \\ \mathbf{0}_{1,4} & \underline{\mathbf{B}}^{(1)} \\ \underline{\mathbf{B}}^{(2)} & \mathbf{0}_{1,4} \\ \mathbf{0}_{1,4} & \underline{\mathbf{B}}^{(2)} \end{pmatrix}, \tag{3.53}$$

where $\underline{\mathrm{B}}^{(1)}$, $\underline{\mathrm{B}}^{(2)}$, and $0_{1,4}$ are described as

$$\underline{\mathbf{B}}^{(1)} = \begin{pmatrix} B_1^{(1)} & B_2^{(1)} & B_3^{(1)} & B_4^{(1)} \end{pmatrix}, \tag{3.54}$$

$$\underline{\mathbf{B}}^{(2)} = \begin{pmatrix} B_1^{(2)} & B_2^{(2)} & B_3^{(2)} & B_4^{(2)} \end{pmatrix}, \tag{3.55}$$

$$\mathbf{0}_{1,4} = \begin{pmatrix} 0 & 0 & 0 & 0 \end{pmatrix}. \tag{3.56}$$

$B_q^{(k)}$ represents a system matrix, contains spreading code and CIR for kth user at qth chip within a symbol. For example, $B_1^{(1)}$ represents a system matrix for user 1 at 1st chip. The spreading codes are used to spread nth data. Note that $q = 1, ..., Q$, $w = 1, ..., W$, and $k = 1, ..., K$.

To discuss behavior of single path JT-TD-SCDMA, the matrix is calculated for $K = 2$ users, $Q = 4$ spreading factor, $N = 2$ transmitted data per user case. For a single path JT, using (3.45), where $W = 1$, the elements of $\underline{\mathbf{B}}^{(1)}$ and $\underline{\mathbf{B}}^{(2)}$ in $\underline{\mathbf{B}}$ can be calculated as

$$\begin{aligned} B_1^{(1)} &= c_1^{(1)} h_1^{(1)}, \\ &\vdots \\ B_4^{(1)} &= c_4^{(1)} h_1^{(1)}, \\ B_1^{(2)} &= c_1^{(2)} h_1^{(2)}, \\ &\vdots \\ B_4^{(2)} &= c_4^{(2)} h_1^{(2)}. \end{aligned} \tag{3.57}$$

From (3.57), we can see that each element of $\underline{\mathbf{B}}^{(1)}$ and $\underline{\mathbf{B}}^{(2)}$ in $\underline{\mathbf{B}}$ contains spreading code and single path CIR.

Multipath Behavior

When multipath channel case is considered, each element in the system matrix $\underline{\mathbf{B}}$ contains multipath CIRs. This can be expressed in the following matrix (for $W = 2$ paths case)

$$\begin{aligned} \underline{\mathbf{B}} &= \underline{\mathbf{C}}^{*T} \underline{\mathbf{H}} \\ &= \begin{pmatrix} \underline{\mathbf{B}}^{(1)} & 0 & \mathbf{0}_{1,4} \\ \mathbf{0}_{1,3} & \hat{B}_4^{(1)} & \underline{\mathbf{B}}^{(1)} \\ \underline{\mathbf{B}}^{(2)} & 0 & \mathbf{0}_{1,4} \\ \mathbf{0}_{1,3} & \hat{B}_4^{(2)} & \underline{\mathbf{B}}^{(2)} \end{pmatrix}, \end{aligned} \tag{3.58}$$

where $\underline{\mathrm{B}}^{(1)}$, $\underline{\mathrm{B}}^{(2)}$, and $0_{1,4}$ are described as in (3.54), (3.55) and (3.56), respectively. $0_{1,3}$ is defined as:

$$\mathbf{0}_{1,3} = \begin{pmatrix} 0 & 0 & 0 \end{pmatrix}. \tag{3.59}$$

Here, each element of (3.58) can be expressed as

$$\begin{aligned} B_1^{(1)} &= c_1^{(1)}h_1^{(1)} + c_2^{(1)}h_2^{(1)}, \\ &\vdots \\ B_4^{(1)} &= c_4^{(1)}h_1^{(1)}, \\ \hat{B}_4^{(1)} &= c_1^{(1)}h_2^{(1)}, \\ B_1^{(2)} &= c_1^{(2)}h_1^{(2)} + c_2^{(2)}h_2^{(2)}, \\ &\vdots \\ B_4^{(2)} &= c_4^{(2)}h_1^{(2)}, \\ \hat{B}_4^{(2)} &= c_1^{(2)}h_2^{(2)}. \end{aligned} \tag{3.60}$$

From (3.60), some elements of the system matrix $\underline{\mathbf{B}}$ contain multipath CIRs. For example, in $B_1^{(1)}$, all paths are multiplied with spreading code and inserted together in one matrix. This will cause a high transmit signal power for the corresponding chip. However, the multipath JT does not increase the whole transmitted signal. It can be seen in $B_4^{(1)}$, where only single path CIR is inserted in one matrix. This will cause a low transmit signal power for the corresponding chip. A presence of signals like $B_1^{(1)}$ in $\underline{\mathbf{B}}$ causes peak, while a presence of signals like $B_4^{(1)}$ causes a low power. The difference of power level for elements in $\underline{\mathbf{B}}$ causes a high peak for certain signal, and low average power within a symbol, leading to high PAPR. The difference of power level is larger if more paths present in the channel; i.e. some elements contain signal from all paths while the others contain signals from only one path.

3.4 Proposed Joint Transmission Technique

It has been discussed in section 3.3.3 that the single path JT-TD-SCDMA can provide lower PAPR than that in conventional TD-SCDMA system. On the opposite, it is also shown in section 3.3.3 that the JT-TD-SCDMA in multipath channel can cause higher PAPR than that in single JT-TD-SCDMA system as shown in (3.60). The multiplied multipath CIRs

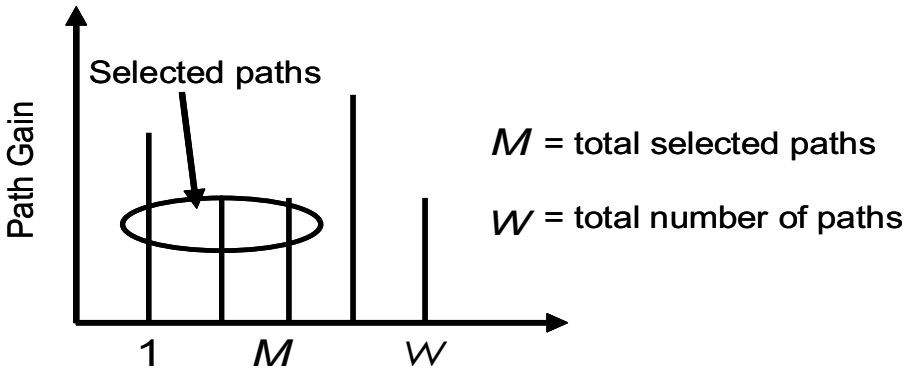

Figure 3.6: Definition for PS I technique

cause a large difference between the largest power and the lowest power, which lead to a high PAPR value. Note that the multipath condition will not affect PAPR of conventional TD-SCDMA because no channel is multiplied before transmission. Though, as the single path JT-TD-SCDMA can perform lower PAPR than that in conventional system, the multipath JT-TD-SCDMA has a potential to have a low PAPR while keeping a simple MS compared to conventional TD-SCDMA. To avoid a high PAPR due to multipath condition in JT-TD-SCDMA, we propose two new approaches of JT technique to reduce the number of paths in multipath channel, named as follows:

- **Path Selection I (PSI)**

  As shown in Fig. 3.6, in PS I, only M first paths of total W paths are selected and inserted into matrix $\underline{\mathbf{H}}$ in (3.49) and (3.50) (e.g., $M = 1$, $W = 4$ means taking $M = 1$ path from $W = 4$ paths)

- **Path Selection II (PSII)**

  In PS II, a threshold is set, and only paths that have path gains above the threshold value are selected to be used in matrix $\underline{\mathbf{H}}$ in (3.49) and (3.50). The threshold concept of PS II is shown in Fig. 3.7. The threshold value is set relative to average power of CIRs. For example, when threshold value is set to 1 dB, it means that the threshold

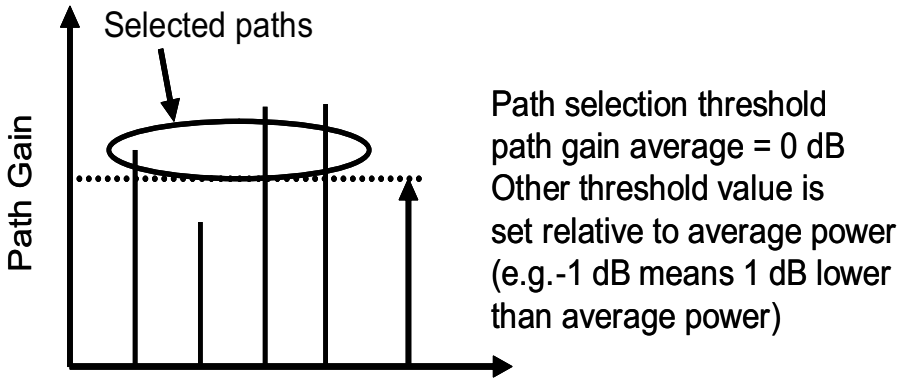

Figure 3.7: Threshold definition for PS II technique

value is 1 dB higher than average power of all paths.

These two different techniques are proposed to determine a better solution for a good technique that can perform a suitable trade-off between PAPR and BER. Note that, the PAPR increases when the number of selected paths increases while, BER degrades when the number of unselected paths increases. The PS I and PS II give different effects to the trade-off because in PS I, the fixed number of paths is selected while in PS II, the number of selected paths changes for each transmission. The adequate technique among the proposed PS I (M/W) and PS II can determine a good technique that improves PAPR with slight BER degradation.

3.5 Data Detection and Signal-to-Noise Power-Ratio

In JT, desired data received at MS can be expressed as

$$\underline{\mathbf{d}}^{(k)} = \underline{\mathbf{D}}^{(k)}\underline{\mathbf{e}}^{(k)} \tag{3.61}$$

where $\underline{\mathbf{D}}^{(k)} = \underline{\mathbf{C}}^{(k)^{*T}}$ is a demodulator matrix that contains spreading code matrix. A detected data containing noise is shown as follows

$$\underline{\hat{\mathbf{d}}}^{(k)} = \underline{\mathbf{D}}^{(k)}(\underline{\mathbf{e}}^{(k)} + \underline{\mathbf{n}}) = \underline{\mathbf{d}}^{(k)} + \underline{\mathbf{D}}^{(k)}\underline{\mathbf{n}}, \tag{3.62}$$

$\underline{\mathbf{n}}$ represents white Gaussian noise vector with variances σ^2. The covarience matrix for noise can be defined as

$$\underline{\mathbf{R}}_{\underline{\mathbf{n}}} = \mathrm{E}\{\underline{\mathbf{n}}\underline{\mathbf{n}}^{*T}\} = 2\sigma^2\underline{\mathbf{I}}. \tag{3.63}$$

From (3.62), it can be seen that no interference exists in the detected data and SNR of the data $\underline{\mathbf{d}}_n^{(k)}$ is expressed as follows

$$\gamma_{JT,n}^{(k)} = \frac{|\underline{\mathbf{d}}_n^k|^2}{2\sigma^2[\underline{\mathbf{D}}^{(k)}\underline{\mathbf{D}}^{(k)*T}]_{n,n}}. \tag{3.64}$$

With (3.64) and the assumption that the noise $\underline{\mathbf{n}}$ is Gaussian distributed, the BER can be derived as [54]

$$\begin{aligned} P_b^{(k)} &= \frac{1}{2}\mathrm{erfc}\left(\sqrt{\frac{\gamma_{JT}^{(k)}}{2}}\right) \\ &= \frac{1}{2}\mathrm{erfc}\left(\sqrt{\frac{|d_n^k|^2}{4\sigma^2[\mathbf{D}^{(k)}\mathbf{D}^{(k)*T}]_{n,n}}}\right). \end{aligned} \tag{3.65}$$

For the proposed PS I and PS II techniques, since the elements of matrix $\underline{\mathbf{H}}$ change from consisting of all paths to certain selected paths, channel mismatch occurs. The channel mismatch might affect data detection at MS. From (3.39), total transmitted signal for PS I and PS II can be written as

$$\hat{\underline{\mathbf{s}}} = \bar{\underline{\mathbf{B}}}^{*T}(\bar{\underline{\mathbf{B}}}\bar{\underline{\mathbf{B}}}^{*T})^{-1}\underline{\mathbf{d}}, \tag{3.66}$$

where $\bar{\underline{\mathbf{B}}} = \underline{\mathbf{B}} - \underline{\mathbf{E}}$ represents a system matrix affected by error $\underline{\mathbf{E}}$ due to the proposed technique. The error $\underline{\mathbf{E}}$ contains unselected paths from real CIR in $\underline{\mathbf{B}}$. Total received signal of (3.66) can be expressed as

$$\bar{\underline{\mathbf{e}}} = \underline{\mathbf{H}}\bar{\underline{\mathbf{s}}} \tag{3.67}$$

and total detected data can be expressed as

$$\bar{\hat{\underline{\mathbf{d}}}} = \underline{\mathbf{B}}\bar{\underline{\mathbf{B}}}^{*T}(\bar{\underline{\mathbf{B}}}\bar{\underline{\mathbf{B}}}^{*T})\underline{\mathbf{d}} + \underline{\mathbf{D}}\underline{\mathbf{n}}, \tag{3.68}$$

where detected data at MS is represented by

$$\begin{aligned}
\underline{\mathbf{d}}^{\bar{\hat{}}(k)} &= \underline{\mathbf{B}}^{(k)}\bar{\underline{\mathbf{B}}}^{*T}(\bar{\underline{\mathbf{B}}}\bar{\underline{\mathbf{B}}}^{*T})^{-1}\underline{\mathbf{d}} + \underline{\mathbf{D}}^{(k)}\underline{\mathbf{n}} \\
&= [\bar{\underline{\mathbf{B}}}^{(k)} + \underline{\mathbf{E}}^{(k)}]\bar{\underline{\mathbf{B}}}^{*T}(\bar{\underline{\mathbf{B}}}\bar{\underline{\mathbf{B}}}^{*T})^{-1}\underline{\mathbf{d}} + \underline{\mathbf{D}}^{(k)}\underline{\mathbf{n}} \\
&= \underline{\mathbf{d}}^{(k)} + \underline{\mathbf{E}}^{(k)}\bar{\underline{\mathbf{B}}}^{*T}(\bar{\underline{\mathbf{B}}}\bar{\underline{\mathbf{B}}}^{*T})^{-1}\underline{\mathbf{d}} + \underline{\mathbf{D}}^{(k)}\underline{\mathbf{n}}.
\end{aligned} \tag{3.69}$$

We can see that detected data for the proposed PS I and PS II techniques in (3.69) contain interference while no interference occurs for conventional JT technique, as shown in (3.62).

From (3.69), data estimation error can be calculated as

$$\underline{\mathbf{d}}^{\bar{\hat{}}(k)} - \underline{\mathbf{d}}^{(k)} = \underline{\mathbf{E}}^{(k)}\bar{\underline{\mathbf{B}}}^{*T}(\bar{\underline{\mathbf{B}}}\bar{\underline{\mathbf{B}}}^{*T})^{-1}\underline{\mathbf{d}} + \underline{\mathbf{D}}^{(k)}\underline{\mathbf{n}}. \tag{3.70}$$

The covariance matrix of the data estimation error in (3.70) can be calculated as

$$\begin{aligned}
\mathrm{R}_{\underline{\mathbf{d}}^{\bar{\hat{}}(k)} - \underline{\mathbf{d}}^{(k)}} &= \mathrm{E}\{(\underline{\mathbf{d}}^{\bar{\hat{}}(k)} - \underline{\mathbf{d}}^{(k)})(\underline{\mathbf{d}}^{\bar{\hat{}}(k)} - \underline{\mathbf{d}}^{(k)})^{*T}\} \\
&= (\underline{\mathbf{E}}^{(k)}\bar{\underline{\mathbf{B}}}^{*T}(\bar{\underline{\mathbf{B}}}\bar{\underline{\mathbf{B}}}^{*T})^{-1}\underline{\mathbf{d}} + \underline{\mathbf{D}}^{(k)}\underline{\mathbf{n}}) \times (\underline{\mathbf{E}}^{(k)}\bar{\underline{\mathbf{B}}}^{*T}(\bar{\underline{\mathbf{B}}}\bar{\underline{\mathbf{B}}}^{*T})^{-1}\underline{\mathbf{d}} + \underline{\mathbf{D}}^{(k)}\underline{\mathbf{n}})^{*T} \\
&= \underline{\mathbf{E}}^{(k)}\bar{\underline{\mathbf{B}}}^{*T}(\bar{\underline{\mathbf{B}}}\bar{\underline{\mathbf{B}}}^{*T})^{-1}(\bar{\underline{\mathbf{B}}}\bar{\underline{\mathbf{B}}}^{*T})^{-1}\underline{\mathbf{B}}\underline{\mathbf{E}}^{(k)*T} \times \underline{\mathbf{d}}\underline{\mathbf{d}}^{*T} + \underline{\mathbf{D}}^{(k)}\underline{\mathbf{D}}^{(k)*T}\underline{\mathbf{n}}\underline{\mathbf{n}}^{*T} \\
&= 2\{\underline{\mathbf{E}}^{(k)}\underline{\mathbf{E}}^{(k)*T}(\bar{\underline{\mathbf{B}}}\bar{\underline{\mathbf{B}}}^{*T})^{-1}\} + 2\sigma^2\underline{\mathbf{D}}^{(k)}\underline{\mathbf{D}}^{(k)*T}.
\end{aligned} \tag{3.71}$$

From the matrix of data estimation error calculated in (3.71), the BER of proposed PS I and PS II can be calculated as

$$\begin{aligned}
P_b^{(k)} &= \frac{1}{2}\mathrm{erfc}\left(\sqrt{\frac{\gamma_{JT}^{(k)}}{2}}\right) \\
&= \frac{1}{2}\mathrm{erfc}\left(\sqrt{\frac{|d_n^k|^2}{4(\mathrm{X}+\mathrm{Y})}}\right)
\end{aligned} \tag{3.72}$$

where

$$\mathrm{X} = \sigma^2[\mathbf{D}^{(k)}\mathbf{D}^{(k)^{*T}}]_{n,n}, \tag{3.73}$$

and

$$\mathrm{Y} = \underline{\mathbf{E}}^{(k)}\underline{\mathbf{E}}^{(k)^{*T}}(\underline{\bar{\mathbf{B}}}\underline{\bar{\mathbf{B}}}^{*T})^{-1}. \tag{3.74}$$

3.6 Simulation and Discussion

Since the PAPR of a transmitted signal is a random variable, it is better to calculate statistical data rather than determine the exact value of PAPR. Thus, we calculate probability of PAPR exceeding a certain threshold level $PAPR_0$. This refers to complementary cumulative distribution function (CCDF) of the PAPR and can be defined as

$$\mathrm{CCDF} = \mathrm{P_r}(\mathrm{PAPR} > \mathrm{PAPR_0}). \tag{3.75}$$

Simulation is done using TD-SCDMA parameters presented in Table 3.1 [52]. Simulation for both single path and multipath are done and discussed in section 3.6.1 and section 3.6.2, respectively. The simulation is done with considering of pulse shaping process, where the transmitted signal $\underline{\mathbf{s}}$ is passed through perfect Nyquist filter (i.e. roll off factor = 1), and oversampled at a sampling rate 4 times higher than original sampling rate.

3.6.1 JT-TD-SCDMA in Single Path Environment

Figure 3.8 shows CCDF of PAPR comparison for single path TD-SCDMA and JT-TD-SCDMA. From Fig. 3.8, we can see that the PAPR of 4 users and 8 users for w/o. JT systems are above 10 dB at CCDF = 10^{-3}. Note that a multiuser CDMA system should have a PAPR lower than 10 dB [42]. We also can see that when JT is applied, PAPR can be reduced for all the number of users compared to the system without JT. The PAPR reduction can be achieved because in JT, the transmitted signal is multiplied with CIRs as shown in

Table 3.1: Simulation Parameters

Modulation method	QPSK
Spreading code	OVSF, complex spreading
Spreading code	16
Channel	Multipath fading case 3 by 3GPP[52] Relative delay [ns] =[0 781 1563 2344] Average power [dB] = [0 -3 -6 -9]
Amplifier model	Rapp model Class AB Output Back-off (OBO) = 5 dB smoothness factor =2

(3.39). The multiplication by CIRs avoids the signal from being influenced by orthogonal code dependency. Thus, signals having large peak power due to a bad combination of orthogonal codes can be reduced. By applying JT, overall transmit signal power increases, so as the average power. This leads to lower PAPR.

Furthermore, from Fig. 3.8, PAPR increases when the number of users increases for both TD-SCDMA and JT-TD-SCDMA. However, the increased value of PAPR in JT-TD-SCDMA is larger than in the conventional TD-SCDMA system when small number of users is active (e.g. from 4 users to 8 users). This occurs because of difference in orthogonal code dependency behavior between small and large number of users. In the conventional TD-SCDMA, smaller number of users can be easily affected by certain combination of orthogonal code that causes consecutive peak power. The JT-TD-SCDMA removes orthogonally of transmit signal, thus mitigates the transmit signal from affected by the bad combination of orthogonal code, so as consecutive peak power. When more users are active in the conventional TD-SCDMA, a probability for all users to use a bad combination of orthogonal codes decreases. Note that orthogonal codes combination is limited by spreading factor. For example, if the number of users is set to spreading factor value, all of orthogonal codes are used, thus a combination of bad orthogonal codes can be avoided. Thus, implementation of JT does not influence the transmit signal much. As a result, a large PAPR improvement can be clearly

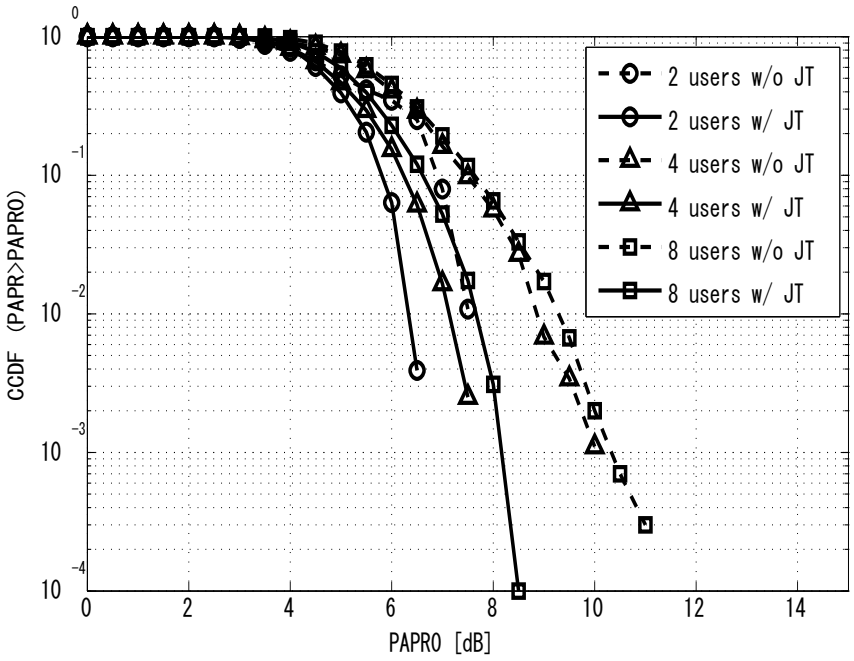

Figure 3.8: PAPR comparison in single path environment for 8 users system

seen for the small number of users compared to the large number of users in JT-TD-SCDMA. This can be seen from PAPR performance for 4 users in Fig. 3.8.

3.6.2 JT-TD-SCDMA in Multipath Environment

Since CIRs are utilized before transmission in JT as shown in (3.39), multipath condition might influence the transmit signal power as well as PAPR. To investigate the effect, we further evaluate PAPR of JT-TD-SCDMA under multipath condition. The results are shown in Fig. 3.9. We can see from Fig. 3.9 that the increasing number of paths used in JT process will increase PAPR value. This is because some elements of the system matrix $\underline{\mathbf{B}}$ contains CIRs of all paths but some other elements contain only CIR of some paths, as shown in (3.60). The difference of power level $\underline{\mathbf{B}}$ is larger if more paths present in the channel; i.e. some elements contain signal from all paths while others contain signals from only one path.

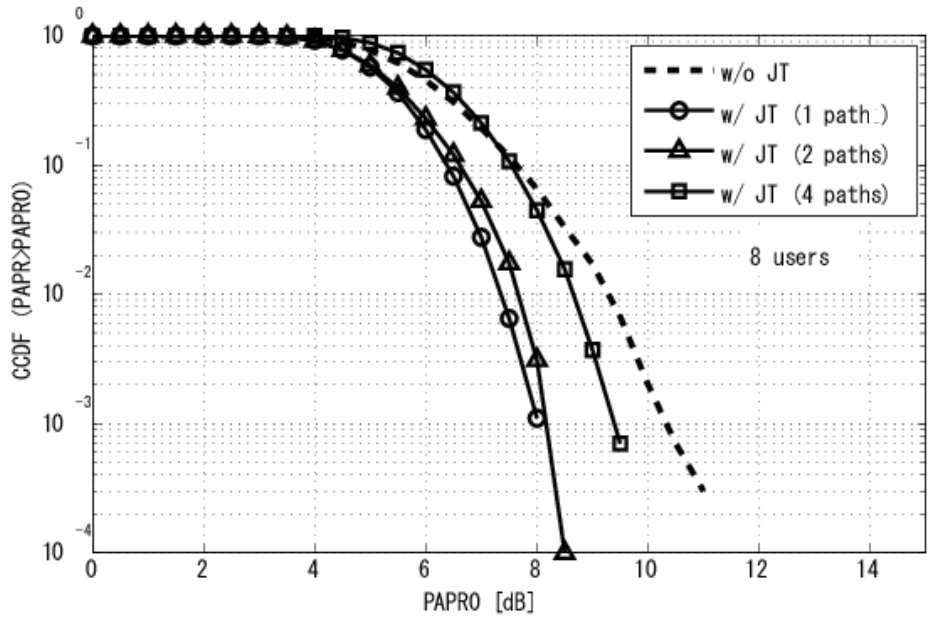

Figure 3.9: PAPR comparison of w/o JT, single path JT and multipath (2, 4 paths) JT environment for 8 users system

This causes large peak power and low average power within a symbol, leading to high PAPR.

To avoid a high PAPR caused by the multipath CIRs in multipath JT-TD-SCDMA, we proposed two different techniques, described in section 3.4. We evaluate the PAPR performance of the proposed techniques in Fig. 3.10. Figure 7 shows PAPR comparison for both PS I and PS II techniques when 8 users are active. PS I (M/W) in Fig. 7 represents M selected path out of W paths. At CCDF = 10^{-3}, the PS I (1/4), PS I (2/4) and PS I (3/4) reduce 1.2 dB, 0.5 dB and 0.4 dB of PAPR, respectively, compared to that in conventional JT system. From the results, for PS I, we can see that PAPR can be reduced when the number of selected paths decreases. For PS II (threshold value = 0 dB), PAPR performance is in between PS I (2/4) and PS I (3/4), 0.6 dB lower than that in conventional JT.

In PS II, the selected number of paths changes depending on threshold value. Note that the threshold value = 0 dB is selected for PS II as the value has a high possibility to reduce

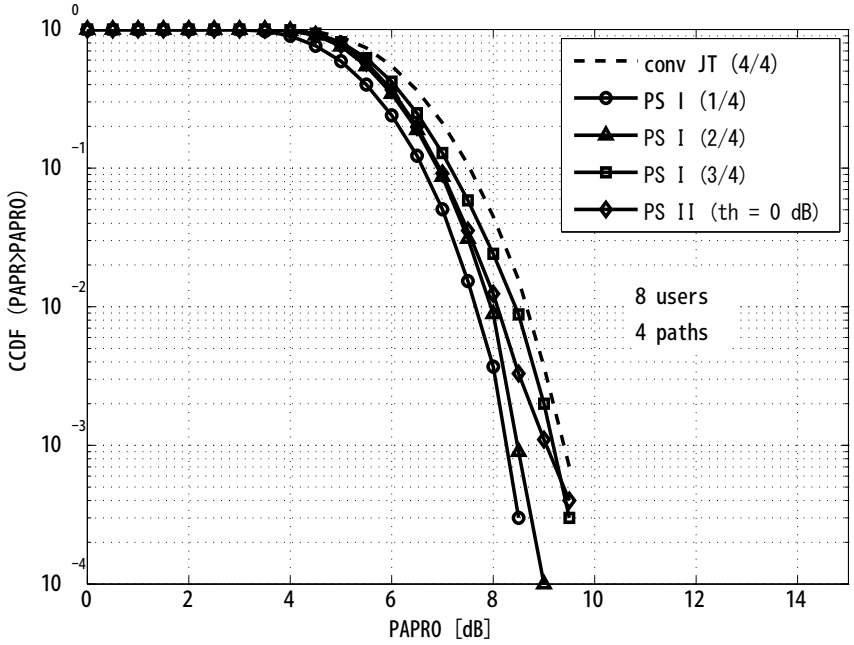

Figure 3.10: PAPR comparison among conventional JT, PS I and PS II for 4 paths 8 users system

PAPR of the system. Table 3.2 shows relation between threshold value and percentiles for the probability distribution function (PDF) of the number of selected paths. For threshold value = 0 dB, 50.69 % of the signals only consist of 1 path, 45.98 % of the signals consists only 2 paths, and the remaining signals consist of 3 paths out of 4 paths. The small number of selected paths can reduce PAPR as same as in PS I. For comparison, the percentiles for PDF of other threshold values are shown in Table 3.2. From Table 3.2, threshold values, 1 dB and 2 dB are not adequate, because no path (0.63 % for 1 dB and 7.77 % for 2 dB) is selected where the channel must exist at least 1 path for the JT process in transmitted. For threshold values of -2 dB and -1 dB, 1.86 % and 0.27 % of the signals select all paths (4 paths), which can increase PAPR of the system. The descriptions stated above are the reasons for selecting threshold value = 0 dB for our proposed PS II technique. Even PS I (1/4) in Fig. 7 performs the smallest PAPR, since there is a trade-off between PAPR and BER, it is unfair to say that

Table 3.2: Relation between threshold value (th) and percentiles for PDF of the number of selected paths (M) for PS II

M (%) / th [dB]	0	1	2	3	4
-2	0.00	23.34	52.30	22.50	1.86
-1	0.00	34.00	53.21	12.52	0.27
0	0.00	50.69	45.98	3.33	0.00
1	0.63	73.15	26.16	0.06	0.00
2	7.77	85.51	6.72	0.00	0.00

the technique is a better solution. To find a good technique among the proposed techniques, we further investigate BER performance for all the techniques, which will be discussed later.

To prove the validity of our simulation, results of simulation and theoretical analysis derived in section 3.5 are compared in Fig. 3.11. Note that the analysis in section 3.5 is derived considering linear amplification process.

In Fig. 3.11, simulation results are compared to theoretical BER performance for conventional JT, proposed PS I and PS II. Note that the theoretical performance is evaluated using percentiles for PDF of the number of selected paths in Table 3.2 and (3.72). It can be seen that the simulation results match theoretical results for all the techniques; conventional JT, PS I and PS II.

As described, the BER performances of the proposed PS techniques need to be evaluated to determine a system with a small PAPR and a good BER performance. BER performances of PS I and PS II are shown in Fig. 3.12. Note that the BER performances in Fig. 9 consider nonlinear amplifier and channel, shown in Table 3.1. From the results, we can see that both the proposed PS I and PS II show BER performance degradation compared to conventional JT when all 4 paths are selected. The reason for BER degradation in the proposed PS I and PS II can be seen from (3.66) to (3.69). In (3.66) the matrix $\underline{\bar{\mathrm{H}}}$ of $\underline{\bar{\mathrm{B}}} = \underline{\mathrm{D}}\underline{\bar{\mathrm{H}}}$ contains only selected paths which are only parts of paths in real CIRs $\underline{\mathrm{H}}$. The difference between $\underline{\bar{\mathrm{H}}}$ in transmitted signal and $\underline{\mathrm{H}}$ in real channel causes channel mismatch. We also can see

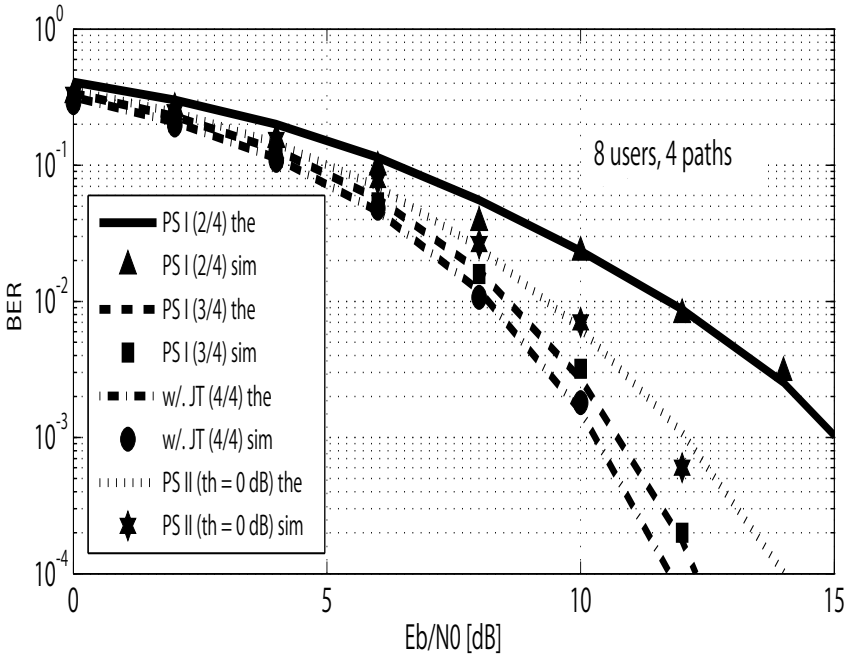

Figure 3.11: BER performance comparison betwen simulation and theoretical analysis for conventional JT (w/ JT), PS I and PS II for 4 paths, 8 users system

that transmitted signal in conventional JT changes when PS I and PS II are applied as shown in (3.66). The change increases interference in data detection shown in (3.70). This causes BER degradation in proposed PS compared to that in conventional JT, which can perfectly eliminate interference as shown in (3.62). The BER degradation can be seen in Fig. 3.12. From (3.66), PS I (1/4) performs the worst performance because 3 remaining paths are treated as interference. The result where the PS I (1/4) performing the worst BER can also be seen in Fig. 3.12. The interference increases owing to the increase of the number of unselected paths. Thus, the PS I (2/4) can provide a better BER than PS I (1/4), as shown in Fig. 3.12.

For PS II (th = 0 dB), a better BER than that in PS I (2/4) can be achieved as the variable number of selected paths (50.69 % for 1 path, 45.98 % for 2 paths and 3.33 % for 3 paths in Table 3.2), mitigates the interferences caused by the channel mismatch. The

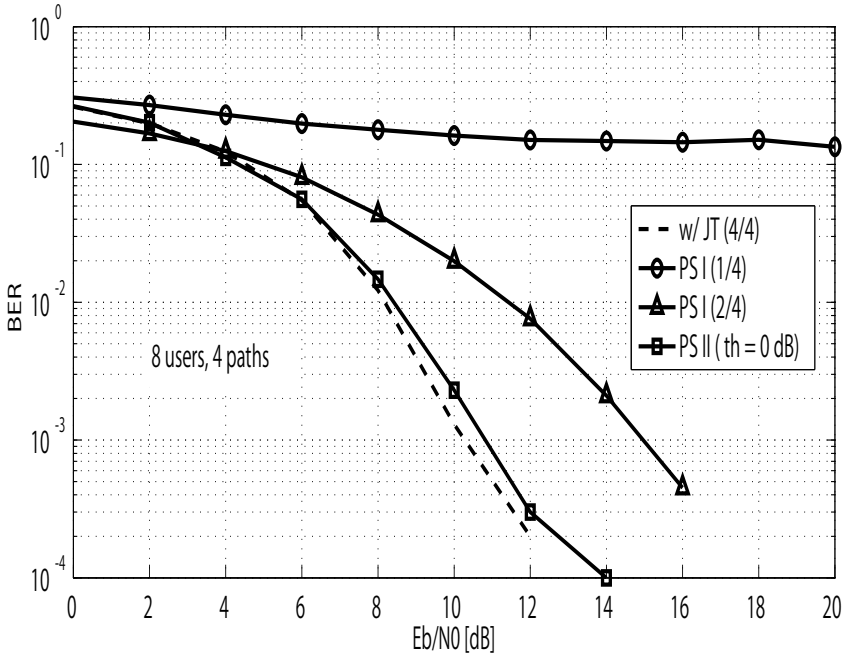

Figure 3.12: BER comparison among conventional JT (w/ JT), PS I and PS II for 4 paths, 8 users

variable number of selected paths in PS II also can give a good trade-off between reducing interferences and a high PAPR caused by increasing the number of paths in JT system. The interference increases owing to the increase of the number of unselected paths. Regarding PAPR evaluation in Fig. 3.10 and BER evaluation in Fig. 3.12, we can say that PS II is a better technique than PS I, because the PS II performs a lower PAPR without severe BER performance degradation than PS I. However, since PAPR improvement in PS II causes a small BER degradation compared with that in conventional JT, some modification needs to be done in the proposed PS II. We combine the proposed PS II with clipping technique (PS II & clip) to achieve both a good BER and PAPR.

To evaluate PS II & clip, we set a threshold value similar to that in the conventional clipping technique, named as clipping level (CL). Transmit signal power over the clipping level will be cut and the clipping level is set as a new transmit signal power. In our simulation,

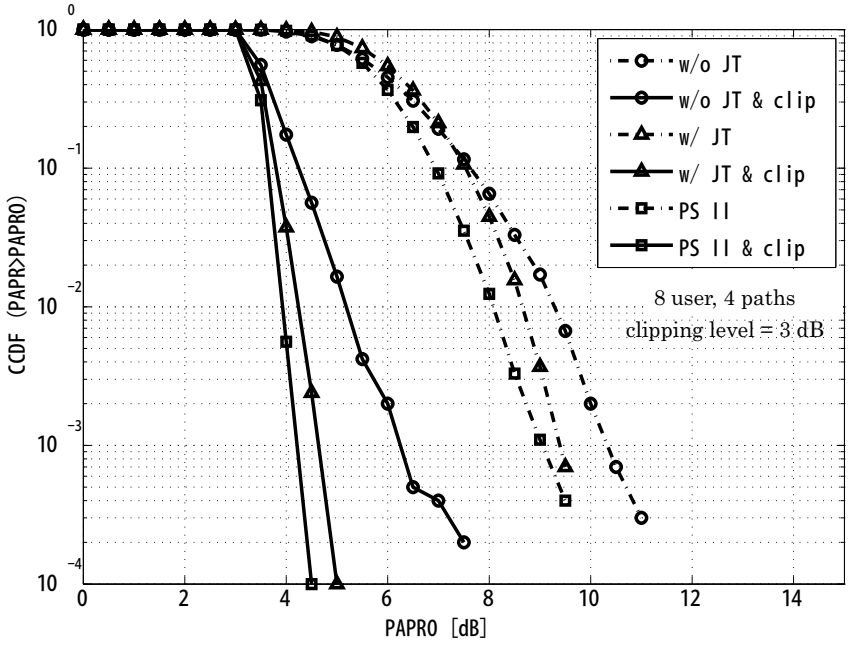

Figure 3.13: PAPR comparison among w/o JT, w/o JT & clip, w/ JT, w/ JT & clip, PS II, and PS II & clip for 4 paths, 8 users system

clipping level is set relative to average transmit power. For example, CL = 3 dB means that the clipping level is set 3 dB higher than average transmit power.

For the sake of comparison, we also evaluate PAPR of conventional clipping technique (w/o JT & clip) and a combination of JT and clipping technique (w/ JT & clip), shown in Fig. 3.13. We can see that when clipping is applied to the w/o. JT, w/. JT and PS II, PAPR reduction can be achieved in all techniques, i.e. w/o. JT & clip outperforms w/o. JT, w/. JT & clip outperforms w/. JT, and PS II & clip outperforms PS II. The clipping technique can clip the signals with a peak higher than clipping level. This can reduce PAPR value of the system. It can also be seen that at ccdf = 10^{-3}, clipping combination of each technique reduces PAPR about 4 dB compared to PAPR of w/o JT, 4.4 dB compared to PAPR of w/. JT, and 4.8 dB compared to PAPR of PS II. From the results, we can say that the combination of clipping with PS II (PSII & clip) provides a good PAPR reduction

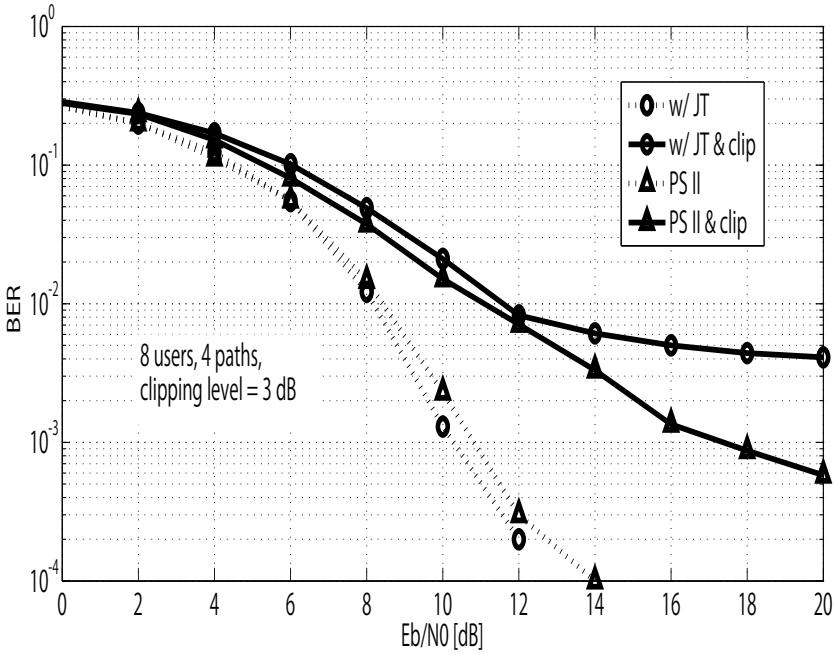

Figure 3.14: BER comparison among w/ JT, w/ JT & clip, PS II, and PS II & clip for 4 paths, 8 users

compared to the combination of clipping with JT (w/ JT & clip).

However, the trade-off between PAPR and BER must be considered. The BER performance has been evaluated and shown in Fig. 3.14. Note that the BER performances in Fig. 11 consider nonlinear amplifier and channel stated in Table 1. We can see that when clipping is applied, the BER degradation occurs for both JT and PS II system. This is because the limit of transmit signal power in clipping technique causes in-band, out-of-band clip noise and peak re-growth after digital analog conversion (DAC), which lead to BER performance degradation [56]. Even the PS II & clip provides a lower PAPR than that in w/ JT & clip, a better BER can be achieved in PS II & clip than that in w/ JT & clip. This is because when PS II is applied, the peak power is reduced as the number of selected paths is reduced. Thus, the peak power that be clipped in PS II & clip is smaller than that in w/. JT & clip. The reduction of clipping process can mitigate in-band, out-of-band clip noise and spectral

Table 3.3: Relation between PAPR value and required E_b/N_0 of proposed techniques

Schemes	**E_b/N_0 [dB] (BER= 10^{-3})**	**PAPR [dB] (CCDF= 10^{-3})**
w/ JT	10	9.5
PS I (1/4)	-	8.3
PS I (2/4)	15	8.5
PS II (th = 0 dB)	11	9.0
w/ JT & clipping	-	4.6
PS II & clipping	17	4.2

re-growth as well as BER degradation.

The relation between PAPR value and required E_b/N_0 of the proposed techniques is summarized in Table 3. From Table 3, the proposed PS II requires 11 dB of E_b/N_0 to achieve BER = 10^{-3}. The result shows that the proposed PS II provides a 0.5 dB low PAPR and requires 0.8 dB more E_b/N_0 than that in conventional JT technique to achieve BER = 10^{-3}. However, as shown in Fig. 10 and Fig. 11, the proposed PS II provides a low PAPR and BER if combined with clipping technique, compared to a combination of conventional JT with clipping technique. From the results, PS II & clip technique can be observed as an effective technique, because the technique provides a low PAPR without severe BER degradation. The BER performance of PS II & clip can also meet the BER requirement (BER=10^{-3}) for 1.28 Mcps TDD-CDMA or TD-SCDMA system as shown in [15]. Note that the BER performances in Fig. 9 and Fig. 11 are evaluated with implementation of convolutional coding technique as standardized for TD-SCDMA (convolutional encoder with code rate = 1/2 and constraint length = 9 with Viterbi decoder) system in [57].

Out-of-band emission or spectral regrowth is the main drawback of clipping technique. However, we did not investigate the spectral regrowth behavior, since the out-of-band spectrum can be mitigated using band pass filter in spread CDMA compared to that in OFDM. Furthermore, the out-of-band emission normally occurs because of clipping technique. In our proposed technique, PS II we select paths that are above threshold value and no signal is

clipped. Thus, no spectral regrowth is predicted. For the combination of PS II and clipping, the signals are firstly selected before clipping. This means that the signals that should be clipped decreases, and this can mitigate spectral regrowth caused by clipping.

3.7 Conclusion

PAPR of JT-TD-SCDMA system for both single path and multipath has been investigated. For single path environment, the result shows that JT technique can reduce PAPR as the CIRs used in transmitted signal increases overall transmitted signal, thus increases average power as well as PAPR. However for multipath environment, only certain transmitted signals in the JT system matrix are affected by multipath. Some elements of the system matrix that contain multipath CIRs cause large peak power, while other elements that contain some paths cause low average of transmit power. The gap between peak and low transmit signal power causes a high PAPR in multipath JT-TD-SDCMA compared to the conventional TD-SCDMA. To avoid a high PAPR in multipath environment, we propose two new techniques of JT named as PS I and PS II. Both techniques are derived by modifying CIRs matrix. In PS I, definite number of paths are selected while in PS II, paths having path gains above certain threshold value are selected. Considering trade-off between PAPR and BER, we further investigated BER performance for each technique. From the results, we can see that taking fewer paths can reduce PAPR but at the same time causes BER performance degradation due to interference. Thus, PS II can be considered a better technique than PS I because variable number of paths of the systems can give a good trade-off between PAPR and BER performance. We further combine the proposed PS II with clipping technique, (PS II & clip). For the sake of comparison, conventional clipping technique (w/o JT & clip) and a combination of JT and clipping (w/ JT & clip) are also evaluated. From the results, proposed PS II & clip performs the lower PAPR without severe BER degradation than the conventional clipping technique. As a result, PS II & clip can be concluded as a

good technique among investigated PAPR reduction techniques.

Chapter 4

Conclusion

This dissertation has provided an impact of channel estimation error and PAPR reduction for precoding technique in TDD-CDMA system. Two different type of TDD systems, TD-CDMA and TD-SCDMA are studied in this research. The impact of channel estimation error is evaluated for pre-rake in TD-CDMA parameter while the PAPR reduction is provided by using JT technique in TD-SCDMA system. The impact of channel estimation is evaluated because precoding usually works well under assumption of perfect channel estimation, which is unrealistic. The PAPR reduction using the JT is proposed to avoid complexity of BS that becoming more complex owing to the replacement of joint detection in MS to BS. The PAPR reduction helps the BS to reduce the complexity and cut cost because a low PAPR allows the BS to use efficient and low cost power amplifier. Our study focuses on having a low BER performance without causing complexity in both BS and MS.

In chapter 2, the impact of channel estimation error in pre-rake TDD-CDMA is studied. We provide numerical analysis for pre-rake under perfect and imperfect channel estimation. The error model of channel estimation is discussed in section 2.3, which consists of amplitude and phase error. For comparison, we also provide numerical analysis for rake technique under perfect and imperfect channel estimation with the same error model as in pre-rake analysis. Computer simulation is done based on TD-CDMA system parameter. From numerical

results and computer simulation, we found that the channel estimation error causes large performance degradation in pre-rake system compared to that in rake system. This occurs because of high orthogonality loss among spreading codes of different users loss increases MAI in pre-rake, which does not affect the rake system. The error also shows that the BER degrades parallel with an increase of Doppler frequency value. The analysis also shows that both amplitude error and phase error increase when Doppler frequency increases.

In chapter 3, we propose a new approach of JT technique to reduce PAPR of the TDD-CDMA system. We provide a path selection technique, where only certain paths are selected instead of all paths processed in JT. Under multipath channel, our proposed path selection technique performs a lower PAPR than that in conventional JT. To enhance the effectiveness of our proposed technique, we combine the proposed path selection technique with clipping technique. We evaluate the proposed technique using numerical analysis and computer simulation. The computer simulation utilizes TD-SCDMA system as simulation parameter. From the results, we found that the proposed technique perform a lower PAPR than that in conventional JT technique. We also found that the combination of proposed technique with clipping technique performs a low PAPR with a good BER performance compared with that in clipping technique.

Bibliography

[1] I. Poole, *Cellular Communications Explained: From Basic to 3G* , Elsevier Publication.

[2] R. Prasad and M. Ruggieri, *Technology Trend in Wireless Communications*, Universal Personal Communications.

[3] M. Peng and W. Wang, "Technologies and Standards for TD-SCDMA Evolution to IMT-advanced,' IEEE Commun. Magazine, pp. 50-58, Dec. 2009.

[4] M. Peng, W. Wang, and H. H. Chen, "TD-SCDMA Evolution," IEEE Vehicular Magazine, pp. 28-41, June 2010.

[5] T. Giannopoulos, V. Paliouras, "Relationship among BER, Power Consumption and PAPR," IEEE Int. Symp. on Wireless Pervasive Computing, pp. 633-637, May 2008.

[6] J. L. Relova, S. Pertega, J. A. Vilar, E. Lopez-Martin, M. Peleteiro, and F. Ares-Pena, "Effects of Cell-Phone Radiation on the Electroencephalographic Spectra of Epileptic Patients [Telecommunications Health & Safety]," IEEE Antennas and Propagation Society, vol. 52, no. 6, pp. 173-179, Dec. 2010.

[7] E. Novakov, "A Low Complexity Ultra-Wideband, Orthogonal Frequency Division Multiplexing Communication System," General Assembly and Scientific Symposium, 2011, pp. 1-4, Aug. 2011.

[8] L. Youjian, "A Low Complexity Protocol for Relay Channels Employing Rateless Codes and Acknowledgement ," IEEE Int. Symp. on Information Theory, pp. 1244-1248, July 2006.

[9] H. Eul, "Complexity Challenges towards 4th Generation Communication solutions ," IEEE/ACM/IFIP Int. Con. on Hardware/Software Codesign and System Synthesis, pp. 123, Sept. 2007.

[10] D. J. Goodman, "Trends in Cellular and Cordless Communications,' IEEE Commun. Magazine, pp. 31-40, June 1991.

[11] I. Martoyo, U. Scliober, and F. Jondral "CDMA versus OFDM, A Performance Comparison in Selective Fading Channels," IEEE Int. Symp. on Spread-Spectrum Tech. & Appl., pp. 139-143, Sept. 2002.

[12] M. Peng and W. Wang, "Technologies and Standards for TD-SCDMA Evolutions to IMT-advanced," IEEE Magazine, vol. 47, pp. 50-58, Dec. 2009.

[13] R. Esmailzadeh and M. Nakagawa, *TDD-CDMA for Wireless Communications*, Artech House, Boston 2003.

[14] 3GPP TS25.233 Spreading and Modulation (TDD).

[15] 3GPP TS 25.102: User Equipment (UE) Radio Transmission and Reception (TDD).

[16] 3GPP TS25.221 Physical Channels and Mapping of Transport Channels onto Physical Channels (TDD).

[17] 3GPP TS36.211; Physical Channels and Modulation.

[18] J. Proakis, *Digital Communications. New York:* McGraw-Hill, 1989.

[19] T. Rappaport, *Wireless Communications*, Prentice Hall, New Jersey, 1996.

[20] G. L. Turin, "Introduction to Spread Spectrum Antimultipath Techniques and Their Application to Urban Digital Radio," Proc.of IEEE, vol. 68, no. 3, Mar. 1980.

[21] R. Esmailzadeh and M. Nakagawa, "Pre-Rake Diversity Combination for Direct Sequence Spread Spectrum Mobile Communication Systems," IEICE Trans. on Commun., vol. E76-B, no. 8, Aug. 1993.

[22] R. Lupas and S. Verdu, "Linear Multiuser Detectors for Synchronous Code-Division-Multiple Access Communications," IEEE Trans. Inform. Theory, vol. 32, pp. 123-136, Jan. 1989.

[23] Z. Zvonar and D. Brady, "Multiuser Detection in Single-path Fading Channels," IEEE Trans. Commun., vol. 42, pp. 1729-1739, Feb. 1994.

[24] 3GPP TS 25.221: User Equipment (UE) radio transmission and reception (TDD).

[25] A. Klein, G. K. Kaleh, P. W. Baier, "Zero forcing and minimum mean-square-error equalization for multiuser detection in code-division multiple-access channels," IEEE Trans. on Vehicular Technology, vol. 45, pp. 276-287, May 1996.

[26] B. Vojcic and W. Jang, "Transmitter Preoding in Synchronous Multiuser Communications," IEEE Trans. Commun., vol. 46, pp. 1346-1355, Oct. 1998.

[27] W. Jang, B. Vojcic and L. Pickholtz, "Joint transmitter-receiver optimization in synchronous multiuser communications over multipath channels," IEEE Trans. Commun., pp.269-278, Feb. 1998.

[28] 3GPP. TSG RAN WG1 699918: Tx Diversity with Joint Predistortion.

[29] P. W. Baier, M. Meurer, T. Weber, and H. Troger, "Joint Transmission and Alternative Rational for the Downlink of TDD CDMA using Multi element Antennas," IEEE Int. Symp. on Spread Spectrum Techniques and Applications, vol. 1, pp. 1-5, Sept. 2000.

[30] M. Meurer, H. Troger, T. Weber, and P. W. Baier, "Synthesis of Joint Detection and Joint Transmission in CDMA downlinks," IET Elec. Lett., vol. 37, pp. 919-920, July 2001.

[31] T. Weber, M. Meurer, and W. Zirwas, "Low complexity energy efficient joint transmission for OFDM multiuser downlinks,"IEEE Int. Symp. on Personal, Indoor and Mobile Radio Communications, vol. 2, pp. 1095 - 1099, Sept. 2004.

[32] R. Esmailzadeh, M. Nakagawa, and A. Jones, "TDD-CDMA for 4th Generation of Wireless Communications," IEEE Wireless Commun., vol. 10, pp. 8-15, Aug. 2003.

[33] R. Esmailzadeh, E. Sourour, M. Nakagawa, "Prerake Diversity Combining in Time-Divison Duplex CDMA Mobile Communication," IEEE Trans, on Vehicular Techology, vol. 48, no.3, May 1999.

[34] J. K. Han, M. W. Lee, and H. K. Park, "Principal Ratio Combining for Pre/Post-Rake Diversity," IEEE Commun. Lett, vol. 6, pp. 234-236, June 2002.

[35] S. Georgoulis and D.G.M. Cruickshank, "Pre-equalization, Transmitter Precoding and Joint Transmission Techniques for TDD-CDMA," Int. Conf. on 3G Mobile Commun. Tech., no. 477, pp. 257-261, March 2001.

[36] E. Sourour and A. Kadous, "The Performance of TDD/CDMA Systems using Pre-Rake combining with Different Diversity Techniques and Imperfect Channel Estimation," IEEE Symp. on Computers and Communications, pp. 280 - 284, July 1997.

[37] E. Kudoh, "On the capacity of DS/CDMA Cellular Mobile Radios under Imperfect Transmitter Power Control," IEICE Trans. on Commun., vol. E76-b, no. 8, Aug. 1993.

[38] M. Pursley, "Performance Evaluation for Phased-coded Spread-spectrum Multiple Access Communication-part1: System analysis,"IEEE Trans. Commun., vol. COM-25, pp.795-799, Aug. 1977

[39] W. H. Press, B. P. Flannery, S. A. Teukolsky, and W. T. Vetterling, *Numerical Recipes the Art of Scientific Computing. New York:* Cambridge Univ. Press, 1986.

[40] http://www.tdscdma-forum.org/en/, "TD-SCDMA Forum TD-SCDMA Milestone".

[41] J. A. Tropp, I. S. Dhillon, R. W. Heath, and T. Strohmer, "CDMA Signature Sequences with Low Peak-to-Average-Power Ratio via Alternating Projection," IEEE Asilomar Conf. On Signals, Systems and Computers, vol. 1, pp. 475-479, Nov. 2003.

[42] V. K. N. Lau, "On the Analysis of Peak-to-Average Ratio (PAR) for IS95 and CDMA2000 Systems," IEEE Trans. on Vehicular Technology, vol. 49, no. 6, pp. 2174-2188, Nov. 2000.

[43] A. Papoulis, *Probability, Random Variables, and Stochastic Processes*, New York: McGraw-Hill, 1984

[44] H. Ochiao and H. Imai, "OFDM-CDMA with peak power reduction based on the spreading sequences," IEEE Int. Conf. on Communications, pp. 1299-1303, June 1998.

[45] L. J. Cimini Jr. and N. R. Sollenberge, "Peak-to-average power ratio reduction of an OFDM signa using partial transmit sequences," IEEE Commun. Lett., vol. 4, pp. 86-88, Feb. 2000.

[46] R. Oneil and L. B. Lopes, "Envelope Variation and Spectral Splatter in Clipped Multicarrier Signals ," IEEE Int. Symp. on Personal, Indoor and Mobile Radio Communications, pp. 71-75, Sept. 1995.

[47] T. Fuji and M. Nakagawa, "Adaptive Clipping Level Control for OFDM Peak Power Reduction using Clipping and Filtering," IEICE Trans. Fundamentals, vol. E85-A, no. 7, pp. 1647-1655, July 2002.

[48] A. E. Jones, T. A. Wilkinson, and S. K. Barton, "Block Coding Scheme for Reduction of Peak to Mean Envelope Power Ratio of Multicarrier Commun.," IEEE Int. Symp. on Personal, Indoor and Mobile Radio Communications, pp. 71-75, , Sept. 1995.

[49] R. W. Bauml, R. F. H. Fisher, and J. B. Huber "Reducing the Peak-to-Average Power Ratio of Multicarrier Modulation by Selecting Mapping ," Elec. Lett. vol. 32, no. 22, pp. 2056-2057, Oct. 1996.

[50] N. B. Harum, Y. Tamura,S. P. W. Jarot, R. Esmailzadeh and M. Nakagawa "Analysis of Performance Degradation due to Channel Estimation Error in Pre-Rake TDD/CDMA," IEEE Int. Symp. on Personal, Indoor and Mobile Radio Communications, vol.1, pp. 921 - 925, Sept. 2003.

[51] J. Wang and T. S. Ng, Advanced in 3G Enhanced Technologies for Wireless Communications, mobile communication series.

[52] 3GPP Technical Specification TS 34.122 V4.5.0, "3rd Generation Partnership Project; Technical Specification Group Radio Access Networks; Base station Conformance (TDD), " June 2002.

[53] X. Zhao and X. Zhang, "Peak to Average Power ratio Analysis in Multicarrier DS-CDMA," IEEE Trans. on Vehicular Technology, vol. 52, no. 3, pp. 561-568, May 2003.

[54] N. Verdu, *Multiuser Detection*, Cambridge U.K, Cambridge University Press, 1998.

[55] N. B. Harum, R. Esmailzadeh, and M. Nakagawa, "Joint Transmission for Space Time Block Coded TD-SCDMA," IEEE Int. Symp. on Personal, Indoor and Mobile Radio Communications, vol. 1, pp. 387-391, Sept. 2005.

[56] T. Jiang and Y. Wu, "An Overview: Peak-to-Average Power Ratio Reduction Techniques for OFDM Signals," IEEE Trans. on Broadcasting, vol. 54, pp. 257-268, no. 2, June 2008.

[57] CWTS TS C103 Multiplexing and Channel Coding.

[58] M. Vollmer, M. Haardt, J. Gotze, "Comparative study of joint-detection techniques for TD-CDMA based mobile radio systems," IEEE Journal on Selected Areas in Communications, vol. 19, pp. 1461-1475, Aug. 2001.

[59] A. N. Barreto and G. Fettweis, "Joint Signal Precoding in the Downlink of Spread-Spectrum Systems," IEEE Trans. on Wireless Commun, vol. 2, no. 3, pp. 511 - 518, May 2003.

Appendix A

Achievements

A.1 Journal Papers

[1] N. B. Harum, Y. Tamura, S. P. W. Jarot, R. Esmaizadeh, and M. Nakagawa, "Analysis of Performance Degradation due to Channel Estimation Error in Pre-Rake TDD/CDMA," IEICE Trans. on Communications, vol. E88-B, no. 6, pp. 2508-2515, June 2005.

[2] N. B. Harum, T. Ohtsuki, and M. Nakagawa, "PAPR Reduction of TDD-CDMA Using Joint Transmission Technique," IEICE Trans. on Communications, vol. E95-B, no. 03, pp. xx-xx, March 2012.

A.2 International Conferences

[1] N. B. Harum, Y. Tamura, S. P. W. Jarot, R. Esmaizadeh, and M. Nakagawa, "Analysis of Performance Degradation due to Channel Estimation Error in Pre-Rake TDD/CDMA," in Proc. IEEE PIMRC 2003, vol. 1, pp.921-925, Beijing, September 2003.

[2] N. B. Harum, R. Esmaizadeh, and M. Nakagawa, "Joint Transmission for Space Time Block Coded TD-SCDMA," in Proc. IEEE PIMRC 2005, vol. 1, pp.387-391, Berlin, September 2005.

[3] N. B. Harum and T. Ohtsuki, "PARR Reduction of TD-SCDMA with Joint Transmission Technique," in Proc. IEEE ISCIT 2010, pp. 366 - 371, Tokyo, October 2010.

A.3 Technical Reports

[1] N. B. Harum, Y. Tamura, S. P. W. Jarot, R. Esmaizadeh, and M. Nakagawa, "Analysis of Performance Degradation due to Channel Estimation Error in Pre-Rake TDD/CDMA," 電子情報通信学会技術研究報告. CS2004-90, pp. 13-18, 2004 年 10 月 22 日.

[2] N. B. Harum, R. Esmaizadeh, and M. Nakagawa, "Joint Transmission for Space Time Block Coded TD-SCDMA," 電子情報通信学会技術研究報告 CS 2004-212, pp. 173-178, 2005 年 1 月 21 日.

[3] N. B. Harum, T. Ohtsuki, and M. Nakagawa, "PAPR reduction of TD-SCDMA using joint transmission technique," 電子情報通信学会技術研究報告 RCS 2010-14, pp. 79-84, 2010 年 4 月 19 日.

[4] N. B. Harum and T. Ohtsuki, "A low PAPR relaying technique of AF relay in OFDM system," 2011 年電子情報通信学会総合大会, B-8-33, 東京都市大, 2011 年 3 月 16 日.

A.4 Patents

[1] A. J. Hoon, J. K. Yung, P. S. Ill, M. Nakagawa, R. Esmailzadeh, and N. B. Harum, [Signal Transmission Apparatus in a Wireless Communication System Using a TDD Scheme and a Method thereof, specially concerned with Obtaining a Diversity Gain, and Improving a Data Transmission Rate], Publication No.: KR1020060075165.

[2] 福井章人、青山隆久、ノルハルヤティ　ビンティ　ハルム、「無線通信基地局装置、無線通信端末装置及び無線通信システム」、国際公開番号：WO/2007/091598.

[3] A. Fukui, T. Aoyama and N. B. Harum, [Radio Communication Base Station Device, Radio Communication Terminal Device, and Radio Communication System], Publication No. EP1983775.

[4] A. Fukui, T. Aoyama and N. B. Harum, [Radio Communication Base Station Device, Radio Communication Terminal Device, and Radio Communication System], Publication No: US 2009/011795A1.

[5] ノルハルヤティ　ビンティ　ハルム, 石井義一、金澤岳史 [無線基地局装置、無線端末装置、無線中継局装置、送信パワー制御方法、無線通信中継方法および無線通信システム], 国際公開番号： WO/2009/110176.

[6] N. B. Harum, Y. Ishii and T. Kanazawa, [Radio Base Station, Radio Terminal Device, Radio Relay Station Device, Transmission Power Control Method, Radio Communication Relay Method, and Radio Communication System], Publication No: US 2011/0159802A1.